Improved PIEZO1 agonism through 4-benzoic acid modification of Yoda1

Gregory Parsonage[1†], Kevin Cuthbertson[2†], Naima Endesh[1], Nicoletta Murciano[3,4], Adam J. Hyman[1], Charlotte H. Revill[2], Oleksandr V. Povstyan[1], Eulashini Chuntharpursat-Bon[1], Marjolaine Debant[1], Melanie J. Ludlow[1], T. Simon Futers[1], Laeticia Lichtenstein[1], Jacob A. Kinsella[1], Fiona Bartoli[1], Maria Giustina Rotordam[3,4], Nadine Becker[3], Andrea Brüggemann[3], Richard Foster[2*], David J. Beech[1*]

[1]Leeds Institute of Cardiovascular and Metabolic Medicine, School of Medicine, University of Leeds, LS2 9JT, UK. [2]School of Chemistry, University of Leeds, LS2 9JT, UK. [3]Nanion Technologies GmbH, Ganghoferstr. 70A, DE - 80339 München, Germany. [4]Saarland University, Theoretical Medicine and Biosciences, Kirrbergerstr. 100, DE - 66424 Homburg, Germany.

*Addresses for correspondence: Professor D. J. Beech, Leeds Institute of Cardiovascular and Metabolic Medicine, LIGHT Building, Clarendon Way, School of Medicine, University of Leeds, Leeds LS2 9JT, UK. E-mail d.j.beech@leeds.ac.uk. Telephone +44 (0) 113 3434323. Dr R. Foster, School of Chemistry, University of Leeds, Leeds LS2 9JT, UK. E-mail r.foster@leeds.ac.uk. Telephone +44 (0) 113 3435759.

[†]Equal contributors

DATA AND MATERIALS AVAILABILITY

The data that support the findings of this study are available from the corresponding author upon reasonable request. Some data may not be made available because of privacy or ethical restrictions. All original data are available in an Excel file. Unique laboratory materials created in the project are available on request (D.J.B. for biological materials and R.F. for chemicals).

FUNDING STATEMENT

AUTHOR CONTRIBUTIONS

G.P., A.J.H. and J.A.K. designed and performed calcium measurement assays. K.C. and C.H.R. designed, synthesized and analysed chemicals. N.E. designed and performed myography assays. O.V.P. designed and performed PIEZO1 patch-clamp experiments and J.A.K. PIEZO2 patch-clamp experiments. N.M., M.G.R., N.B. and A.B. designed automated patch-clamp experiments. N.M. and M.G.R. performed automated patch-clamp assays. T.S.F. and L.L. bred and maintained genetically engineered mice. M.J.L. generated cell lines. G.P., N.E., N.M. and O.V.P. made the figures. G.P. orchestrated the figure designs, data analysis and data transparency. CHR generated the supplementary chemistry information. E.C.-B. made intellectual contribution and performed PIEZO2 and HeLa cell experiments with M.D. and F.B.. G.P. and D.J.B. interpreted data and wrote most of the manuscript with input from

M.G.R., R.F., O.V.P., N.M., E.C.-B. and M.D.. D.J.B. and R.F. conceptualised the study, supervised the project team and generated funding.

ETHICS APPROVAL STATEMENT

All animal experiments were authorised by the University of Leeds Animal Welfare and Ethics Committee and the UK Home Office under the authority of the Project Licences P606320FB and PP8169223.

PERMISSION TO REPRODUCE INFORMATION FROM OTHER SOURCES

Not applicable.

DECLARATION OF TRANSPARENCY AND SCIENTIFIC RIGOUR

This Declaration acknowledges that this paper adheres to the principles for transparent reporting and scientific rigour of preclinical research as stated in the BJP guidelines for Design and Analysis, and Animal Experimentation, and as recommended by funding agencies, publishers and other organisations engaged with supporting research.

AUTHOR DETAILS

First name	Last name (surname)	Affiliation	Email	ORCID ID
Gregory	Parsonage	University of Leeds	g.parsonage@leeds.ac.uk	0000-0002-3666-5288
Kevin	Cuthbertson	University of Leeds	kevincuthbertson@live.co.uk	No ID
Naima	Endesh	University of Leeds	n.e.m.endesh@leeds.ac.uk	No ID
Nicoletta	Murciano	Nanion Technologies GmbH and Saarland University	Nicoletta.Murciano@nanion.de	0000-0002-8046-7297
Adam	Hyman	University of Leeds	adamhyman3@outlook.com	0000-0002-3666-5288

Charlotte	Revill	University of Leeds	c.h.revill@leeds.ac.uk	No ID
Oleksandr	Povstyan	University of Leeds	o.povstyan@leeds.ac.uk	0000-0002-6998-3944
Eulashini	Chuntharpursat-Bon	University of Leeds	medechu@leeds.ac.uk	0000-0002-0767-6877
Marjolaine	Debant	University of Leeds	m.debant@leeds.ac.uk	0000-0001-5988-3395
Melanie	Ludlow	University of Leeds	mjbettale@gmail.com	No ID
T. Simon	Futers	University of Leeds	t.s.futers@leeds.ac.uk	0000-0003-3810-190X
Laeticia	Lichtenstein	University of Leeds	l.lichtenstein@leeds.ac.uk	0000-0003-3900-786X
Jacob	Kinsella	University of Leeds	umjki@leeds.ac.uk	0000-0002-4759-1771
Fiona	Bartoli	University of Leeds	f.bartoli@leeds.ac.uk	0000-0001-9487-9551
Maria Giustina	Rotordam	Nanion Technologies and Saarland University	Giustina.Rotordam@nanion.de	No ID
Nadine	Becker	Nanion Technologies	Nadine.Becker@nanion.de	No ID
Andrea	Brüggemann	Nanion Technologies	andrea@nanion.de	0000-0002-7325-6715
Richard	Foster	University of Leeds	r.foster@leeds.ac.uk	0000-0002-2361-3884
David	Beech	University of Leeds	d.j.beech@leeds.ac.uk	0000-0002-7683-9422

88
89
90 **KEYWORDS**
91

Calcium channel, Non-selective cation channel, Mechanical force, Pharmacology, Medicinal chemistry, Vascular biology, Endothelial cell.

WHAT IS ALREADY KNOWN ABOUT THIS SUBJECT

PIEZO1 channel is an important mechanical force sensor

Options for pharmacological modulation of PIEZO1 are limited

WHAT THIS STUDY ADDS

Novel PIEZO1 agonists and new agonism structure-activity relationships

Improved PIEZO1 agonism

CLINICAL SIGNIFICANCE

Potential foundations for treating diseases linked genetically to PIEZO1, such as lymphatic dysplasia

ABSTRACT

Background and Purpose: PIEZO1 forms mechanically activated calcium-permeable non-selective cation channels in numerous species and cell types. Options for pharmacological modulation are limited and so we modified a PIEZO1 small-molecule agonist (Yoda1) to advance capability for modulation.
Experimental Approach: Medicinal chemistry generated Yoda1 analogues that were tested in intracellular calcium and patch-clamp assays on cultured cells exogenously expressing human or mouse PIEZO1 or mouse PIEZO2, physico-chemical assays and wire myography assays on vein from mice in which there was genetic disruption of PIEZO1.
Key Results: A Yoda1 analogue (KC159) containing 4-benzoic acid instead of the pyrazine of Yoda1 and its potassium salt (KC289) have equivalent or improved reliability, efficacy and potency compared to Yoda1 in functional assays. Tested against over-expressed mouse PIEZO1 in calcium assays, potency order is KC289 (150)>KC159 (280)>Yoda1 (600) (EC_{50}s in parentheses, nM). There is selectivity for PIEZO1 over other membrane proteins and the physico-chemical properties are more suited to physiological conditions than those of Yoda1. Vasorelaxant effects occur that are consistent with PIEZO1 agonism. 2-benzoic acid substitution, by contrast, fails to generate a modulator.
Conclusion and Implications: 4-Benzoic acid modification of Yoda1 improves PIEZO1 agonism. We suggest naming this new modulator Yoda2. It should be a useful tool compound in physiological assays and facilitate efforts to identify a binding site. Such compounds may have therapeutic potential, for example in diseases linked genetically to PIEZO1 such as lymphatic dysplasia.

NON-STANDARD ABBREVIATIONS

139
140 EC$_{50}$, concentration for 50% effect; HEK, human embryonic kidney; GFP, green fluorescent
141 protein; TRPC, transient receptor potential canonical; DMEM, Dulbecco's minimum essential
142 medium; HUVEC, Human Umbilical Vein Endothelial Cells; ECGM-2, Endothelial Cell Basal
143 Medium 2; EDTA, ethylenediamine tetraacetic acid; HeLa cells, immortal cells named after
144 Henrietta Lacks; GAPDH, glyceraldehyde 3-phosphate dehydrogenase; HEPES, 4-(2-
145 hydroxyethyl)-1-piperazineethanesulfonic acid; DMSO, dimethyl sulphoxide; PTFE,
146 polytetrafluoroethylene; RED, rapid equilibrium dialysis; TAM, tamoxifen; L-NAME, L-N^G-nitro
147 arginine methyl ester; PE, phenylephrine; EC, endothelial cell; Cdh5, Cadherin 5; NOS3,
148 endothelial nitric oxide synthase; mPIEZO1, mouse PIEZO1; hPIEZO1, human PIEZO1;
149 mPIEZO2, mouse PIEZO2; siPIEZO1, short-interfering RNA targeted to PIEZO1 expression;
150 siPIEZO2, short-interfering RNA targeted to PIEZO2 expression; siCtrl, control short-
151 interfering RNA; M-Stim, mechanical stimulation.
152
153 **INTRODUCTION**
154
155 PIEZO1 is a mechanically activated calcium ion (Ca^{2+})-permeable non-selective cation
156 channel subunit (Coste et al., 2010; Murthy, Dubin & Patapoutian, 2017). It assembles as
157 trimers to form a central ion pore (Guo & MacKinnon, 2017; Jiang, Yang, Jiang & Xiao, 2021).
158 Its N-terminal propeller blade-like structures curve and indent the membrane, most likely to
159 enable response to increased membrane tension (De Vecchis, Beech & Kalli, 2021; Guo &
160 MacKinnon, 2017; Yang, Lin, Chen, Li, Li & Xiao, 2022; Young, Lewis & Grandl, 2022).
161 Channel activation leads to Ca^{2+} influx and intracellular Ca^{2+} elevation and thus cellular effects
162 due to the second messenger roles of Ca^{2+}. The channels are widely expressed and have
163 diverse functions, including in blood flow sensing by endothelium (Li et al., 2014; Rode et al.,
164 2017; Wang, Chennupati, Kaur, Iring, Wettschureck & Offermanns, 2016) and detection of
165 cyclical force in innate immunity (Solis et al., 2019). Mutations in human *PIEZO1* associate
166 with anaemia (Zarychanski et al., 2012), malarial resistance (Ma et al., 2018), lymphatic
167 dysplasia (Fotiou et al., 2015) and varicose vein disease (Fukaya et al., 2018), suggesting
168 important roles in red blood cell, vascular wall and other human biology (Beech & Kalli, 2019;
169 Jiang, Yang, Jiang & Xiao, 2021).
170
171 The pharmacology available for PIEZO1 is limited and so the opportunities for PIEZO1
172 manipulation and therapeutic drug discovery are restricted. Most importantly so far, screening
173 of a library of small-molecules revealed a promising agent called Yoda1, named in reference
174 to the "may the force be with you" phrase of the Star Wars films (Syeda et al., 2015). This
175 substance (2-[5-[[(2,6-dichlorophenyl)methyl]thio]-1,3,4-thiadiazol-2-yl]pyrazine) is an agonist
176 of mouse and human PIEZO1 channels (Syeda et al., 2015). It does not activate the only
177 related channel, PIEZO2, in studies of mouse PIEZO2 overexpressed in HEK 293 cells (Syeda
178 et al., 2015). Yoda1 is used extensively in the field and, while some concern has been raised
179 about its suitability, it appears to be a valuable tool compound (Beech & Kalli, 2019). It
180 activates PIEZO1 channels reconstituted in lipid bilayers (Syeda et al., 2015) and may act
181 somewhere in the propeller blade region proximal to the ion pore domain, putatively serving
182 as a "molecular wedge" to lower the threshold for mechanical activation (Botello-Smith et al.,
183 2019). Despite the synergy with mechanical force (Syeda et al., 2015), direct application of
184 Yoda1 in the absence of exogenous force is often sufficient to cause strong PIEZO1 channel
185 activation (Evans et al., 2018), perhaps because there is already endogenous force acting on
186 the channel (e.g., from the substrate or cell-cell contact). Therefore, Yoda1 is a test agent to
187 determine the presence of functional PIEZO1 channels and indicate physiological roles of
188 PIEZO1. Nevertheless, although Yoda1 is a useful tool compound, it has limitations such as
189 its relatively low potency and aqueous solubility (Syeda et al., 2015).
190
191 A potential route to improving PIEZO1 pharmacology is through better understanding of the
192 structure-activity relationships of Yoda1. Integrity of the 2,6-dichlorophenyl moiety is important
193 (Evans et al., 2018; Syeda et al., 2015) with only limited possibilities for modification with

194 retained activity (Li, Xiong, Yan, O'Brien & Schuller de Almeida, 2021). The pyrazine moiety
195 at the other end of the molecule, however, appears to be less critical while still important for
196 agonism (Evans et al., 2018). Therefore, we hypothesized that modification of the pyrazine
197 could be a route to improved agonism and physico-chemical properties.
198
199
200 **METHODS**
201
202 Stable cell lines
203
204 HEK T-REx™ 293 cells that overexpress human PIEZO1 upon induction with tetracycline were
205 generated as previously described (Rode et al., 2017). PIEZO1-GFP7 was used as a PCR
206 template to clone human PIEZO1 coding sequence into pcDNA™4/TO between HindIII and
207 EcoRI restriction sites. PIEZO1 was amplified as two fragments using the following primers:
208 (HindIII-PIEZO1-Fw: AATAAGCTTATGGAGCCGCACGTG and BamHI-Int.PIEZO1-Rv:
209 AATGGATCCCCCTGGACTGTCG) and (BamHI-Int. PIEZO1-Fw:
210 AATGGATCCTCCCCGCCACGGA and EcoRI-PIEZO1-Rv:
211 AATGAATTCTTACTCCTTCTCACGAGT). The two fragments were fused using BamHI
212 restriction site, resulting in the full-length PIEZO1 coding sequence with the c4182a silent
213 mutation. HEK T-REx™ 293 cells (Invitrogen) were transfected with pcDNA4/TO-PIEZO1
214 using Lipofectamine 2000 (Thermo Fisher Scientific). Subsequently cells were treated with 10
215 μg mL^{-1} blasticidin and 200 μg mL^{-1} zeocin (InvivoGen) to select stably transfected cells.
216 Single cell clones were isolated and analysed individually. Expression was induced by treating
217 the cells for 24 hours with 10 ng mL^{-1} tetracycline and analysed by quantitative RT-PCR and
218 western blot. These cells are referred to as hPIEZO1-TREx.
219 HEK T-REx™ cells that constitutively overexpress murine PIEZO1 were generated as
220 previously described (Blythe et al., 2019). pcDNA3 mouse PIEZO1 IRES GFP, a gift from
221 Ardem Patapoutian (Coste et al., 2010), was used as a template to clone the mouse PIEZO1
222 coding sequence into pcDNA4/TO. Overlapping mouse PIEZO1 (forward primer 5'-
223 GTAACAACTCCGCCCCATTG-3' and reverse primer 5'-GCTTCTACTCCCTCTCACGTGTC-
224 3') and pcDNA4/TO (forward primer 5'-
225 GACACGTGAGAGGGAGTAGAAGCCGCTGATCAGCCTCGACTG-3' and reverse primer 5'-
226 CAATGGGGCGGAGTTGTTAC-3') PCR products were assembled using Gibson Assembly
227 (New England Biolabs). This construct does not contain tetracycline operator sequences. HEK
228 T-REx™ 293 cells were transfected with pcDNA4/TO-mPIEZO1 using Lipofectamine 2000
229 (Invitrogen) and treated with 200 μg mL^{-1} zeocin to select stably transfected cells. Individual
230 clones were isolated and analyzed for expression using Yoda1 and intracellular Ca^{2+}
231 measurements. These cells are referred to as mPIEZO1-TREx.
232
233 HEK 293 cells stably expressing tetracycline-regulated human TRPC5 have been described
234 previously (Zeng et al., 2004). For the TRPC5 expressing cells, selection was achieved by
235 including 5 μg mL^{-1} blasticidin and 400 μg mL^{-1} zeocin in the cell medium. To induce
236 expression, cells were incubated with 1 μg mL^{-1} tetracycline for 24 h prior to experiments.
237 These cells are referred to as hTRPC5-TREx.
238
239 **PIEZO2 and cell transfection**
240
241 Mouse PIEZO2 (mPIEZO2) pCMV-Sport6 was a gift from Ardem Patapoutian (Coste et al.,
242 2015), obtained via Addgene (Addgene plasmid # 81073; http://n2t.net/addgene:81073;
243 RRID:Addgene_81073). It was sequenced for validation. Transient transfection of the plasmid
244 was achieved using Lipofectamine 3000 in HEK293 cells, 48 hr prior to measurements being
245 made.
246
247 **Cell culture**
248

HEK T-REx™ 293 cells were maintained in DMEM supplemented with 10% heat-inactivated fetal calf serum, 100 units mL^{-1} penicillin and 100 µg mL^{-1} streptomycin (Sigma-Aldrich). Stably transfected HEK T-REx™ 293 cells continued to receive 10 µg mL^{-1} blasticidin, and 200 µg mL^{-1} zeocin in maintenance cultivation. Non-transfected HEK T-REx™ 293 cells were used as control cells.

Human Umbilical Vein Endothelial Cells (HUVEC) purchased from PromoCell (# C-12203) were maintained in Endothelial Cell Basal Medium (ECGM-2, PromoCell # C-22111) supplemented with: 500 pg mL^{-1} recombinant human vascular endothelial growth factor 165, 10 ng mL^{-1} recombinant human basic fibroblast growth factor, 200 ng mL^{-1} hydrocortisone, 22.5 µg mL^{-1} heparin, and 2% (vol./vol.) foetal calf serum. Antibiotic-antimycotic (Gibco #15240062) was also added and resulted in final concentrations of 10 U mL^{-1} penicillin, 10 U mL^{-1} streptomycin, and 250 ng mL^{-1} amphotericin B. HUVEC were passaged at a maximum seeding ratio of 1:4 (parent:daughter flask) after 3 to 6 days' growth, when they had reached densities of between 3.4 to 6.6 x 10^4 cells cm^{-2}. After washing the cell monolayer with D-PBS [Sigma # D8537], 2 mL pre-warmed 0.05% Trypsin-EDTA (Gibco # 25300054) was added to 75 cm^2 flasks until the cells had detached (between 2-5 minutes at 37°C). 8 mL complete ECGM2 medium was added to inhibit the trypsin, the cells were counted, their density adjusted before seeding into fresh vessels for maintenance cultivation or experimental purposes. The medium for maintenance of cultures was completely refreshed every 48 hours. HUVEC were used for experiments after a minimum of 3 and a maximum of 5 passages. All cells were grown at 37°C and in 5% CO_2 humidified incubator.

Hela and HEK 293 cells were purchased from ATCC and maintained in DMEM supplemented with 10% heat-inactivated fetal calf serum, 100 units.mL^{-1} penicillin and 100 µg.mL^{-1} streptomycin (Sigma-Aldrich).

RNA interference

Cells were transfected using using Opti-MEM^{TM} I Reduced Serum Medium (ThermoFisher Scientific) and Lipofectamine 2000 (ThermoFisher Scientific). For transfection of cells in 6-well plates, 20 nmol siRNA (siCtrl : Dharmacon ON-TARGETplus Non-targeting Control Pool, D-001810-10-05 ; siPIEZO2 : Dharmacon ON-TARGETplus SmartPool PIEZO2, L-013925-02-0005 and PIEZO1 : Sigma-Aldrich, GCAAGUUCGUGCGCGGAUU[DT][DT]) and 3 µL of Lipofectamin 2000 complexed in 200 µL of Opti-MEM were added to 0.8 mL cell culture medium per well. The culture medium was changed 4 hours post transfection and cells were used for experiments 48 hr later. RNA isolation and RT-qPCR: RNA was isolated using Trizol according to manufacturer's protocol. 1 µg of total RNA was reverse transcribed using the iScript™ cDNA Synthesis Kit (Bio-Rad), according to the manufacturer's instructions. qPCR was performed using SyBR Green (Bio-Rad). qPCR reactions were performed on a LightCycler® 480 Real Time PCR System (Roche). Samples were analysed using the comparative CT method, and expressed as percentage of GAPDH housekeeping gene. The sequences of PCR primers (synthesized by Integrated DNA Technologies) were:

Species	Gene	Forward (5'-3')	Reverse (5'-3')
Homo sapiens	*PIEZO1*	CGTCTTCGTGGAGCAGATG	GCCCTTGACGGTGCATAC
	PIEZO2	GACAGACGAAGCAGCACAGA	GTGCTTTCTTCCAACTCGCC
	GAPDH	GCCTCAAGATCATCAGCAAT	GGACTGTGGTCATGAGTCCT
Mus musculus	*Piezo1*	TGAGCCCTTCCCCAACAATAC	CTGCAGGTGGTTCTGGATATAG
	Piezo2	AGAGTCGGAAAAGAGATACCCTC	CCAGACGATACAGATGAGAAGGA

Ca^{2+} measurement

296 HEK 293-TREx cells and their stably-transfected derivatives or transiently transfected HEK
297 293 or HeLa cells were seeded at a density of 7.5 x 10^4 cells per well into poly-D-Lysine-
298 coated 96-well plates. The plates were either commercially pre-coated with poly-D-Lysine
299 (Greiner Bio-One # 655946) or (Greiner Bio-One # 655090) were coated in-house with 35 μL
300 of a 10 μg mL^{-1} poly-D-Lysine (Bio-Techne, Cultrex # 3439-100-01) in sterile deionised water
301 per well for at least 24 hours and rinsed 3 times with 100 μL per well sterile D-PBS before
302 addition of cells. HUVEC were seeded into tissue culture-treated 96-well plates (Greiner Bio-
303 One #655090) at a density of either 2.5 x 10^4 cells 24 h before experimentation, or 1.25 x 10^4
304 cells 48 h before experimentation. Cells were incubated with 2 μM Fura-2-AM (Molecular
305 Probes™) in the presence of 0.01% (weight/vol.) pluronic F127 (Sigma-Aldrich #P2443) in
306 standard bath solution (SBS) for 1 h at 37°C. Cells were washed with SBS for 30 min at room
307 temperature. Alternatively, if inhibitors were being tested, these were added at this time,
308 immediately following a wash in SBS. (-)-Englerin A (Akbulut et al., 2015) was used in SBS
309 containing 0.01% pluronic acid as a dispersing agent to minimise aggregation of compound.
310 Unless otherwise stated, the final concentration of DMSO was 0.2% (vol./vol.). Working 2000X
311 stock solutions of test compounds were freshly made in DMSO and diluted 1000-fold in SBS
312 during the 30-minute SBS wash/inhibitor preincubation period to obtain 2X solutions for
313 injection. When testing the highest concentration of Yoda1, KC159 and KC289 (30 μM), the
314 final DMSO concentration was 0.6% (vol./vol.). Measurements were made at room
315 temperature on a 96-well fluorescence plate reader (FlexStationIII, Molecular Devices,
316 Sunnyvale, CA, USA) controlled by Softmax Pro software v7.0.3. Recipient wells containing
317 80 μL SBS/ 0.2% (vol./vol.) DMSO vehicle or inhibitor compound received 80 μL 2X compound
318 at an injection rate of 1 μL s^{-1}, and the pipette introduced liquids from a height setting of 70
319 μL. No trituration was performed. For recordings using Fura-2, the change in intracellular
320 calcium was indicated as the ratio of Fura-2 emission (510 nm) intensities at 340 and 380 nm
321 excitation. Photomultipliers were set to medium sensitivity. SBS contained: 130 mM NaCl, 5
322 mM KCl, 8 mM D-glucose, 10 mM HEPES, 1.2 mM $MgCl_2$, 1.5 mM $CaCl_2$ and the pH was
323 adjusted to 7.4 with NaOH. The solution was filtered through a 0.2 μm bottle-top filter prior to
324 use, and handled aseptically thereafter.
325
326 We did not randomize compounds in the multiwell plate Ca^{2+} assays because of the risk of it
327 introducing errors due to the complexity of constructing and analysing randomized plates. We
328 did, however, take steps to minimize the risk of systematic errors by altering the position of
329 specific compounds in the plate to test for the possibility of position-related effects, for which
330 we found no evidence.
331
332 **Patch-clamp recording**
333
334 For manual patch-clamp, macroscopic transmembrane ionic currents of mPIEZO1 HEK-TREx
335 cells (or control HEK-TREx cells) were recorded using the standard whole-cell configuration
336 for patch-clamp in voltage-clamp mode. For studies of HEK 293 cells overexpressing PIEZO2
337 (or control HEK 293 cells), the outside-out patch configuration was used in voltage-clamp
338 mode. All recordings were made using an AXOpatch 200B amplifier (Axon Instruments, Inc.,
339 USA) equipped with Digidata 1550B hosted by a PC running pClamp 10.7 software (Molecular
340 Devices, USA) at room temperature. The cells were maintained during the experiment in an
341 external salt buffer solution (SBS) of the following composition: 135 mM NaCl, 5 mM KCl, 1.5
342 mM $CaCl_2$, 1.2 mM $MgCl_2$, 8 mM D-glucose, 10 mM HEPES (titrated to pH 7.4 with NaOH).
343 Patch pipettes were fire-polished and had a resistance of 4–7 MΩ when filled with the pipette
344 solution of the following composition: 145 mM CsCl, 2 mM $MgCl_2$, 10 mM HEPES, 1 mM
345 EGTA, 5 mM Na_2ATP, 0.1 mM Na_2GTP and the pH was titrated to 7.2 with CsOH (whole-cell
346 experiments). For outside-out experiments, Na_2ATP and Na_2GTP were omitted. For whole-
347 cell experiments, cells were held at 0 mV and current amplitude was monitored by application
348 of ramp voltage protocol from -100 mV to +100 mV at 10 s intervals. Currents were measured
349 at -100 mV and +100 mV. Test compounds were applied in the external solution using a bath
350 perfusion system. SBS flow was applied to the cells for 1 min before the addition of

compounds. For outside-out experiments the patches were held at -80 mV and currents were activated by application of 100-ms pressure pulse from 0 to 75 mmHg applied directly to the patch pipette with an interval of 12.387 s using High Speed Pressure Clamp HSPC-1 System (ALA Scientific Instruments, USA). Current records were analogue-filtered at 1 kHz and digitally acquired at 10 kHz. Data were analysed and plotted using pClamp 10.7 and MicroCal Origin 2018 (MicroCal software, USA).

For automated patch-clamp, cells were cultured and harvested according to Nanion's standard cell culture protocol (Obergrussberger et al., 2014). hPIEZO1-TREx cells were induced to express PIEZO1 by incubation with 0.5 µg ml^{-1} tetracycline 24 hours prior to experiments. Whole cell patch-clamp recordings were conducted on HEK-TREx, hPIEZO1-TREx and mPIEZO1-TREx cells according to Nanion's standard procedure for the SyncroPatch 384, using medium resistance (4-5 MΩ) chips (Obergrussberger et al., 2018). Cells were held at -80 mV for the duration of the experiment. The channel was activated by mechanical forces in the absence and presence of the agonists. To stimulate PIEZO1 channels mechanically (mechanical stimulation, M-Stim), we dispensed 20 µL of solution (either reference or agonist) locally to the cell at a pipetting speed of 110 µL.s^{-1} in synchrony with a triggered recording of the current response at the holding potential. The internal solution contained: 110 mM KF, 10 mM KCl, 10 mM NaCl, 10 mM HEPES, 10 mM EGTA pH adjusted to 7.2 with KOH, and the external solution contained: 140 mM NaCl, 4 mM KCl, 2 mM $CaCl_2$, 1 mM $MgCl_2$, 5 mM Glucose, 10 mM HEPES, pH adjusted to 7.4 with NaOH, and 0.1% DMSO to match the DMSO concentration of the compound solutions. For PIEZO1 stimulation, KC159, KC157 or Yoda1 was applied directly onto the cells via a pipette application. One chip of the SyncroPatch 384 is equipped with 384 wells served by 384 robotic pipettes and connected to 384 individual amplifiers, allowing us to test 384 distinct cells in one experiment. We tested the effect of each specified analogue on mPIEZO1-, hPIEZO1- and untransfected HEK-TREx cells in parallel and in comparison to mechanical and Yoda1 stimulation. To estimate the EC_{50} values, 4 concentrations of each agonist were tested per cell line in one chip, with each cell receiving single concentrations, and the concentration response curve was calculated across the whole chip (384 cells). Only cells with seal resistance >0.3 GΩ, series resistance <20 MΩ and cell capacitance >5 pF and <40 pF were used for analysis. We considered responding cells as the cells treated with the agonist that displayed current with peak amplitude >-100 pA and area under the curve (AUC) >-10 pA.

Chemical synthesis

Analogues of Yoda1 were synthesised using a 4-step synthetic route utilising a Suzuki-coupling to introduce diversity (Scheme X) whilst compound **KC289** is the potassium salt of **KC159**, synthesised by treating **KC159** with KOH. All synthesised chemicals were purified by column chromatography or trituration and determined as >97% pure by ^{1}H NMR (proton nuclear magnetic resonance) and ^{13}C NMR (carbon-13 nuclear magnetic resonance). Synthetic and analytical details are reported in the Supporting Information (SI).

Eurofins Hit Profiling Screen PP70

These experiments were performed by Eurofins Scientific and the methods below are from this company's information (https://www.eurofins.co.uk/). ‡Membrane protein/ membrane amounts may have varied and the concentrations used were adjusted as necessary. KC289 was tested at 5 µM.

Acetylcholine M2: Human recombinant muscarinic M2 receptors expressed in CHO-K1 cells were used in modified Tris-HCl buffer pH 7.4. An 8 µg‡ aliquot was incubated with 0.8 nM [^{3}H]N-Methylscopolamine for 120 minutes at 25°C. Non-specific binding was estimated in the presence of 1 µM atropine. Receptors were filtered and washed, the filters were counted to determine [^{3}H]N-Methylscopolamine specifically bound.

406

407 Acetylcholine M3: Human recombinant muscarinic M3 receptors expressed in CHO-K1 cells
408 were used in modified Tris-HCl buffer pH 7.4. A 12 µg[‡] aliquot was incubated with 0.8 nM
409 [^{3}H]N-Methylscopolamine for 120 minutes at 25°C. Non-specific binding was estimated in the
410 presence of 1 µM atropine. Receptors were filtered and washed, the filters were then counted
411 to determine [^{3}H]N-Methylscopolamine specifically bound.

412

413 Adenosine A1: This assay measured binding of [^{3}H]DPCPX to adenosine A1 receptors. CHO-
414 K1 cells stably transfected with a plasmid encoding the human adenosine A1 receptor were
415 used to prepare membranes in modified HEPES pH 7.4 using standard techniques. A 10 µg[‡]
416 aliquot of membrane was incubated with 1 nM [^{3}H]DPCPX for 90 minutes at 25°C. Non-specific
417 binding was estimated in the presence of 100 µM R(-)-PIA. Membranes were filtered and
418 washed 3 times and the filters were counted to determine [^{3}H]DPCPX specifically bound.

419

420 Adenosine A2A: This assay measured binding of [^{3}H]CGS-21680 to human adenosine A2A
421 receptors. HEK 293 (human embryonic kidney) cells stably transfected with a plasmid
422 encoding the human adenosine A2A receptor were used to prepare membranes in modified
423 Tris-HCl pH 7.4 buffer using standard techniques. A 15 µg[‡] aliquot of membrane was
424 incubated with 50 nM [^{3}H]CGS-21680 for 90 minutes at 25°C. Non-specific binding was
425 estimated in the presence of 50 µM NECA. Membranes were filtered and washed 3 times and
426 the filters were counted to determine [^{3}H]CGS-21680 specifically bound.

427

428 Adrenoceptor alpha1A: Submaxillary glands of male Wistar derived rats weighing 175 ± 25 g
429 were used to prepare adrenergic α1A receptors in modified Tris-HCl buffer pH 7.4. A 5 mg[‡]
430 aliquot was incubated with 0.25 nM [^{3}H]Prazosin for 60 minutes at 25°C. Non-specific binding
431 was estimated in the presence of 10 µM phentolamine. Membranes were filtered and washed,
432 the filters were then counted to determine [^{3}H]Prazosin specifically bound.

433

434 Adrenoceptor alpha1B: Livers of male Wistar derived rats weighing 175 ± 25 g were used to
435 prepare adrenergic α1B receptors in modified Tris-HCl buffer pH 7.4. A 5 mg[‡] aliquot was
436 incubated with 0.25 nM [^{3}H]Prazosin for 60 minutes at 25°C. Non-specific binding was
437 estimated in the presence of 10 µM phentolamine. Membranes were filtered and washed, the
438 filters were then counted to determine [^{3}H]Prazosin specifically bound.

439

440 Adrenoceptor alpha2A: Human recombinant adrenergic α2A receptors expressed in CHO-K1
441 cells were used in modified Tris-HCl buffer pH 7.4. A 2 µg[‡] aliquot was incubated with 1.5 nM
442 [^{3}H]Rauwolscine for 60 minutes at 25°C. Non-specific binding was estimated in the presence
443 of 10 µM WB-4101. Receptors were filtered and washed, the filters were then counted to
444 determine [^{3}H]Rauwolscine specifically bound. KC289 was screened at 5 µM.

445

446 Adrenoceptor beta1: Human recombinant adrenergic β1 receptors expressed in CHO-K1 cells
447 were used in modified Tris-HCl buffer pH 7.4. A 25 µg‡ aliquot of membrane was incubated
448 with 0.03 nM [^{125}I]Cyanopindolol for 120 minutes at 25°C. Non-specific binding was estimated
449 in the presence of 100 µM S(-)-propranolol. Membranes were filtered and washed 3 times and
450 the filters were counted to determine [^{125}I]Cyanopindolol specifically bound.

451

452 Adrenoceptor beta2: This assay measured binding of [^{3}H]CGP-12177 to human adrenergic b2
453 receptors. Mammalian CHO-hNBR1 cells stably transfected with a plasmid encoding the
454 human adrenergic b2 receptor were used to prepare membranes in modified Tris-HCl pH 7.4
455 buffer using standard techniques. A 50 µg[‡] aliquot of membrane was incubated with 0.2 nM
456 [^{3}H]CGP-12177 for 60 minutes at 25°C. Non-specific binding was estimated in the presence
457 of 10 µM ICI-118551. Membranes were filtered and washed 3 times and the filters were
458 counted to determine [^{3}H]CGP-12177 specifically bound.

459

Cav1.2 (L-type): Cerebral cortices of Wistar derived rats weighing 175 ± 25 g were used to prepare membranes in Tris-HCl buffer pH 7.4. A 2.5 mg‡ aliquot was incubated with 0.1 nM [³H]Nitrendipine for 90 minutes at 25°C. Non-specific binding was estimated in the presence of 1 µM nitrendipine. Membranes were filtered and washed, the filters were then counted to determine [³H]Nitrendipine specifically bound.

CB1 Human Cannibinoid: Human recombinant cannabinoid CB1 receptors expressed in rat hematopoietic Chem-1 cells were used in modified HEPES buffer pH 7.4. A 5 µg‡ aliquot of membrane was incubated with 2 nM [³H]SR141716A for 60 minutes at 37°C. Non-specific binding was estimated in the presence of 10 µM CP 55,940. Membranes were filtered and washed 4 times and the filters were counted to determine [³H]SR141716A specifically bound.

Dopamine D1: This assay measured binding of [³H]SCH-23390 to human dopamine D1 receptors. CHO cells stably transfected with a plasmid encoding the human dopamine D1 receptor were used to prepare membranes in modified Tris-HCl pH 7.4 buffer using standard techniques. A 20 µg‡ aliquot of membrane was incubated with 1.4 nM [³H]SCH-23390 for 120 minutes at 37°C. Non-specific binding was estimated in the presence of 10 µM (+)-butaclamol. Membranes were filtered and washed 3 times and the filters were counted to determine [3H]SCH-23390 specifically bound.

Dopamine D25: This assay measured binding of [³H]Spiperone to human dopamine D25 (D2B) receptors. CHO cells stably transfected with a plasmid encoding the human dopamine D25 receptor were used to prepare membranes in modified Tris-HCl pH 7.4 buffer using standard techniques. A 15 µg‡ aliquot of membrane was incubated with 0.16 nM [³H]Spiperone for 120 minutes at 25°C. Non-specific binding was estimated in the presence of 10 µM haloperidol. Membranes were filtered and washed 3 times and the filters were counted to determine [3H]Spiperone specifically bound.

GABA A (1): Whole brains (except cerebellum) of male Wistar derived rats weighing 175 ± 25 g were used to prepare GABAA agonist site receptors in Tris-HCl buffer pH 7.4. A 10 mg‡ aliquot was incubated with 1 nM [³H]Muscimol for 10 minutes at 4°C. Non-specific binding was estimated in the presence of 0.1 µM muscimol. Membranes were filtered and washed, the filters were then counted to determine [3H]Muscimol specifically bound. GABA A (2): Whole brain (except cerebellum) of male Wistar derived rats weighing 175 ± 25 g were used to prepare GABAA central benzodiazepine membrane receptor in Na-K phosphate buffer pH 7.4. A 5 mg‡ aliquot was incubated with 1 nM [³H]Flunitrazepam for 60 minutes at 25°C. Non-specific binding was estimated in the presence of 10 µM diazepam. Membranes were filtered and washed, the filters were then counted to determine [³H]Flunitrazepam specifically bound.

Glutamate: Cerebral cortices of Wistar derived rats weighing 175 ± 25 g were used to prepare glutamate NMDA phencyclidine receptors in Tris-HCl buffer pH 7.4. A 6.3 mg‡ aliquot was incubated with 4 nM [³H]TCP for 45 minutes at 25°C. Non-specific binding was estimated in the presence of 1 µM dizocilpine ((+)-MK-801). Membranes were filtered and washed, the filters were then counted to determine [³H]TCP specifically bound.

Histamine H1: Human recombinant histamine H1 receptor expressed in CHO-K1 cells were used in modified Tris-HCl buffer pH 7.4. A 10 µg‡ aliquot was incubated with 1.2 nM [³H]Pyrilamine for 180 minutes at 25°C. Non-specific binding was estimated in the presence of 1 µM pyrilamine. Receptor proteins were filtered and washed, the filters were then counted to determine [³H]Pyrilamine specifically bound.

Imidazoline I2: Brains (except cerebella) of male Wistar derived rats weighing 175 ± 25 g were used to prepare imidazoline I2 receptors in modified Tris-HCl buffer pH 7.4. A 15 mg‡ aliquot was incubated with 2 nM [³H]Idazoxan for 30 minutes at 25°C. Non-specific binding was

514   estimated in the presence of 1 µM idazoxan. Membranes were filtered and washed, the filters
515   were then counted to determine [³H]Idazoxan specifically bound.
516
517   mu Opioid: Human opiate µ receptors expressed in CHO-K1 cells were used in modified Tris-
518   HCl buffer pH 7.4. An 11 µg‡ aliquot was incubated with 0.6 nM [³H]Diprenorphine for 60
519   minutes at 25°C. Nonspecific binding was estimated in the presence of 10 µM naloxone.
520   Membranes were filtered and washed, the filters were then counted to determine
521   [³H]Diprenorphine specifically bound.
522
523   nAChR (alpha1): Human Nicotinic Acetylcholine α1 receptors expressed in RD cells were
524   used in 150 mM NaCl, 4 mM KCl, 2.3 mM CaCl₂. An aliquot was incubated with 0.6 nM [¹²⁵I]α-
525   Bungarotoxin for 120 minutes at 25°C. Nonspecific binding was estimated in the presence of
526   1 µM α-Bungarotoxin. Membranes were filtered and washed, the filters were then counted to
527   determine [¹²⁵I]α-Bungarotoxin specifically bound.
528
529   nAChR Nicotinic Acetylcholine: Human Nicotinic Acetylcholine receptors expressed in IMR-
530   32 cells were used in 20 mM HEPES, pH 7.5, 150 mM NaCl, 1.5 mM KCl, 2 mM CaCl₂, 1 mM
531   MgSO₄. An aliquot was incubated with 0.10 nM [¹²⁵I] Epibatidine for 60 minutes at 25°C.
532   Nonspecific binding was estimated in the presence of 300 µM (-)-Nicotine. Membranes were
533   filtered and washed, the filters were then counted to determine [¹²⁵I] Epibatidine specifically
534   bound.
535
536   Norepinephrine Transporter: Human norepinephrine transporters expressed in dog kidney
537   MDCK cells were used in modified Tris-HCl buffer pH 7.4. A 40 µg‡ aliquot was incubated with
538   0.2 nM [¹²⁵I]RTI-55 for 3 hours at 4°C. Non-specific binding was estimated in the presence of
539   10 µM desipramine. Membranes were filtered and washed, the filters were then counted to
540   determine [¹²⁵I]RTI-55 specifically bound.
541
542   PDE: This assay measured binding of [³H]Rolipram to rolipram binding sites. Whole brains
543   (except cerebellum) of male Wistar derived rats weighing 175 ± 25 g were prepared in modified
544   Tris-HCl pH 7.4 buffer using standard techniques. A 180 µg‡ aliquot of membrane was
545   incubated with 1.8 nM [³H]Rolipram for 60 minutes at 4°C. Non-specific binding was estimated
546   in the presence of 10 µM rolipram. Membranes were filtered and washed 3 times and the filters
547   were counted to determine [³H]Rolipram specifically bound.
548
549   Phorbol Ester: This assay measures binding of [³H]PDBu to phorbol ester receptors. Brains
550   (except cerebella) membranes of male ICR derived mice weighing 20 ± 2 g were prepared in
551   modified Tris-HCl pH 7.4 buffer using standard techniques. A 20 µg‡ aliquot of membrane was
552   incubated with 3 nM [³H]PDBu for 60 minutes at 25°C. Non-specific binding was estimated in
553   the presence of 1 µM PDBu. Membranes were filtered and washed 3 times and the filters were
554   counted to determine [³H]PDBu specifically bound.
555
556   Potassium Channel (hERG): Human recombinant potassium channel HERG expressed in
557   human HEK 293 cells were used in modified HEPES buffer pH 7.4. A 10 µg‡ aliquot was
558   incubated with 1.5 nM [³H]Astemizole for 60 minutes at 25°C. Non-specific binding was
559   estimated in the presence of 10 µM Astemizole. Channel proteins were filtered and washed,
560   the filters were then counted to determine [³H]Astemizole specifically bound.
561
562   Potassium Channel (KATP): This assay measured binding of [³H]Glyburide to voltage
563   insensitive ATP-sensitive potassium channel sites [KATP]. HIT-T15 Syrian hamster pancreatic
564   b cells were used to prepare membranes in modified MOPS pH 7.4 buffer using standard
565   techniques. A 100 µg‡ aliquot of membrane was incubated with 5 nM [³H]Glyburide for 120
566   minutes at 25°C. Non-specific binding was estimated in the presence of 1 µM glyburide.
567   Membranes were filtered and washed 3 times and the filters were counted to determine
568   [³H]Glyburide specifically bound.

569

570 Prostanoid EP4: Human recombinant prostanoid EP4 receptors expressed in Chem-1 cells
571 were used in modified MES buffer pH 6.0. A 3 µg/ml[‡] aliquot was incubated with 1 nM
572 [^{3}H]PGE$_2$ for 120 minutes at 25°C. Non-specific binding was estimated in the presence of 10
573 µM PGE$_2$. Receptors were filtered and washed, the filters were then counted to determine
574 [^{3}H]PGE$_2$ specifically bound.

575

576 Serotonin (5-HT2B): This assay measured binding of [^{3}H]Lysergic acid diethylamide (LSD) to
577 human serotonin 5-HT2B receptors. CHO-K1 cells stably transfected with a plasmid encoding
578 the human serotonin 5-HT2B receptor were used to prepare membranes in modified Tris-HCl
579 pH 7.4 buffer using standard techniques. A 30 µg[‡] aliquot of membrane protein was incubated
580 with 1.2 nM [^{3}H]LSD for 60 minutes at 37°C. Non-specific binding was estimated in the
581 presence of 10 µM serotonin. Membranes were filtered and washed 3 times and the filters
582 were counted to determine [^{3}H]LSD specifically bound.

583

584 Sigma 1: This assay measured binding of [3H]Haloperidol to sigma δ1 receptors. Human
585 Jurkat cells were used to prepare membranes in potassium phosphate buffer pH 7.5 using
586 standard techniques. A 140 µg[‡] aliquot of membrane was incubated with 8 nM [^{3}H]Haloperidol
587 for 4 hours at 25°C. Non-specific binding was estimated in the presence of 10 µM Haloperidol.
588 Membranes were filtered and washed 3 times and the filters were counted to determine
589 [^{3}H]Haloperidol specifically bound.

590

591 Sodium Ion Channel: This assay measured binding of [3H]Batrachotoxinin to the site 2 of the
592 sodium channel-batrachotoxin. Whole brain (except cerebellum) membranes of male Wistar
593 derived rats weighing 175 ± 25 g were prepared in modified HEPES/Tris-HCl containing 40
594 mg/ml LqTx (alpha scorpion toxin from Leiurus quinquestriatus) to block site 2 at pH 7.4 buffer
595 using standard techniques. A 7.5 mg[‡] aliquot of membrane was incubated with 5 nM
596 [^{3}H]Batrachotoxinin for 60 minutes at 37°C. Non-specific binding was estimated in the
597 presence of 100 µM veratridine. Membranes were filtered and washed 3 times and the filters
598 were counted to determine [^{3}H]Batrachotoxinin specifically bound.

599

600 **Aqueous solubility**

601

602 Standard curves for each test compound were constructed. DMSO-dissolved test compounds
603 were added to universal aqueous buffer (45 mM ethanolamine, 45 mM KH$_2$PO$_4$, 45 mM KOAc,
604 pH 7.4): acetonitrile 80:20 (298.5 µL) at a final DMSO concentration of 0.5%. Samples were
605 incubated at room temperature with 300 rpm shaking for 30 min. 200 µL of each well was
606 transferred to a 96-well polypropylene V-bottomed collection plate and absorbance readings
607 were taken at 250 - 500 nm in 10 nm increments. Thus the λ_{max} was identified at which
608 concentration versus absorbance was plotted to provide standard curves.

609

610 For estimating aqueous solubility 2 µL of 50 mM test compound in DMSO was added to 398
611 µL of universal aqueous buffer and the samples were incubated for 1.5 hours with 300 rpm
612 shaking at room temperature. After filtration through hydrophilic PTFE 0.2 µm filters, 160 µL
613 sample was transferred to wells of a 96-well polypropylene V-bottomed collection plate and
614 40 µL acetonitrile was added to each well. Absorbance readings were taken at 250-500 nm in
615 10 nm increments. Solubility was calculated at the appropriate λ_{max} with reference to the
616 standard curve.

617

618 Kinetic and thermodynamic solubility assays were also performed by Malvern PanAnalytical
619 (UK). Briefly, 1000 µL of 0.1 M phosphate buffer (pH 7.4) received either; 25 µL of a 10 mM
620 DMSO stock of test compound (for kinetic solubility assays) or; 1 mg of test compound (for
621 thermodynamic solubility assays). The mixtures were shaken on an orbital mixer to reach
622 equilibrium for 1 or 24 hours, respectively. The equilibrated solution was centrifuged, the
623 supernatant removed to a fresh vial and then re-centrifuged. High and low dilution samples

were prepared from the secondary supernatant and quantified by LC-MSMS against a standard curve.

Microsomal half-life

Compound half-lives were measured by Malvern PanAnalytical (UK). Briefly, microsomal mouse liver microsomes (1 mg protein/ mL) were pre-incubated with NADPH cofactor solution at 37°C. Biotransformation was initiated by addition and mixing of 1 µM test compound in a final volume of 350 µL. 25 µL aliquots were removed at 5 minute intervals for 35 minutes and quenched in 300 µL ice cold methanol containing internal standard. The protein in the samples was then precipitated by centrifugation at 4°C, and the supernatant analysed by LC-MS/MS to quantify the test parent compound remaining at each time-point.

Plasma protein binding

Mouse plasma protein binding was measured by Rapid Equilibrium Dialysis (RED) performed by Malvern PanAnalytical (UK). Briefly, mouse plasma was warmed to 37°C for 10 minutes and test compound stock solution added to achieve a 5 µM solution. 500 µL of dialysis buffer was added to one side of the chamber of the device insert (Piercenet, Dialysis membrane MWCO 8000) housed within a heated Teflon block, and the incubation initiated by the addition of 300 µL of the test compound protein solution to the opposite chamber. Equilbrium was reached by shaking the device on an orbital mixer at 37°C for 4 hours. 50 µL aliquots from the buffer and the plasma chambers were transferred into separate wells of a deep well plate. 50 µL of plasma were added to the buffer samples, and 50 µL of buffer were added to the plasma samples. 300 µL of ice cold acetonitrile containing internal standard were added to precipitate the protein. Samples were then centrifuged (2700 x g at 4°C for 20 minutes) to pellet the protein and the supernatant analysed by LC-MS/MS to quantify the % input compound unbound to plasma protein with reference to a standard curve.

Stability in plasma

Pooled heparinised mouse plasma was warmed to 37°C for 10 minutes, mixed and cleared of aggregated protein by centrifugation. Aliquots of the clear supernatant were transferred into the assay plate. Following equilibration to 37°C, biotransformation was initiated by adding and mixing of 1 µM compound solution in a final incubation volume of 300 µL. 25 µL aliquots were removed at 0, 5, 15, 30, 60, and 120 minutes and quenched in 300µL ice cold acetonitrile containing internal standard. After storing the samples at -20°C for a minimum of 4 hours, the protein in the samples was precipitated by centrifugation at 4°C and the supernatants analysed by LC-MS/MS to quantify the % input test compound remaining.

Mice

The mouse was selected for animal ex vivo studies because it is the smallest known mammalian species that can be used to provide blood vessels suitable for myography and enable suitable genetic manipulation, which in this study was used to test the role of PIEZO1. The portal vein was selected as the tissue to study because our pilot studies had shown that this blood vessel has a robust response to PIEZO1 agonists that is more reliable and larger than we have observed for other blood vessels. Animal studies are reported in compliance with the ARRIVE guidelines (Kilkenny, Browne, Cuthill, Emerson & Altman, 2010; McGrath & Lilley, 2015). All animal experiments were authorised by the University of Leeds Animal Ethics Committee and the UK Home Office under the authority of the UK Home Office Project Licences P606320FB and PP8169223.

All mice were housed in GM500 individually ventilated cages (Animal Care Systems) at 21°C, 50-70% humidity and with a 12 hour alternating light/dark cycle. They had *ad libitum* access

679   to water and RM1 diet (SpecialDiet Services, Witham, UK) with bedding from Pure'o Cell
680   (Datesand, Manchester, UK). The number of cage companions was up to 5. Animals were
681   visually inspected and weighed at a minimum of weekly intervals for welfare-related
682   assessments. Local animal welfare advice and steps were taken in the rare cases of concern
683   for an animal or animals. The genetically modified mice did not display any obvious adverse
684   effects. Animals weighed 25-35 g.

685

686   Genotypes were determined by a service using real-time PCR with specific probes designed
687   for each gene (Transnetyx, Cordova, TN). C57BL/6 J mice from the University of Leeds with
688   *PIEZO1* gene flanked with LoxP sites (PIEZO1^{flox}) (Li et al., 2014) were used to generate
689   tamoxifen (TAM)-inducible disruption of the *PIEZO1* gene in the endothelium. PIEZO1$^{flox/flox}$
690   mice were crossed with mice expressing cre recombinase under the Cadherin5 promoter
691   (Tg(Cdh5-cre/ERT2)1Rha and inbred to obtain PIEZO1$^{flox/flox}$/Cdh5-cre mice (Rode et al.,
692   2017). TAM (Sigma-Aldrich) was dissolved in corn oil (Sigma-Aldrich) at 20 mg mL^{-1}. Mice
693   were injected intra-peritoneally with 75 mg kg^{-1} TAM for 5 consecutive days and studies were
694   performed 10–14 days later. PIEZO1$^{flox/flox}$/Cdh5-cre mice that received TAM injections are
695   referred to as PIEZO1$^{\Delta EC}$. PIEZO1$^{flox/flox}$ littermates (lacking Cdh5-cre) that received TAM
696   injections were the controls (control genotype). For experiments, mice were males aged 12–
697   16 weeks. Only male mice were used in order to reduce variability that might arise due to sex
698   differences and reproductive cycle. TAM injections and genotyping were performed by a
699   researcher independently from the myographer, such that the genotypes were blind to the
700   myographer. The different genotypes were studied at random as they became available,
701   depending on the genotypic spread of each litter.

702

703   The study sought to address the 3Rs by using in vitro cell-based (non-animal) technical
704   approaches as much as possible (i.e., Replacement), only using animals once the aim and
705   design of such studies was informed by the in vitro studies (i.e., Reduction).

706

707   **Myography**

708

709   Mice were anaesthetized with isoflurane (5% induction, 1.5% maintenance) in 95% O_2
710   according to Schedule 1 procedure approved by the UK Home Office. The portal vein was
711   quickly dissected and placed in Krebs solution. The Krebs PV solution consisted of (in mM):
712   118 mM NaCl, 4.7 mM KCl, 2.5 mM $CaCl_2$, 1.2 mM KH_2PO_4, 1.2 mM $MgSO_4(7H_2O)$, 25.2 mM
713    $NaHCO_3$ and 11.1 mM glucose. By means of a dissecting microscope, adhering perivascular
714   tissue was carefully removed and the vein was cut into 1-mm segments.

715

716   Vein segments were mounted onto two thin stainless-steel wires in an isometric myograph
717   (Multi Wire Myograph System 620 M from Danish Myograph Technology, DMT), for which the
718   force transducer was calibrated once per month according to the manufacturer's instructions.
719   The recording chamber was filled with gassed Krebs solution (95% O_2/5% CO_2, pH 7.4). The
720   segments were then stretched to a normalized internal diameter according to the
721   manufacturer's instructions. The mounted rings were kept in a 5 mL chamber containing Krebs
722   solution at 37°C and continuously bubbled with a gas mixture of 95% O_2 and 5% CO_2 (pH 7.4).
723   After an equilibration period of 60 minutes the contractile function of the vessel was tested by
724   replacing the Krebs solution by 60 mM K^+ solution. Following washout, the vein was contracted
725   once with 10 µM phenylephrine (PE) and then Yoda1, KC159 or KC289 was applied with the
726   concentrations of 0.1 to 10 µM. The nitric oxide synthase inhibitor, N^G-nitro-L-arginine methyl
727   ester (L-NAME, 100 µM) was pre-incubated for 20 minutes before the PIEZO1 modulator.

728

729   Since the anticipated effect of test compounds was to cause vessel relaxation, phenylephrine
730   (PE) was applied to induce tension and the maximum value of this tension was defined as 0%
731   relaxation (no relaxation). The value of tension immediately prior to application of PE was
732   defined as 100% relaxation. Data are normalised to these values because, otherwise, the

733 intrinsic variability in the absolute amount of tension induced by PE obscured exploration of
734 the relaxant effect of compounds.
735
736 **Reagents**
737
738 Unless stated otherwise, all commercially available chemicals were purchased from Sigma-
739 Aldrich. Stocks of chemicals were reconstituted in DMSO and stored at -20 °C unless stated
740 otherwise. Fura-2-AM was dissolved at 1 mM. Pluronic acid F-127 was stored at 10% (w/v) in
741 DMSO at room temperature in the dark. Yoda1 (Tocris) was stored at 10 mM. All Yoda1
742 analogues were synthesised in-house and purified (for more information, see Supporting
743 Information) and prepared as 10 mM stock solutions. (-)-Englerin A was prepared as a 10 mM
744 stock solution and stored at -80°C. PE was dissolved in distilled water to make a stock solution
745 of 100 mM. L-NAME was dissolved in distilled water to make a stock solution of 100 mM.
746
747 **Data analysis**
748
749 OriginPro 2020 (OriginLab) and Prism 9 (GraphPad) were used for all data analysis. For
750 intracellular Ca^{2+} ($Ca^{2+}i$) measurements, technical intra-experiment replicates were used to
751 improve confidence in the data. Analysis of individual experiments was performed to obtain
752 mean ± SEM values. For collated analysis of independent experiments, where normal
753 distributions were not evidenced by Shapiro-Wilk normality tests, non-parametric distributions
754 were assumed and therefore median values were used. To compare the agonistic activity of
755 Yoda1 analogues, background readings taken for the first 25 s prior to compound injection
756 were subtracted and the resulting median peak values were compared ($\Delta Ca^{2+}i$). Data
757 subjected to statistical analysis arose from at least 5 independent experiments (n=5). For
758 comparisons between two sets of paired data, Wilcoxon's signed rank tests were used. For
759 comparisons of two sets of unpaired data, two-tailed Mann-Whitney signed rank tests were
760 performed. For multiple comparisons (Figure 1D), Kruskal-Wallis ANOVA was used. Datasets
761 in Figure 10 and 10 SI 1 satisfied the Shapiro-Wilk normality test, and therefore Repeated-
762 Measure One-Way ANOVA was applied, followed by a Tukey's post-hoc test. Data for Figure
763 10 SI 1Aii were not normally distributed, and so a Friedmann test for paired non-parametric
764 data followed by a Dunn's post-hoc test was applied. $p < 0.05$ was deemed significant
765 throughout. EC_{50} estimates from appropriately saturating concentration-response curves were
766 fitted with a standard Hill-equation (Hill1 function in OriginPro 2020 software).
767
768 DataControl 384 (Nanion Technologies GmbH), Prism 9 (GraphPad) and OriginPro 2020
769 (OriginLab) were used for all analysis of automated patch clamp data. For manual and
770 automated patch-clamp data, N represents the number of cells recorded from successfully in
771 each experimental condition, sampled from 2 to 6 batches of cells or 384-well chips in
772 automated patch-clamp. For manual patch-clamp experiments, each cell/patch recording (N)
773 is considered as an independent experiment because each was made independently at a
774 separate time, using a separate coverslip of cells and using a separate patch pipette. In some
775 instances, more than one such independent recording was made from the same batch of
776 cultured/ transfected cells. These N values are considered as independent. Each cell was
777 studied alone and from a separate cover slip in the case for manual patch-clamp. To estimate
778 the EC_{50} values of the agonists in automated patch-clamp studies, the peak current in the
779 presence of the agonist was normalized to the peak current in the presence of the reference
780 solution. Single-point concentration response curves were fitted with a standard Hill equation
781 to estimate EC_{50} values. $p < 0.05$ was deemed significant. For automated patch-clamp
782 experiments we included some data for n<5 (Figure 7A, B). We did not apply a statistical test.
783 We suggest that the results are, nevertheless, useful because of the high number of
784 independent replicates per experiment (i.e., separate recordings from separate wells in each
785 recording chip, which are referred to as N). Such replicates are a feature of, and a rationale
786 for, this automated technology, which is an innovation for the type of research shown here but
787 already commonly used in the pharmaceutical industry for other ion channel studies to

788 increase throughput and avoid waste from large volumes of independent cell cultures and
789 minimise cost from expensive specially engineered plates. As a general strategy, our study
790 used multiple independent technical approaches to address the same or similar questions.
791 These multiple approaches include Ca^{2+} measurement, patch-clamp and vascular contraction
792 assays. In this way, the overall conclusions do not rely on a single approach such as
793 automated patch-clamp.

795 OriginPro 2020 was used for the analysis of myography data. Myography traces show
796 readings taken every 0.5 or 1 s, smoothed with the Savitzky-Golay filter set to 70 points. To
797 compare the agonistic activity of Yoda1 analogues, basal vessel tension prior to compound
798 injection was subtracted. Maximal tension in the presence of phenylephrine (PE) alone was
799 used to define 0% relaxation. The tension value prior to PE application was defined as 100%
800 relaxation. Following the addition of test compounds, tension readings were taken at the last
801 time point of the treatments and expressed as percentage relaxation.

803 Group sizes were not always equal because we did more experiments with analogues that
804 were most active or newest. We have fully represented what we did rather than excluding
805 data. While our target was 5, our observation of unexpected variability in effects of some
806 compounds caused us to increase the number in some cases in an effort to increase the
807 robustness of our conclusions.

809 Statistical analysis was undertaken only for studies where each group size was at least n=5.
810 Group size is the number of independent values. Statistical analysis was done using these
811 independent values (i.e., not treating technical replicates as independent values).

813 For multigroup studies with parametric variables, post hoc tests were conducted only if F in
814 ANOVA (or equivalent) achieved the chosen necessary level of statistical significance and
815 there was no significant variance inhomogeneity.

817 Potential outlier data points were retained in data analysis and presentation.

819 The identities of compounds and cell lines were not blinded to investigators. This is a limitation
820 of the study that may have introduced bias.

822 The work complies with BJP's recommendations and requirements on experimental design
823 and analysis (Curtis et al., 2018). A separate "Compliance with BJP Declaration of
824 Transparency and Scientific Rigour" document is provided. A separate data transparency
825 spreadsheet document is provided containing all data.

827 **Nomenclature of targets and ligands**

829 Key protein targets and ligands in this article are hyperlinked to corresponding entries in
830 http://www.guidetopharmacology.org, and are permanently archived in the Concise Guide to
831 PHARMACOLOGY 2021/22 (Alexander et al., 2021).

834 **RESULTS**

836 **4-benzoic acid substitution in Yoda1 improves PIEZO agonism**

838 We replaced the pyrazine ring of Yoda1 with a 2-, 3- or 4- benzoic acid group (**KC157,** 2-
839 benzoic acid; **KC158,** 3-benzoic acid; **KC159**, 4-benzoic acid), a 3- or 4- benzamide group
840 (**KC162**, 3-benzamide; **KC161,** 4-benzamide) or a potassium salt of the 4-benzoic acid
841 (**KC289**) (Figure 1A). Each analogue was tested for its ability to evoke intracellular calcium
842 ion (Ca^{2+}_i) elevation in cells overexpressing human PIEZO1, compared directly with Yoda1 at

843 the same concentration of 10 μM (Figure 1B and 1C). **KC159** and **KC289** evoke robust
844 responses that are larger than those of Yoda1 (Figure 1B-D). The other analogues fail to evoke
845 responses (Figure 1B and 1C). Yoda1, **KC159** and **KC289** fail to evoke responses in a similar
846 cell line that expressed TRPC5 Ca^{2+}-permeable cation channel in place of PIEZO1, suggesting
847 that Ca^{2+} signals need PIEZO1 (Figure 1 SI 1). The selectivity of 5 μM **KC289** was further
848 investigated via Eurofins' Hit Profiling Screen PP70 to obtain binding data for 30 proteins
849 including ion channels and receptors (SI Table 1). There is modest interaction with Adenosine
850 A2A and Prostanoid EP4 receptors and little or no binding to others (SI Table 1). The data
851 suggest that the 4-benzoic acid analogue (**KC159**) and its potassium salt (**KC289**) are PIEZO1
852 agonists.

4-benzoic acid substitution improves physico-chemical properties

856 Physico-chemical properties are important in physiological assays and therapeutics. Kinetic
857 and thermodynamic solubility assays conducted by Malvern PanAnalytical were used to
858 assess aqueous solubility and other properties. In both, **KC159** and **KC289** showed better
859 solubility than Yoda1 in phosphate-buffered saline at physiological pH (SI Table 2). Our in-
860 house solubility data suggested that **KC159** and **KC289** are at least 160 times more soluble
861 in aqueous buffer than Yoda1 (Figure 1 SI 2). A microsomal stability assay performed by
862 Malvern PanAnalytical yielded half-lives of 29.6 and 24.6 min, at least 20 times longer than for
863 Yoda1 (SI Table 2). The fractions of **KC159** and **KC289** bound to plasma proteins are
864 relatively high (99.4 and 99.35 %) but are lower than that of Yoda1 (SI Table 2). A plasma
865 stability assay indicated good stability over 2 hours for Yoda1, **KC159** and **KC289** (SI Table
866 2). The data suggest that key physico-chemical properties are better in **KC159** and **KC289**
867 than Yoda1.

4-benzoic acid substitution improves concentration-response data for human PIEZO1

871 Because of the potential advantages, we investigated **KC159** and **KC289** in more detail. We
872 first attempted to construct concentration-response curves using cells overexpressing human
873 PIEZO1, comparing the effects of Yoda1, **KC159** and **KC289** at concentrations up to 30 μM
874 in Ca^{2+} assays. Yoda1 causes concentration-dependent increases in intracellular Ca^{2+} but a
875 saturating effect is not observed at the highest concentration and its effects are highly variable
876 (Figure 2A and 2B, Figure 2 SI 1). **KC159** and **KC289** also do not produce saturating effects
877 but a saturating inflection point occurs at 10 μM **KC289**, suggesting that a maximum is
878 approached at approximately 30 μM. The effects of **KC159** and **KC289** are less variable than
879 those of Yoda1, particularly at high concentrations (Figure 2A and 2B, Figure 2 SI 1). We
880 performed similar experiments with human umbilical vein endothelial cells (HUVECs), which
881 are a physiologically relevant cell type that endogenously expresses PIEZO1. Again, the
882 effects of Yoda1 are the most variable and in this cell system saturating inflection points occur
883 at 3 - 10 μM for both **KC159** and **KC289** (Figure 2C and 2D, Figure 2 SI 1). Estimated
884 concentrations for 50% effect (EC_{50}s) for **KC159** and **KC289** are 2.28 μM and 1.14 μM
885 respectively (Figure 2D). The data suggest that **KC159** and **KC289** provide more consistency
886 than Yoda1 in concentration-response studies.

4-benzoic acid substitution improves efficacy and potency at mouse PIEZO1

890 Previous work suggested that Yoda1 is more potent at mouse compared with human PIEZO1
891 (Blythe et al., 2019; Evans et al., 2018; Syeda et al., 2015). We therefore studied cells
892 overexpressing mouse PIEZO1. As with human PIEZO1, **KC159** and **KC289** evoke larger
893 responses than Yoda1 and **KC157** is inactive (Figure 3A and 3B). **KC158**, **KC161** and **KC162**
894 exhibit agonist effects in the mouse PIEZO1 overexpression system, although their effects are
895 slower to develop and smaller than those of Yoda1 (Figure 3A and 3B). Concentration-
896 response curves were generated in parallel to directly compare Yoda1, **KC159** and **KC289**.

897   Similar to human PIEZO1, the responses to **KC159** and **KC289** are less variable than those
898   to Yoda1 (Figure 4A and 4B, Figure 4 SI1). In contrast to human PIEZO1, all compounds
899   produce effects that are saturating or approaching saturation at the highest concentrations
900   tested (Figure 4A and 4B). Therefore, EC_{50}s were compared by fitting Hill equations (Figure
901   4C). EC_{50}s are 0.6 μM (Yoda1), 0.28 μM (**KC159**) and 0.15 μM (**KC289**). The data suggest
902   that **KC159** and **KC289** are more efficacious and potent than Yoda1 at mouse PIEZO1 with a
903   rank order of potency of **KC289**>**KC159**>Yoda1. **KC289** is approximately 4 times more potent
904   than Yoda1.

906   **Agonism is confirmed by manual patch-clamp**

908   An important technique in ion channel studies is manual patch-clamp. Its throughput is limited
909   and so we focused on a comparison of Yoda1 and **KC159** in cells overexpressing mouse
910   PIEZO1. Mechanical stimulus due to fluid flow through the recording chamber causes a small
911   current in PIEZO1-expressing but not control (i.e., null) cells that lacked transfection with
912   PIEZO1 (Figure 5A-C i *cf* ii and iii). **KC159** increases current in PIEZO1-expressing but not
913   null cells, seen as outward current at positive voltages and inward current at negative voltages,
914   with reversal near 0 mV as expected for PIEZO1 currents (Figure 5B-Ci, iii). The effect is
915   similar to that of Yoda1 (Figure 5B-Cii). Current reaches a peak and then declines to a plateau
916   in the continuous presence of **KC159** or Yoda1 (Figure 5B-Cii, iii). The plateau current
917   disappears when **KC159** or Yoda1 is washed from the chamber (Figure 5B-Cii, iii). The
918   application of DMSO only (the solvent for Yoda1 and KC159) evoked no change in current in
919   6 independent recordings from cells overexpressing mouse PIEZO1. The data further suggest
920   that **KC159** is an agonist of PIEZO1. They suggest that the responses to a single high
921   concentration are similar to those of Yoda1.

923   **Improved agonism is confirmed by high throughput patch-clamp**

925   For comparative electrophysiological studies, we performed high-throughput automated
926   patch-clamp on cells overexpressing human or mouse PIEZO1 in comparison to null cells that
927   lacked the overexpression of PIEZO1. Mechanical stimulation alone (M-Stim only) was caused
928   by fluid flow from the compound application pipette, which we expected would cause shear
929   stress on the cells and possibly also a compression force. M-Stim only elicits small transient
930   inward currents at the holding potential of -80 mV in both human and mouse PIEZO1 cells
931   (Figure 6A-E). Inclusion of 10 μM **KC159** greatly amplifies the currents (Figure 6A-E). In
932   mouse PIEZO1 cells, the currents show a sustained component that is 26±8 % (mean ±
933   standard deviation) of the peak current amplitude, which is not seen in human PIEZO1 cells
934   (-4±2% of peak current) (Figure 6B, Figure 6 SI 1). There are little or no responses in empty
935   cells (Figure 6C-E). **KC157** mostly fails to evoke responses (Figure 6D, Figure 6 SI 1).

937   We next performed paired comparisons with Yoda1. **KC159** causes more cells to respond
938   compared with Yoda1, most notably for mouse PIEZO1 (Figure 7A and B). **KC157** is largely
939   ineffective (Figure 7A and B). Yoda1 responses are highly variable and concentration-
940   dependence is lacking (Figure 7C and 7D). **KC159** elicits concentration-dependent increases
941   in current in human and mouse PIEZO1 cells (Figure 7E and 7F). Maximum responses are
942   not certain and so EC_{50}s are only estimates at 1.67 and 1.54 μM for human and mouse
943   respectively. The data suggest that **KC159** is more reliable and effective as a PIEZO1 agonist
944   than Yoda1 and more effective at mouse compared with human PIEZO1.

946   **KC159 and KC289 relax the mouse portal vein**

948   Previous studies have suggested that PIEZO1 channels signal to endothelial nitric oxide
949   synthase (NOS3) to generate nitric oxide (NO) and thereby cause endothelium-dependent
950   blood vessel relaxation (Beech & Kalli, 2019). We used this effect to investigate **KC159** and
951   **KC289** in a physiological assay. The portal vein was studied because of evidence that PIEZO1

952 is important in the hepatic circulation (Caolo et al., 2020; Hilscher et al., 2019; Li et al., 2014;
953 Rode et al., 2017). Vessel wall tension was recorded ex vivo using wire myography and
954 smooth muscle contraction was evoked by the α_1-adrenoceptor agonist phenylephrine (PE)
955 so that endothelium-dependent relaxation could be observed (e.g., Figure 8A). Yoda1, **KC159**
956 and **KC289** cause concentration-dependent relaxation (Figure 8A). **KC159** and **KC289**
957 concentration-response curves reach saturation, thus enabling calculation of EC$_{50}$s of 1.14
958 µM and 1.20 µM respectively (Figure 8A). Yoda1 effects are more variable and no saturation
959 occurs (Figure 8A). The data suggest that **KC159** and **KC289** are suitable for use in a
960 physiological assay and are an improvement on Yoda1.

KC289-evoked relaxation is NO dependent

964 To investigate if **KC289** causes relaxation via NOS3 we incubated portal vein with N^G-Nitro- l-
965 Arginine Methyl Ester (L-NAME), which is a substrate inhibitor of NOS3. L-NAME abolishes
966 the relaxant effect of **KC289** (Figure 8B). Effects of L-NAME in the absence of **KC289** are
967 shown in Figure 8 SI 1. We had technical difficulty removing endothelium from portal vein
968 without damaging the smooth muscle layer and so we could not test the endothelium-
969 dependence of the KC289 response. The data suggest that **KC289** acts to stimulate NOS3
970 and NO production, as expected for a PIEZO1 agonist.

KC289-evoked relaxation is endothelial PIEZO1 dependent

974 To determine the role of endothelial PIEZO1 in **KC289** responses we compared portal vein of
975 control mice with that of matched mice in which endothelial PIEZO1 expression was
976 conditionally deleted at the adult stage (PIEZO1$^{\Delta EC}$), as previously described (Caolo et al.,
977 2020; Rode et al., 2017). **KC289**-evoked relaxation is inhibited by endothelial PIEZO1 deletion
978 and a contractile response often becomes evident at 10 µM (Figure 8C). Variable spontaneous
979 oscillatory contractions occurred in these experiments, regardless of PIEZO1 deletion. This
980 may explain the wide variability in the overall data and response to KC289. For transparency,
981 all original traces are provided (Figure 8 SI 2). The mechanism of the contractile effect of
982 KC289 was not investigated but it may relate to PIEZO1 expressed in smooth muscle cells or
983 another cell type of the vessel.

KC289-evoked relaxation is inhibited by Dooku1

987 Dooku1 is an analogue of Yoda1 that antagonises the action of Yoda1 (Evans et al., 2018).
988 Pre-incubation with 10 µM Dooku1 reduces relaxations evoked by **KC159** and **KC289** (Figure
989 8 SI 3). Dooku1 also consistently inhibits the PE response (Figure 8 SI 3), as previously
990 reported in studies of mouse aorta (Evans et al., 2018). The data suggest that **KC159** and
991 **KC289** cause relaxation via a site that is the same as the one mediating effects of Yoda1.

Effects of 3- and 4-benzamide and 3-benzoic acid analogues

995 In view of the effect of Dooku1 described above, we tested if there are inhibitory actions of the
996 new Yoda1 analogues by pre-treating cells at 10 µM for 30 minutes prior to adding 2 µM Yoda1
997 (Figure 9 and Figure 9 SI 1). All except **KC157** and **KC161** inhibit the action of Yoda1 on
998 human PIEZO1 (Figure 9A, Figure 9 SI 1). Only **KC157** fails to inhibit the action of Yoda1 on
999 mouse PIEZO1 (Figure 9B, Figure 9 SI 1). **KC159** and **KC289** are agonists and so they may
1000 inhibit the effect of Yoda1 simply by pre-activating the channels. **KC158**, **KC161** and **KC162**
1001 are also agonists of mouse PIEZO1 (Figure 3). **KC158** and **KC162** appear to inhibit the Yoda1
1002 response without pre-activating human PIEZO1 (Figure 9A, Figure 9 SI 1, Figure 1B and 1C)
1003 but we noticed an elevated baseline Ca^{2+} signal for **KC161** and **KC162** in the pre-incubation
1004 protocol, suggesting that these compounds are actually slowly acting mild agonists (Figure 9
1005 SI 2). The data suggest that 3-benzamide (**KC162**), 4-benzamide (**KC161**) and 3-benzoic acid

(**KC158**) analogues are mild, slowly acting, agonists that may also inhibit the effect of Yoda1, as if they are partial agonists. Only the 2-benzoic acid analogue (**KC157**) lacks agonist or antagonist properties.

Relationship to PIEZO2

Yoda1 was discovered in a chemical screen of HEK 293 cells overexpressing mouse PIEZO1 and mouse PIEZO2 but Yoda1 was subsequently found not to activate mouse PIEZO2 overexpressed alone (Syeda et al., 2015). To investigate **KC159** and **KC289** in relation to PIEZO2 we compared HEK 293 cells overexpressing mouse PIEZO1, mouse PIEZO2 or neither ("non-transfected cells") (Figure 10, Figure 10 SI 1, Figure 10 SI 2). Ca^{2+} elevations evoked by **KC159** or **KC289** in HEK 293 cells overexpressing mouse PIEZO2 are not different from background signals in non-transfected cells and contrast with the larger responses when mouse PIEZO1 is overexpressed (Figure 10A). The background signals may have been due to endogenous human PIEZO1 channels of these HEK 293 cells (Dubin et al., 2017). To investigate the relevance to native PIEZO2, we studied HeLa cells because they natively express PIEZO2 (TheHumanProteinAtlas, 2022). Yoda1, **KC159** and **KC289** evoked Ca^{2+} elevations in HeLa cells (Figure 10B). To determine the relevance to PIEZO2, we used RNA interference to deplete its expression (Figure 10 SI 2). There is PIEZO1 in HeLa cells (Geng et al., 2020) and so we depleted its expression too (Figure 10 SI 2). PIEZO2 depletion partially suppresses responses to **KC159**, **KC289** and Yoda1, but with greater effect on responses to **KC159** and **KC289** (Figure 10B). Responses to Yoda1, **KC159** and **KC289** are all partly suppressed by PIEZO1 depletion (Figure 10B). Depletion of PIEZO1 and PIEZO2 further suppresses the responses (Figure 10B). The data suggest that like Yoda1, **KC159** and **KC289** are not agonists of overexpressed mouse PIEZO2 but may agonise native human PIEZO2, at least when it is natively coexpressed with PIEZO1.

DISCUSSION AND CONCLUSIONS

In this study, we modified Yoda1 with the aim of improving capability for PIEZO1 modulation in physiological settings. Our data suggest that modification of Yoda1's pyrazine moiety is a route to better agonism and physico-chemical properties. Specifically, benzoic acid substitution with carboxylate is beneficial, with the 4-position being critical. Substitution at the 2-position generates an inactive compound while the 3-position leads to inferior agonism. The 2-position analogue can serve as a negative control comparator compound. When there is 4-benzamide instead of 4-benzoic acid, there is weak or no agonism. Since 4-benzoic acid and 4-benzamide occupy a similar molecular volume, it may be the neutral charge of 4-benzamide at physiological pH that impairs agonism. The potassium salt of the 4-benzoic acid analogue (**KC289**) is superior to the analogue itself (**KC159**). Its improved aqueous solubility is likely to be a factor in this. **KC159** and **KC289** are nevertheless both advances on Yoda1 in PIEZO1 agonism.

An important next step would be determination of a binding site or binding sites for Yoda1, **KC159** and **KC289**, particularly if such a site or sites could be characterised at atomic resolution. There could then be better rational design and understanding of PIEZO1 modulators. Surface plasmon resonance studies suggest binding of Yoda1 between residues 1 and 2190 of mouse PIEZO1 (in total it comprises 2547 residues) (Wang et al., 2018). Computer simulations have suggested a pocket away from the C-terminal region of the central ion pore and mutagenesis data point to importance of residues such as alanine at position 1718 (Botello-Smith et al., 2019). **KC289** could help future structural determination studies by enabling incubation of PIEZO1 with a higher concentration of compound and perhaps conferring stronger binding. Our data suggest greater effect and potency of **KC159** and **KC289** at mouse compared with human PIEZO1, so mouse PIEZO1 may be the most promising route to binding site determination. Moreover, comparisons of mouse and human sequences could indicate what is optimal for binding and efficacy. However, we suggest caution in such

1061 inferences because the expression of mouse PIEZO1 may have been better than human
1062 PIEZO1 in our studies, possibly creating an impression of greater efficacy and sensitivity
1063 through greater receptor reserve.

1064

1065 Various factors can explain differences in apparent efficacy and potency. In addition to
1066 receptor reserve, aqueous solubility could be important. Our estimates suggest aqueous
1067 solubility of Yoda1 only up to the low μM range. We used it up to 30 μM and other groups
1068 report use of higher concentrations. Inclusion of a solvent such as dimethylsulphoxide in the
1069 buffer (as we did) may aid solubility but partial precipitation could still occur and potentially
1070 explain variability in Yoda1 effects. **KC159** and **KC289** have better aqueous solubility and so
1071 this may be why they show less variability in effect. Another factor explaining differences in
1072 apparent efficacy and potency could be complexity in the transduction pathway between
1073 channel activation and effect. When tested against over-expressed mouse PIEZO1 in Ca^{2+}
1074 assays, the EC$_{50}$s for **KC289** and **KC159** were 0.15 and 0.28 μM, whereas in mouse portal
1075 vein relaxation, the EC$_{50}$s were 1.2 and 1.14 μM. The portal vein effects occur via PIEZO1, so
1076 a high concentration of compound may be required to overcome non-linearity in the signalling.

1077

1078 The EC$_{50}$ we report for Yoda1 is lower (i.e., 'better') than that reported in some other studies
1079 (Lacroix, Botello-Smith & Luo, 2018; Syeda et al., 2015). There could be several reasons,
1080 including different channel expression levels and experiment conditions, but we note that we
1081 found considerable variability in the effect of Yoda1, such that we also sometimes observed
1082 high EC$_{50}$s in individual experiments. We suggest that such differences may arise due to the
1083 limited aqueous solubility of Yoda1 at concentrations relevant to EC$_{50}$ determination, causing
1084 Yoda1 to variably precipitate out of solution. In support of this hypothesis, our new more
1085 soluble analogues had less variable effects.

1086

1087 Manual patch-clamp enables comparisons of the efficacy and potency of compounds but its
1088 utility is restricted by the low throughput of recording from one cell at a time. Therefore, we
1089 explored automated patch-clamp technology, which has the potential to increase throughput
1090 greatly. The arising data support our findings from 96-well Ca^{2+} measurements by suggesting
1091 that **KC159** has advantages over Yoda1 and that **KC157** (the 2-position analogue) is inactive.
1092 Differences between mouse and human PIEZO1 are again evident. In this regard, we
1093 observed an intriguing sustained response of mouse but not human PIEZO1. In these
1094 experiments, there was a rapid small-volume application of compound followed by rapid
1095 retraction of double the volume. Reversal of the **KC159** effect occurs after washout in manual
1096 patch recordings, but these recordings were on a slower timescale. We speculate that the
1097 rapid retraction in the automated system insufficiently removes **KC159** in the short timeframe
1098 of the recordings, leaving residual compound at low concentration. This low concentration may
1099 cause the sustained current evident in mouse but not human PIEZO1 because **KC159** has
1100 apparent great efficacy and potency at mouse PIEZO1. This hypothesis is supported by failure
1101 to observe sustained current when applying Yoda1, which is less effective than **KC159**.

1102

1103 A limitation of our efficacy comparison of Figure 3 is that the effects of the various analogues
1104 may not have been compared at equal saturation for all compounds. This is challenging to
1105 overcome because of the limited aqueous solubility of this series of compounds, despite our
1106 improvements. Therefore, we cannot exclude that some of the compounds would be more
1107 effective if tested at higher concentrations, if they were to be retained in aqueous solution.

1108

1109 Yoda1, **KC159** and **KC289** are tool compounds for laboratory and potentially in vivo animal
1110 studies aimed at determining functions of PIEZO1 and informing potential drug discovery
1111 projects. We do not yet know if they have therapeutic relevance or suitability (e.g., distribution
1112 and safety features) for use in humans. Nevertheless, there is potential clinical value. A
1113 disease area to consider is malaria because gain-of-function mutation in PIEZO1 is associated
1114 with protection against malaria (Ma et al., 2018) and so this effect might be mimicked by a

PIEZO1 agonist acting on wild-type PIEZO1. Another area to consider is lymphoedema because loss-of-function mutations in PIEZO1 are associated with generalized lymphatic dysplasia (Fotiou et al., 2015) and so PIEZO1 agonism might be beneficial if partially functional channels are still available.

Despite Yoda1's value and apparent selectivity, its use at relatively high concentrations could make it especially vulnerable to as-yet unknown off-target effects. Moreover, **KC159** and **KC289** are analogues of Yoda1 but they are not the same chemicals and may not have the same selectivity profile. We provide evidence for their selectivity: there is small or no activation of Ca^{2+} or electrophysiological signals in control (null) HEK 293 cells without PIEZO1 overexpression; they do not activate mouse PIEZO2 or human TRPC5 overexpressed in HEK 293 cells; genetic disruption of PIEZO1 inhibits vasorelaxation; and a commercial selectivity screen suggests little or no binding to a range of other proteins other than potential modest effects on A2A and EP4 receptors (SI Table 1). We did not further investigate the relevance of the latter receptors but the strong inhibitory effect of genetic disruption of PIEZO1 on the effect of KC289 suggests that PIEZO1-independent effects do not contribute, or are minor contributors, in portal vein.

Although **KC159** and **KC289** did not activate overexpressed mouse PIEZO2 channels, knockdown of native human PIEZO2 in HeLa cells partially inhibited responses to **KC159** and **KC289**. These data suggest that the new Yoda1 analogues (such as KC289) may have the ability to activate PIEZO2 channels in a species- or context- dependent manner. This warrants further investigation using electrophysiological approaches and overexpressed human PIEZO2 because there are currently limited possibilities for chemically modulating PIEZO2 channels. Although PIEZO2 siRNA (siPIEZO2) has no significant effect on PIEZO1 mRNA abundance, there is a visual impression of a potential small off-target effect on PIEZO1 (Figure 10 SI 1B). This does not detract from the observation that siPIEZO2 is more effective against responses evoked by **KC159** and **KC289** than Yoda1 (Figure 10B). Therefore, we cautiously suggest that some Yoda1 analogues may cross over to PIEZO2 and thereby provide a route to PIEZO2 agonism.

In conclusion, this study supports the idea that Yoda1 provides a template for developing a series of useful PIEZO1 modulators. The structure-activity requirements are quite strict and seem to be relatively inflexible at the 2,6-dichlorophenyl moiety (Evans et al., 2018) but our data suggest better opportunity at the pyrazine moiety. Here we show value of 4-benzoic acid substitution and improvement on Yoda1 for PIEZO1 agonism in terms of efficacy, potency and physico-chemical properties (e.g., aqueous solubility). We suggest calling the potassium salt of this analogue (i.e., KC289) Yoda2 and propose its potential value as a tool compound in physiological assays and for facilitating efforts to identify a binding site. In addition, we suggest consideration of Yoda2 or a variant thereof in disease conditions such malaria and lymphoedema.

REFERENCES

Akbulut Y, Gaunt HJ, Muraki K, Ludlow MJ, Amer MS, Bruns A*, et al.* (2015). (-)-Englerin A is a potent and selective activator of TRPC4 and TRPC5 calcium channels. Angew Chem Int Ed Engl 54**:** 3787-3791.

Alexander SP, Mathie A, Peters JA, Veale EL, Striessnig J, Kelly E*, et al.* (2021). THE CONCISE GUIDE TO PHARMACOLOGY 2021/22: Ion channels. Br J Pharmacol 178 Suppl 1**:** S157-S245.

Beech DJ, & Kalli AC (2019). Force Sensing by Piezo Channels in Cardiovascular Health and Disease. Arterioscler Thromb Vasc Biol 39**:** 2228-2239.

Blythe NM, Muraki K, Ludlow MJ, Stylianidis V, Gilbert HTJ, Evans EL*, et al.* (2019). Mechanically activated Piezo1 channels of cardiac fibroblasts stimulate p38 mitogen-activated protein kinase activity and interleukin-6 secretion. J Biol Chem 294**:** 17395-17408.

Botello-Smith WM, Jiang W, Zhang H, Ozkan AD, Lin YC, Pham CN*, et al.* (2019). A mechanism for the activation of the mechanosensitive Piezo1 channel by the small molecule Yoda1. Nat Commun 10**:** 4503.

Caolo V, Debant M, Endesh N, Futers TS, Lichtenstein L, Bartoli F*, et al.* (2020). Shear stress activates ADAM10 sheddase to regulate Notch1 via the Piezo1 force sensor in endothelial cells. Elife 9.

Coste B, Mathur J, Schmidt M, Earley TJ, Ranade S, Petrus MJ*, et al.* (2010). Piezo1 and Piezo2 are essential components of distinct mechanically activated cation channels. Science 330**:** 55-60.

Coste B, Murthy SE, Mathur J, Schmidt M, Mechioukhi Y, Delmas P*, et al.* (2015). Piezo1 ion channel pore properties are dictated by C-terminal region. Nat Commun 6**:** 7223.

Curtis MJ, Alexander S, Cirino G, Docherty JR, George CH, Giembycz MA*, et al.* (2018). Experimental design and analysis and their reporting II: updated and simplified guidance for authors and peer reviewers. Br J Pharmacol 175**:** 987-993.

De Vecchis D, Beech DJ, & Kalli AC (2021). Molecular dynamics simulations of Piezo1 channel opening by increases in membrane tension. Biophys J 120**:** 1510-1521.

Dubin AE, Murthy S, Lewis AH, Brosse L, Cahalan SM, Grandl J*, et al.* (2017). Endogenous Piezo1 Can Confound Mechanically Activated Channel Identification and Characterization. Neuron 94**:** 266-270 e263.

Evans EL, Cuthbertson K, Endesh N, Rode B, Blythe NM, Hyman AJ*, et al.* (2018). Yoda1 analogue (Dooku1) which antagonizes Yoda1-evoked activation of Piezo1 and aortic relaxation. Br J Pharmacol 175**:** 1744-1759.

Fotiou E, Martin-Almedina S, Simpson MA, Lin S, Gordon K, Brice G*, et al.* (2015). Novel mutations in PIEZO1 cause an autosomal recessive generalized lymphatic dysplasia with non-immune hydrops fetalis. Nat Commun 6**:** 8085.

Fukaya E, Flores AM, Lindholm D, Gustafsson S, Zanetti D, Ingelsson E*, et al.* (2018). Clinical and Genetic Determinants of Varicose Veins. Circulation 138**:** 2869-2880.

Geng J, Liu W, Zhou H, Zhang T, Wang L, Zhang M*, et al.* (2020). A Plug-and-Latch Mechanism for Gating the Mechanosensitive Piezo Channel. Neuron 106**:** 438-451 e436.

Guo YR, & MacKinnon R (2017). Structure-based membrane dome mechanism for Piezo mechanosensitivity. Elife 6.

Hilscher MB, Sehrawat T, Arab JP, Zeng Z, Gao J, Liu M*, et al.* (2019). Mechanical Stretch Increases Expression of CXCL1 in Liver Sinusoidal Endothelial Cells to Recruit Neutrophils, Generate Sinusoidal Microthombi, and Promote Portal Hypertension. Gastroenterology 157**:** 193-209 e199.

Jiang Y, Yang X, Jiang J, & Xiao B (2021). Structural Designs and Mechanogating Mechanisms of the Mechanosensitive Piezo Channels. Trends Biochem Sci 46**:** 472-488.

Kilkenny C, Browne W, Cuthill IC, Emerson M, & Altman DG (2010). Animal research: Reporting in vivo experiments: The ARRIVE guidelines. British Journal of Pharmacology 160**:** 1577-1579.

Lacroix JJ, Botello-Smith WM, & Luo Y (2018). Probing the gating mechanism of the mechanosensitive channel Piezo1 with the small molecule Yoda1. Nat Commun 9**:** 2029.

Li H, Xiong J, Yan W, O'Brien C, & Schuller de Almeida M (2021). PIEZO1 agonists for the promotion of bone formation. International Patent Application WO 2021/067943 A1.

Li J, Hou B, Tumova S, Muraki K, Bruns A, Ludlow MJ*, et al.* (2014). Piezo1 integration of vascular architecture with physiological force. Nature 515**:** 279-282.

Ma S, Cahalan S, LaMonte G, Grubaugh ND, Zeng W, Murthy SE*, et al.* (2018). Common PIEZO1 Allele in African Populations Causes RBC Dehydration and Attenuates Plasmodium Infection. Cell 173**:** 443-455 e412.

McGrath JC, & Lilley E (2015). Implementing guidelines on reporting research using animals (ARRIVE etc.): new requirements for publication in BJP. British Journal of Pharmacology 172**:** 3189-3193.

Murthy SE, Dubin AE, & Patapoutian A (2017). Piezos thrive under pressure: mechanically activated ion channels in health and disease. Nat Rev Mol Cell Biol 18**:** 771-783.

Obergrussberger A, Goetze TA, Brinkwirth N, Becker N, Friis S, Rapedius M*, et al.* (2018). An update on the advancing high-throughput screening techniques for patch clamp-based ion channel screens: implications for drug discovery. Expert Opin Drug Discov 13**:** 269-277.

Obergrussberger A, Haarmann C, Rinke I, Becker N, Guinot D, Brueggemann A*, et al.* (2014). Automated Patch Clamp Analysis of nAChalpha7 and Na(V)1.7 Channels. Curr Protoc Pharmacol 65**:** 11 13 11-48.

Rode B, Shi J, Endesh N, Drinkhill MJ, Webster PJ, Lotteau SJ*, et al.* (2017). Piezo1 channels sense whole body physical activity to reset cardiovascular homeostasis and enhance performance. Nat Commun 8**:** 350.

Solis AG, Bielecki P, Steach HR, Sharma L, Harman CCD, Yun S*, et al.* (2019). Mechanosensation of cyclical force by PIEZO1 is essential for innate immunity. Nature 573**:** 69-74.

Syeda R, Xu J, Dubin AE, Coste B, Mathur J, Huynh T*, et al.* (2015). Chemical activation of the mechanotransduction channel Piezo1. Elife 4.

TheHumanProteinAtlas (2022). PIEZO2. Human Protein Atlas https://www.proteinatlas.org/ENSG00000154864-PIEZO2/cell+line.

Wang S, Chennupati R, Kaur H, Iring A, Wettschureck N, & Offermanns S (2016). Endothelial cation channel PIEZO1 controls blood pressure by mediating flow-induced ATP release. J Clin Invest 126**:** 4527-4536.

Wang Y, Chi S, Guo H, Li G, Wang L, Zhao Q*, et al.* (2018). A lever-like transduction pathway for long-distance chemical- and mechano-gating of the mechanosensitive Piezo1 channel. Nat Commun 9**:** 1300.

1280 Yang X, Lin C, Chen X, Li S, Li X, & Xiao B (2022). Structure deformation and curvature
1281 sensing of PIEZO1 in lipid membranes. Nature 604**:** 377-383.

1283 Young M, Lewis AH, & Grandl J (2022). Physics of mechanotransduction by Piezo ion
1284 channels. J Gen Physiol 154.

1286 Zarychanski R, Schulz VP, Houston BL, Maksimova Y, Houston DS, Smith B*, et al.* (2012).
1287 Mutations in the mechanotransduction protein PIEZO1 are associated with hereditary
1288 xerocytosis. Blood 120**:** 1908-1915.

1290 Zeng F, Xu SZ, Jackson PK, McHugh D, Kumar B, Fountain SJ*, et al.* (2004). Human TRPC5
1291 channel activated by a multiplicity of signals in a single cell. J Physiol 559**:** 739-750.
1292
1293
1294

Figure 1
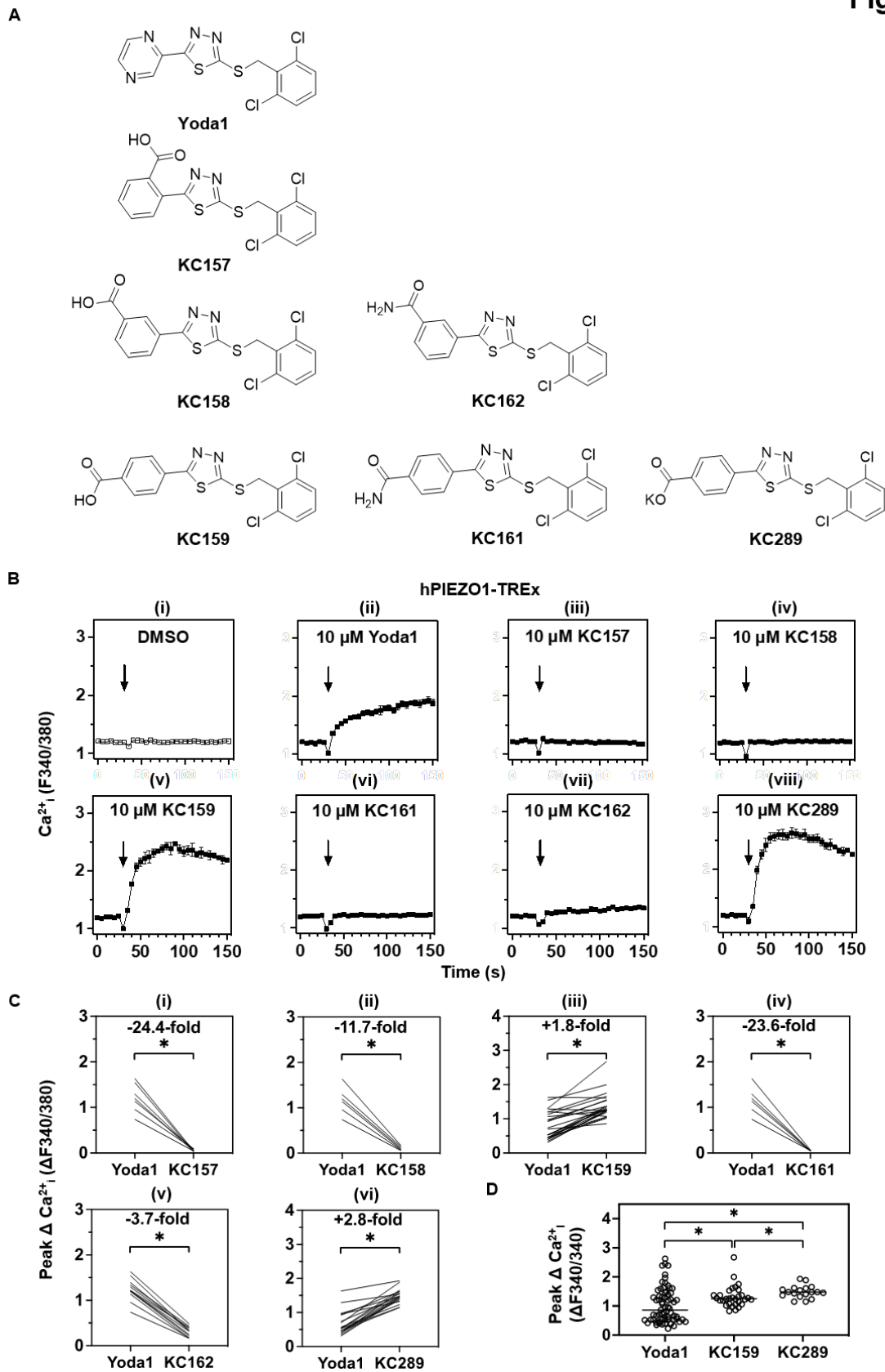
Figure 1. Yoda1 analogues and their effects on human PIEZO1

1298 (A) Structures of Yoda1 and analogues in which the pyrazine moiety has been altered. **KC157,**
1299 2-benzoic acid; **KC158,** 3-benzoic acid; **KC159**, 4-benzoic acid; **KC162**, 3-benzamide;
1300 **KC161,** 4-benzamide; **KC289,** 4-benzoic acid (potassium salt).
1301 (B) Intracellular Ca^{2+} measurements from a single experiment (n=1) in which hPIEZO1-TREx
1302 cells were acutely exposed to; (i) DMSO vehicle, or 10 µM; (ii) Yoda1, (iii) **KC157**, (iv) **KC158**,
1303 (v) **KC159**, (vi) **KC161**, (vii) **KC162**, (viii) **KC289**. Arrows indicate the time at which the
1304 indicated compound was added to the cells, following a 30 s background read. Mean ± SEM
1305 values from 3 technical replicates are shown.
1306 (C) Paired, background-subtracted (change above background, Δ), peak intracellular Ca^{2+}
1307 measurement comparisons of hPIEZO1-TREx cells treated with 10 µM indicated compound.
1308 Each plot shows mean peak values from independent experiments (**KC157**, n=7; **KC158**, n=6;
1309 **KC159**, n=25; **KC161**, n=6; **KC162**, n=12, **KC289**, n=18). Paired sample Wilcoxon signed
1310 rank test results comparing the median values of the collated experiments are shown as: * p
1311 < 0.05. Median fold-differences compared to Yoda1 are also indicated.
1312 (D) Background-subtracted (Δ) peak intracellular Ca^{2+} measurements for hPIEZO1-TREx cells
1313 treated with 10 µM indicated compound. Each symbol shows a mean peak value from an
1314 independent experiment (Yoda1, n=67; **KC159**, n=30; **KC289**, n=18). Kruskal-Wallis ANOVA
1315 results comparing the median values of each treatment pair are shown as: * p < 0.05.
1316

Figure 1 SI 1
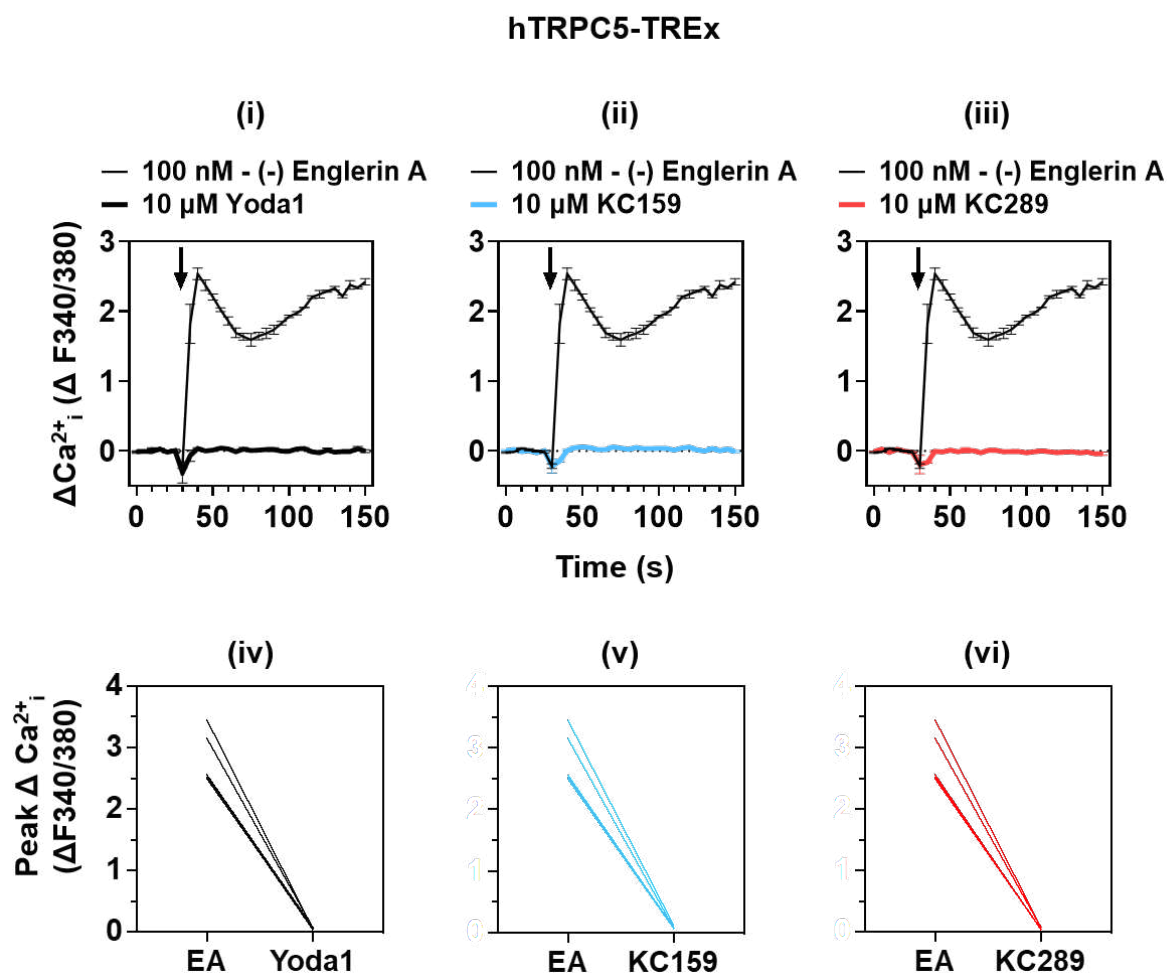
hTRPC5-TREx

Figure 1 SI 1 Lack of agonism at TRPC5 channels

(upper panel) Background-subtracted (Δ) intracellular Ca^{2+} measurements from a single experiment in which hTRPC5-TREx cells were acutely exposed to 10 µM (i) Yoda1, (ii) **KC159**, (iii) **KC289**. Arrows indicate the time at which the indicated compound was added to the cells, following a 30 s background read. The positive control stimulus (100 nM - (-) Englerin A is shown for comparison. Mean ± SEM values from 3 technical replicates are shown.

(lower panel) Paired, background-subtracted (Δ) peak intracellular Ca^{2+} measurement comparisons of hTRPC5-TREx cells treated with 100 nM (-)–Englerin A (EA) versus 10 µM (iv) Yoda1, (v) **KC159**, and (vi) **KC289**. Each plot shows mean peak values from independent experiments (n=5 for all compounds).

SI Table 1

Assay Name	Gene / Subfamily Name	Binding Assay Type	Catalogue #	Organism	% Inhibition
Acetylcholine M2 (Muscarinic)	CHRM2	GPCR (Antagonist Radioligand)	252710	Human	10
Acetylcholine M3 (Muscarinic)	CHRM3	GPCR (Antagonist Radioligand)	252810	Human	1
Adenosine A1	ADORA1	GPCR (Antagonist Radioligand)	200510	Human	-4
Adenosine A2A	**ADORA2A**	**GPCR (Agonist Radioligand)**	**200610**	**Human**	**40**
Adrenoceptor alpha1A	ADRA1A	GPCR (Antagonist Radioligand)	203100	Rat	3
Adrenoceptor alpha1B	ADRA1B	GPCR (Antagonist Radioligand)	203200	Rat	6
Adrenoceptor alpha2A	ADRA2A	GPCR (Antagonist Radioligand)	203630	Human	14
Adrenoceptor beta1	ADRB1	GPCR (Antagonist Radioligand)	204010	Human	11
Adrenoceptor beta2	ADRB2	GPCR (Antagonist Radioligand)	204110	Human	-2
Cav1.2 (L-type)	CACNA1C	Calcium Ion Channel (Dihydropyridine Site)	214600	Rat	20
CB1 Human Cannabinoid	CNR	GPCR (Antagonist Radioligand)	217050	Human	5
Dopamine D1	DRD1	GPCR (Antagonist Radioligand)	219500	Human	9
Dopamine D2S	DRD2	GPCR (Antagonist Radioligand)	219700	Human	1
GABA A	GABAA	(Non-Selective) Ion Channel [3H] Muscimol (Agonist Radioligand)	226500	Rat	12
GABA A	GABAA	(Non-Selective) Ion Channel [3H] Flunitrazepam (Agonist Radioligand)	226600	Rat	1
Glutamate	Ionotropic	(Non-Selective) Ion Channel [3H] TCP	233000	Rat	0
Histamine H1	HRH1	GPCR (Antagonist Radioligand)	239610	Human	-7
Imidazoline I2	Imidazoline	Central (Antagonist Radioligand)	241000	Rat	13
mu Opioid	OPRM1	GPCR (Antagonist Radioligand)	260410	Human	-10
nAChR (alpha1)	CHRNA1	Ion Channel, Bungarotoxin (Antagonist Radioligand)	258700	Human	-3
nAChR Nicotinic Acetylcholine	-	Ion Channel Binding, Epibatidine (Antagonist Radioligand binding)	258590	Human	-5
Norepinephrine Transporter	SLC6A2	Transporter (Antagonist Radioligand)	204410	Human	-9
PDE	Phosphodiesterase	(Non-Selective) [3H] Rolipram (Antagonist Radioligand)	270000	Rat	5
Phorbol Ester	-	Phorbol Ester	264500	Mouse	9
Potassium Channel (hERG)	KCNH2	Potassium Ion Channel [3H] Astemizole (Antagonist Radioligand)	265900	Human	3
Potassium Channel (KATP)	KCNJ11	Potassium Ion Channel (Antagonist Radioligand)	265600	Hamster	0
Prostanoid EP4	**PTGER4**	**GPCR (Agonist Radioligand)**	**268420**	**Human**	**63**
Serotonin (5-HT2B)	HTR2B	GPCR [3H]LSD (Agonist Radioligand)	271700	Human	-1
Sigma 1	SIGMAR1	Non-Selective (Antagonist Radioligand)	278110	Human	2
Sodium Ion Channel	Sodium Ion Channel	(Non-Selective) Sodium Ion Channel [3H] Batrachotoxinin (Site 2)	279510	Rat	-3

1330
1331 **SI Table 1. Binding results for 30 targets.**

1332   Data are for KC289 at 5 μM. 'Phorbol ester' is a binding assay that targets protein kinase Cs
1333   and potentially other proteins. Data were produced by Eurofins Scientific
1334   (https://www.eurofins.co.uk/).

SI Table 2

Assay	Repeat	Yoda1 Values	Yoda1 Mean	KC159 Values	KC159 Mean	KC289 Values	KC289 Mean
Kinetic solubility (µM) (0.1 M phosphate buffer, pH 7.4)	1 2	0.2 3.8	2	76.6 1.5	39.1	17.8 10.2	14
Thermodynamic solubility (µM) (0.1 M phosphate buffer, pH 7.4)	1 2	0.44 0.3	0.37	11.9 7.7	9.8	46 8.9	27.5
Mouse Microsomal $t_{1/2}$ (min)	1 2	1.0 1.2	1.1	37.2 21.9	29.6	31.8 17.3	24.6
Mouse Plasma Protein Binding (% Fraction Unbound)	1 2	<0.1 0.1	<0.1	0.4 0.8	0.6	0.5 0.8	0.65
Mouse plasma stability (% compound remaining after 2 hours)	1 2 3	nd 119 115	117	69 96 92	85.7 ± 14.6 (S.D.)	125 110 98	111 ± 13.5 (S.D.)

SI Table 2. Physico-chemical properties of Yoda1, KC159 and KC289.
Data were produced by Malvern PanAnalytical (https://www.malvernpanalytical.com/).
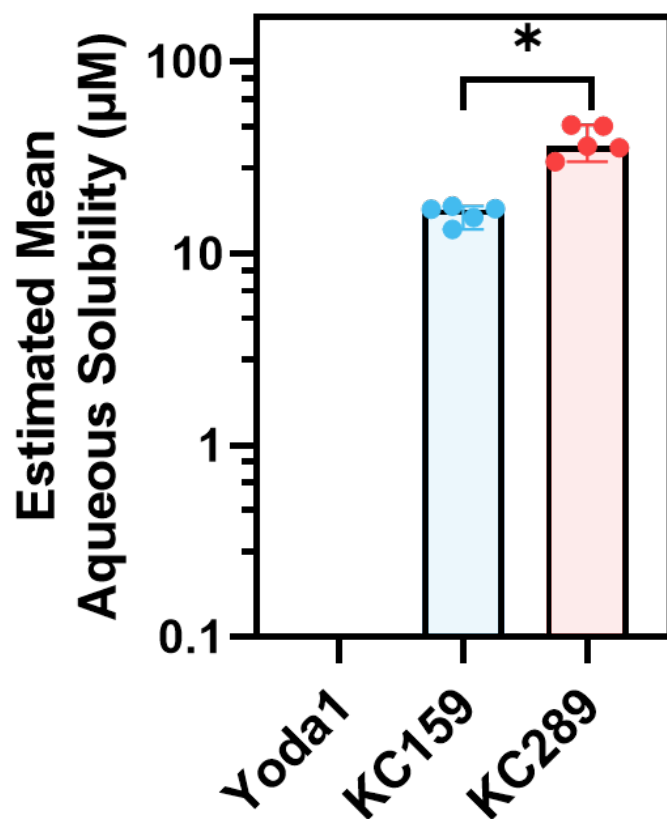
Figure 1 SI 2

1339
1340 **Figure 1 SI 2. In-house solubility comparisons for Yoda1, KC159 and KC289.**
1341 Estimated solubility of Yoda1, **KC159**, and **KC289** in universal aqueous buffer. Median values
1342 with data range from 5 independent experiments are shown (n=5). The lower limit of detection
1343 for the assay was 0.1 μM. Data for Yoda1 were below this limit, suggesting that Yoda1 was
1344 poorly soluble in these conditions. Results of a two-tailed Mann-Whitney rank comparison of
1345 the median values of the collated experiments are shown as: * $p < 0.05$.
1346
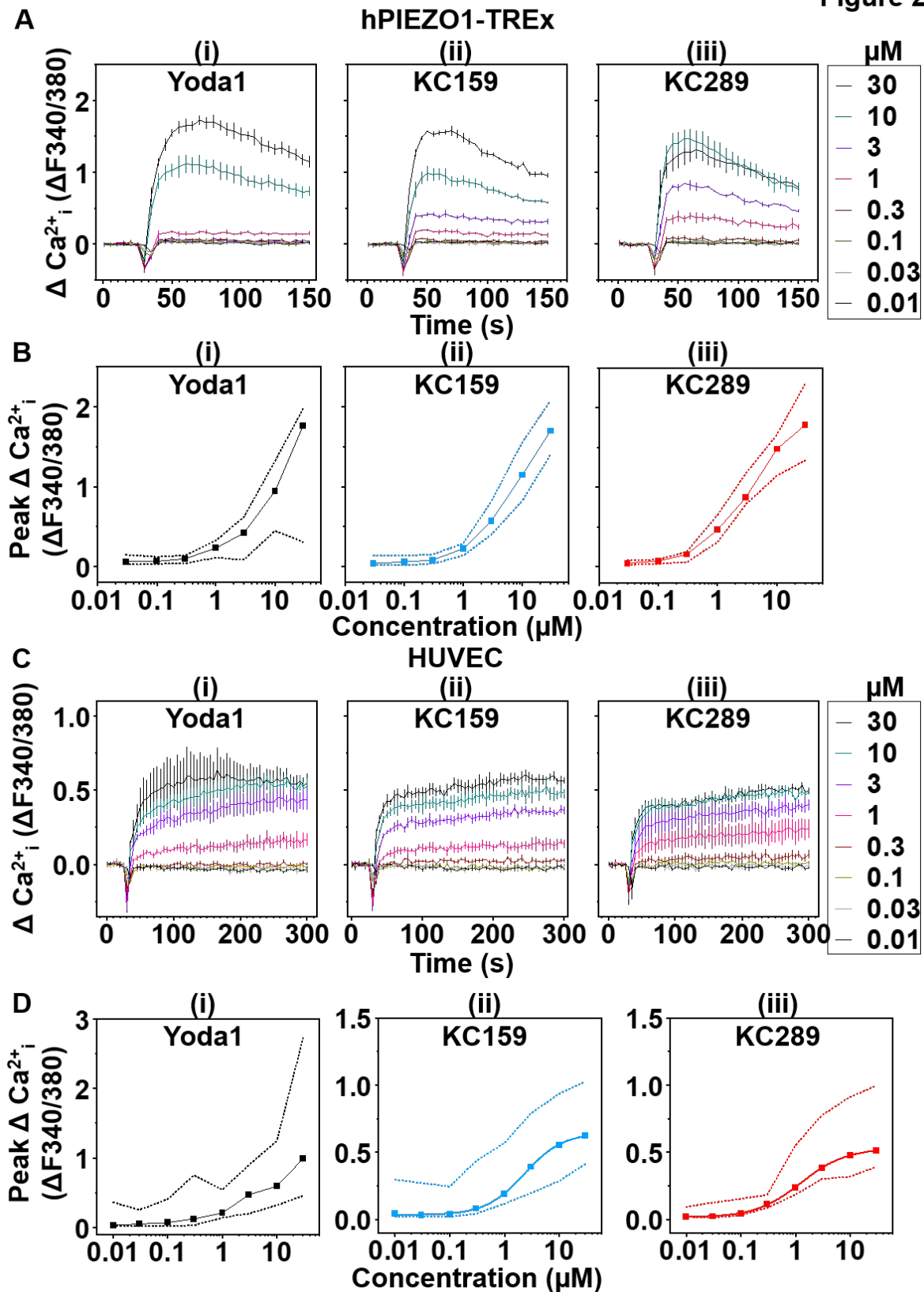
Figure 2

Figure 2. 4-benzoic acid improves concentration-response data for human PIEZO1
(A) Background-subtracted (Δ) intracellular Ca²⁺ measurements from a single experiment (n=1) in which hPIEZO1-TREx cells were exposed to the indicated concentrations of; (i) Yoda1, (ii) **KC159**, (iii) **KC289**. Mean ± SEM values from 3 technical replicates are shown.

1352   (B) Background-subtracted (Δ) peak intracellular Ca^{2+} measurements of hPIEZO1-TREx cells
1353   treated with the indicated concentration range of; (i) Yoda1, (ii) **KC159**, (iii) **KC289.** Median
1354   peak values and the data range from collated experiments are shown (Yoda1, n=12; **KC159**,
1355   n=17; **KC289**, n=7).
1356   (C) Background-subtracted (Δ) intracellular Ca^{2+} measurements from a single dose-response
1357   experiment (n=1) in which HUVEC were exposed to the indicated concentrations of; (i) Yoda1,
1358   (ii) **KC159**, (iii) **KC289**. Mean ± SEM values from 3 technical replicates are shown.
1359   (D) Background-subtracted (Δ) peak intracellular Ca^{2+} measurements of HUVEC treated with
1360   the indicated concentration range of; (i) Yoda1, (ii) **KC159**, (iii) **KC289.** Median peak values
1361   and the data range from collated experiments are shown (Yoda1, n=9; **KC159**, n=9, **KC289**,
1362   n=6). Fitted curves constructed using the Hill equation are shown in (ii) and (iii).
1363
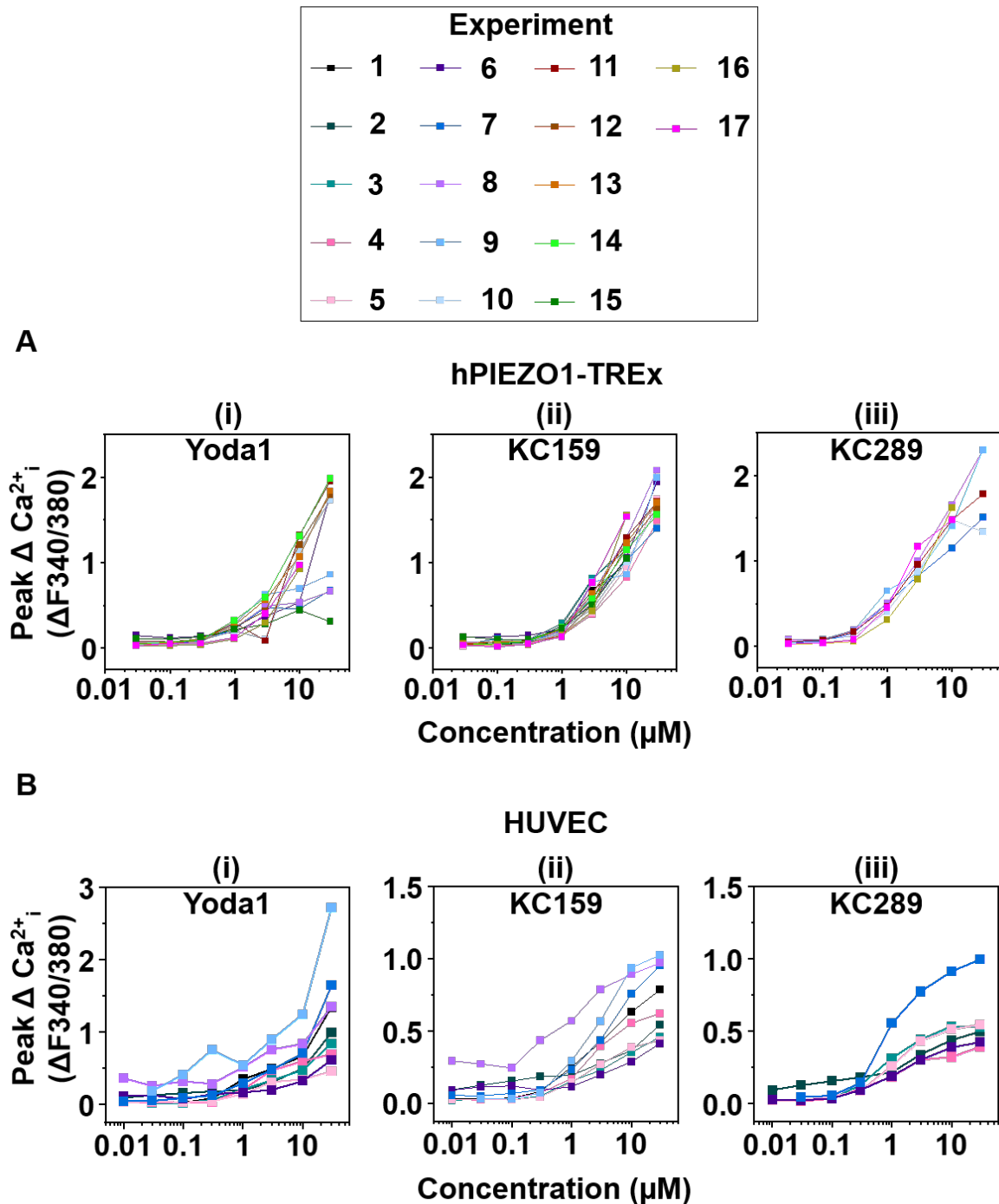
Figure 2 SI 1 Supporting data for Figure 2

(A) Background-subtracted (Δ) peak intracellular Ca^{2+} measurements from individual experiments in which hPIEZO1-TREx cells were exposed to the indicated concentrations of: (i) Yoda1 (n=12); (ii) **KC159** (n=17); (iii) **KC289** (n=7). Mean values from 2 to 5 technical replicates are shown for each of the individual experiments.

(B) Background-subtracted (Δ) peak intracellular Ca^{2+} measurements from individual experiments in which HUVECs were exposed to the indicated concentrations of: (i) Yoda1 (n=9); (ii) **KC159** (n=9); (iii) **KC289** (n=6). Mean values from 2 to 5 technical replicates are shown for each of the individual experiments.
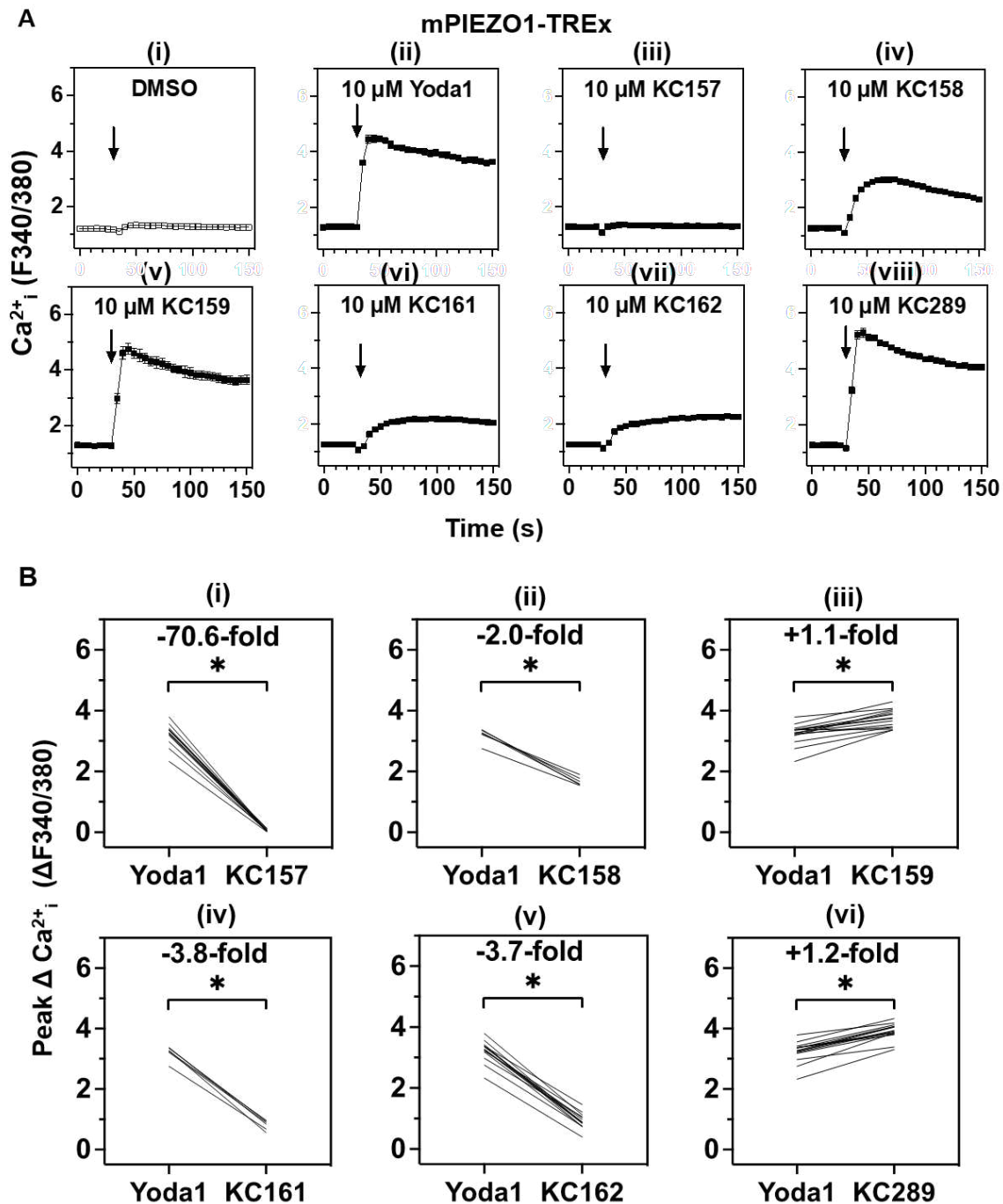
Figure 3

Figure 3. 4-benzoic acid improves efficacy at mouse PIEZO1

(A) Intracellular Ca^{2+} measurements from a single experiment in which mPIEZO1-TREx cells were acutely exposed to; (i) DMSO vehicle, or 10 µM; (ii) Yoda1, (iii) **KC157**, (iv) **KC158**, (v) **KC159**, (vi) **KC161**, (vii) **KC162**, (viii) **KC289**. Arrows indicate the time at which the indicated compound was added to the cells, following a 30 s background read. Mean ± SEM values from 5 technical replicates are shown. (B) Paired, background-subtracted (Δ), peak intracellular Ca^{2+} measurement comparisons of mPIEZO1-TREx cells treated with 10 µM indicated compound. Each plot shows mean peak values from independent experiments (**KC157**, n=15; **KC158**, n=6; **KC159**, n=15; **KC161**, n=6; **KC162**, n=15, **KC289**, n=15). Paired sample Wilcoxon signed rank test results comparing the median values of the collated

1387   experiments are shown as: * p < 0.05. Median fold-differences compared to Yoda1 are also
1388   indicated.
1389
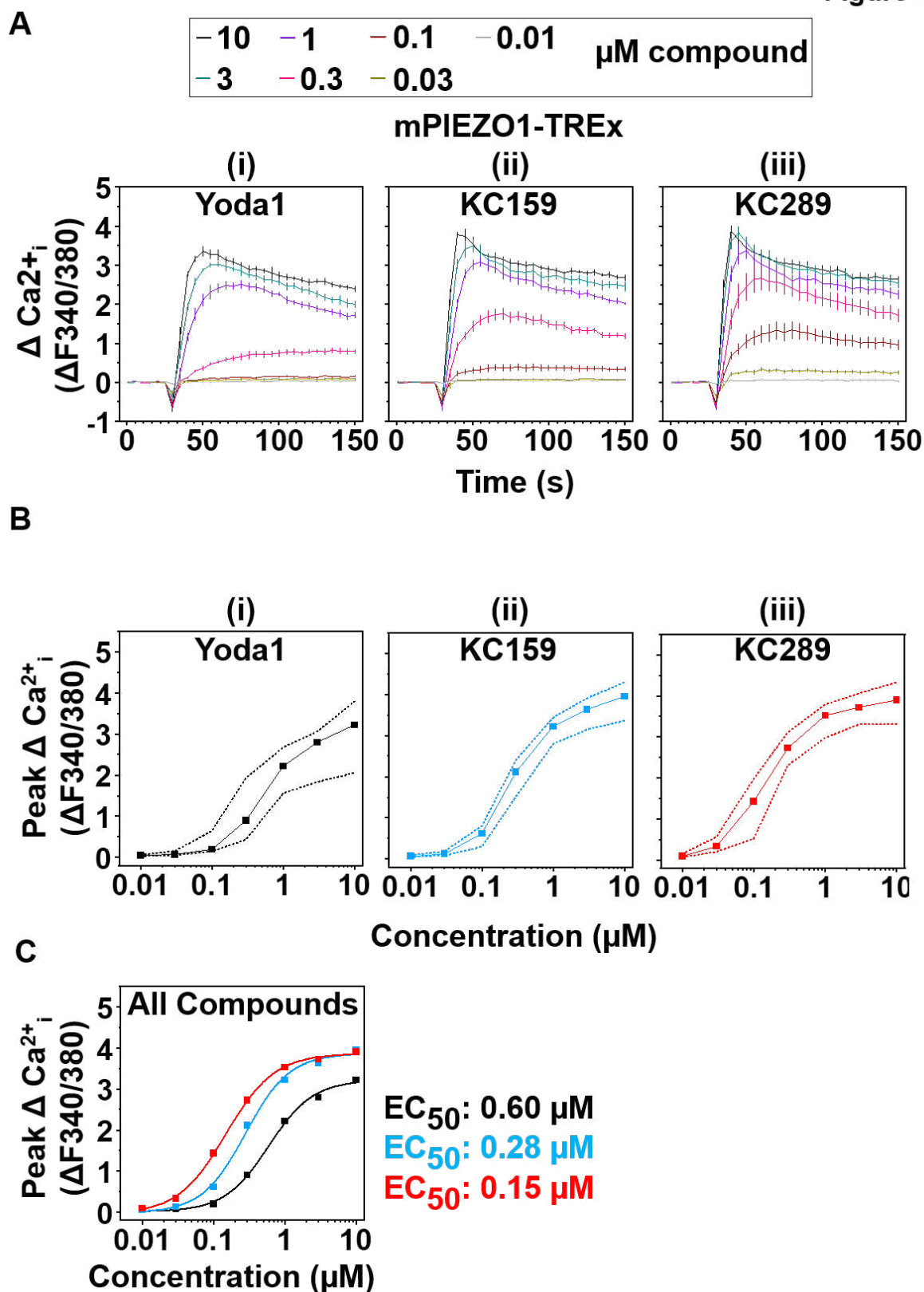
Figure 4

Figure 4. 4-benzoic acid improves potency at mouse PIEZO1
(A) Intracellular Ca^{2+} measurements from a single experiment (n=1) in which mPIEZO1-TREx
cells were exposed to the indicated concentrations of; (i) Yoda1, (ii) **KC159**, (iii) **KC289**. Mean
± SEM values from 4 technical replicates are shown.

1395   (B) Background-subtracted (Δ) peak intracellular Ca^{2+} measurements of mPIEZO1-TREx cells
1396   treated with the indicated concentration range of; (i) Yoda1, (ii) **KC159**, (iii) **KC289.** Median
1397   peak values and the data range from collated experiments are shown (n=12 for all
1398   compounds).
1399   (C) Median peak values for each compound were used to construct fitted curves from the Hill
1400   equation, and the respective EC_{50} values are indicated.
1401

Figure 4 SI 1
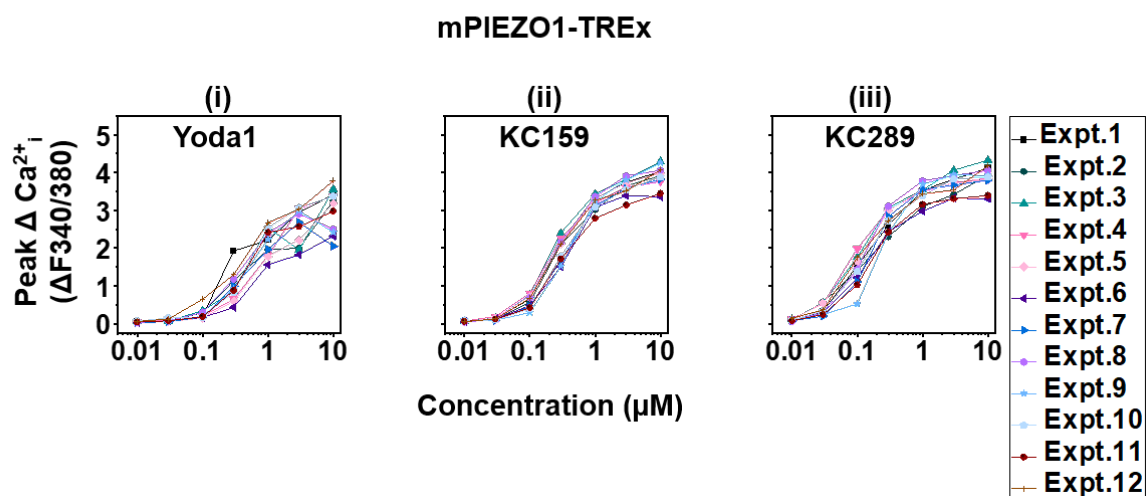
mPIEZO1-TREx

1402
1403 **Figure 4 SI 1 Supporting data for Figure 4**
1404 Background-subtracted (Δ) peak intracellular Ca^{2+} measurements from individual experiments
1405 in which mPIEZO1-TREx cells were exposed to the indicated concentrations of; (i) Yoda1, (ii)
1406 **KC159**, (iii) **KC289**. Mean values from 2 or 3 technical replicates are shown for each of the
1407 individual experiments (n=12 for all compound tests).
1408
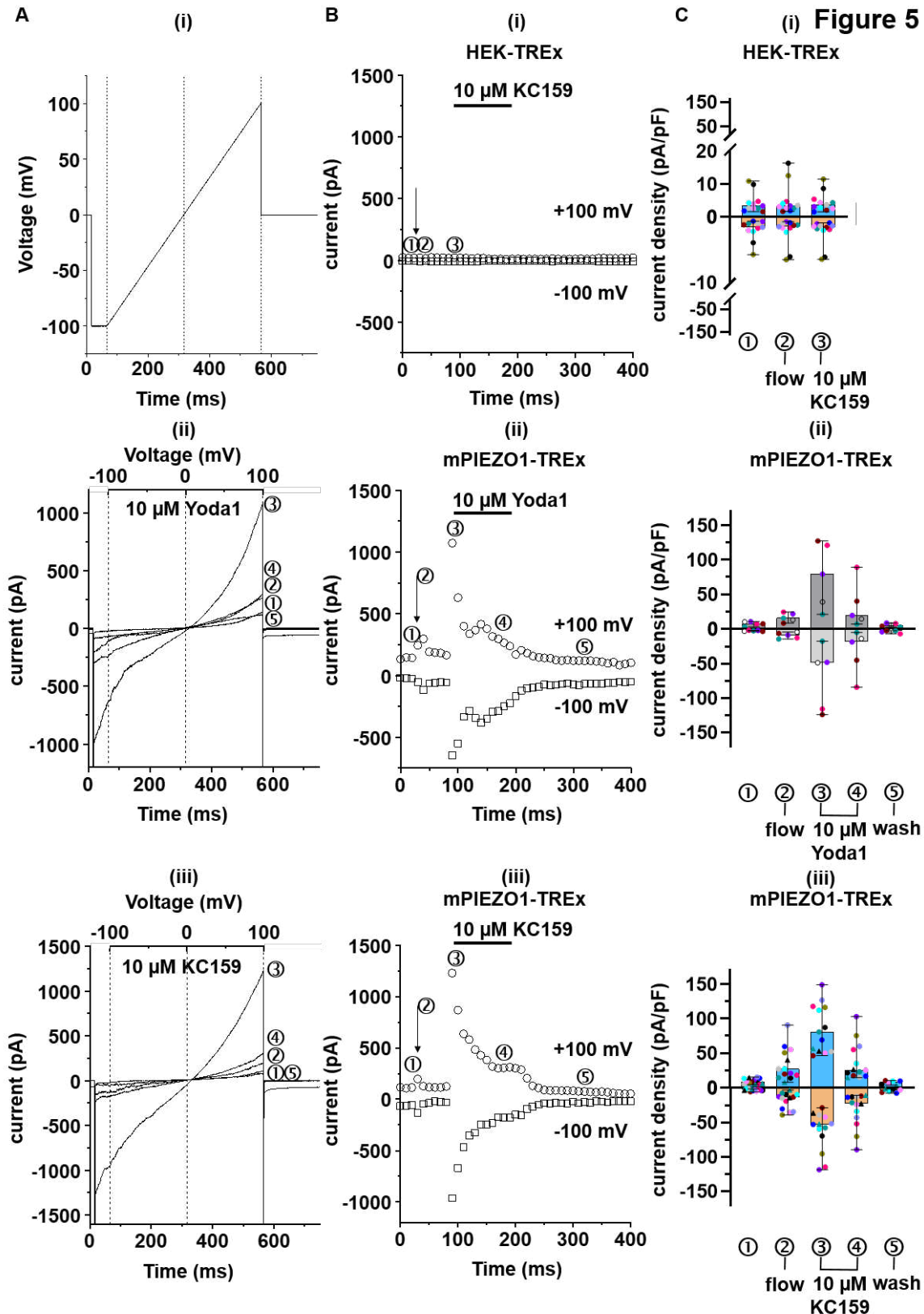
1409
Figure 5. PIEZO1 agonism confirmed by manual patch-clamp
(A) (i) Ramp voltage protocol used for cell stimulation. Dashed gridlines show time points where the ramp starts (-100 mV), reverses (0 mV) and ends (+100 mV). They also match the lines in (ii) and (iii) which show representative (N=1) whole-cell currents activated in mPIEZO1-TREx channels by 10 µM (ii) Yoda1, or (iii) **KC159**. The circled numbers indicate currents at

1415 the following stages of the experiment; ① control; ② after the start of SBS flow; ③ (maximal)

1416 after application of the indicated compound; ④ 100 ms after application of compound; ⑤

1417 after bath solution (SBS) washout of compound. The circled numbers correspond to those

1418 shown in all subsequent plots.

1419 (B) Time-resolved plots of representative experiments (N=1); (i) HEK-TREx control (null) cell

1420 treated with fluid flow and then flow plus 10 µM **KC159**; (ii) mPIEZO1-TREx cell treated with

1421 flow and then flow plus 10 µM Yoda1; (iii) mPIEZO1-TREx cell treated with flow and then flow

1422 plus 10 µM **KC159**. Arrow indicates the start of SBS flow. Circles indicate currents measured

1423 at +100 mV of the ramp, and squares those measured at -100mV. The currents were recorded

1424 every 10 s.

1425 (C) Collated data for experiments as exemplified in (A) and (B). Current densities (pA/pF)

1426 measured at +100 mV are shown on the upper y-axis (blue for KC159, dark grey for Yoda1),

1427 and those measured at -100 mV on the lower y-axis (orange for KC159, light grey for Yoda1).

1428 Individual data points of different cells are shown with different colours. Bars indicate the

1429 median ± range. (i) HEK-TREx control cells treated with 10 µM **KC159**: ① (N=11); ② (N=11);

1430 ③ (N=11). (ii) mPIEZO1-TREx cells treated with 10 µM Yoda1: ① (N=5); ② (N=5); ③ (N=5);

1431 ④ (N=5) and; ⑤ (N=5). (iii) mPIEZO1-TREx cells treated with 10 µM **KC159**: ① (N=13); ②

1432 (N=13); ③ (N=13); ④ (N=13) and; ⑤ (N=6).

1433

1434

Figure 6
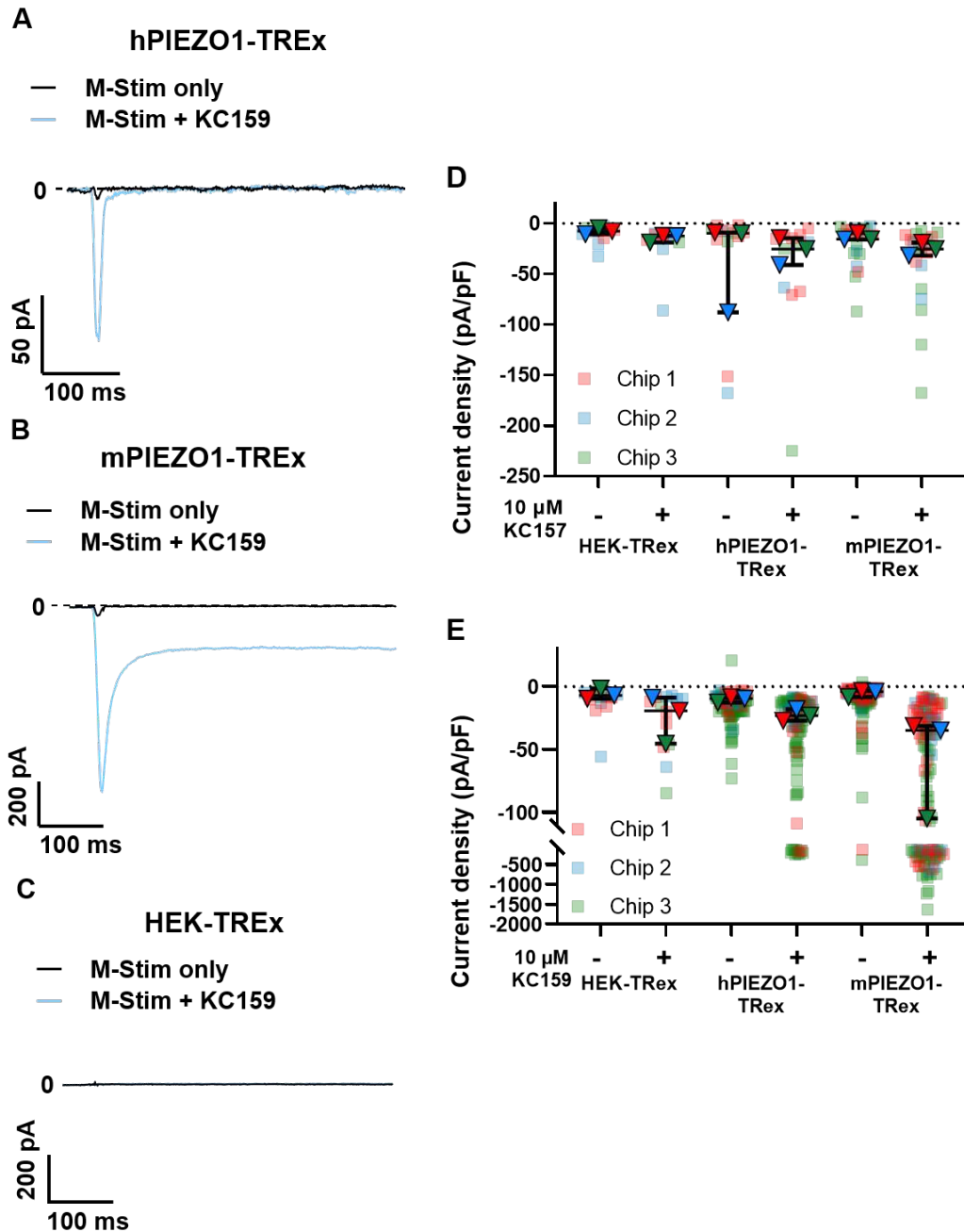
1435
1436 **Figure 6. Improved agonism seen by automated patch-clamp**
1437 (A, B, C) Averaged traces for PIEZO1-mediated currents activated by mechanical stimulation
1438 (M-Stim) on the SyncroPatch384 in the absence (black traces) and presence of 10 µM **KC159**
1439 (blue traces) from: (A) hPIEZO1-TREx (N=44); (B) mPIEZO1-TREx (N=46) and (C)
1440 untransfected HEK-TREx (N=55).
1441 (D and E) Current densities elicited by M-Stim in the absence and presence of 10 µM: (D)
1442 **KC157** or; (E) **KC159** in untransfected HEK-TREx, hPIEZO1-TREx and mPIEZO1-TREx cells.
1443 Each square represents the peak current density of a single cell, with median values and
1444 ranges indicated in black. Only data for cells defined as responding (see Methods) are
1445 included in the plots. Recordings were made from cells on 3 different 384-well recording chips
1446 and the data from these chips are distinguished by red, blue and green colour with the filled
1447 triangles indicating the median values for each chip. (D) HEK-TREx M-Stim (N=10), HEK-

1448   TREx M-Stim + **KC157** (N=10), hPIEZO1-TREx M-Stim (N=12), hPIEZO1-TREx M-Stim +
1449   **KC157** (N=12), mPIEZO1-TREx M-Stim (N=20), mPIEZO1-TREx M-Stim + **KC157** (N=20).
1450   (E) HEK-TREx M-Stim (N=13), HEK-TREx M-Stim + **KC159** (N=13), hPIEZO1-TREx M-Stim
1451   (N=94), hPIEZO1-TREx M-Stim + **KC159** (N=94), mPIEZO1-TREx M-Stim (N=113),
1452   mPIEZO1-TREx M-Stim + **KC159** (N=113).
1453

Figure 6 SI 1

A

B
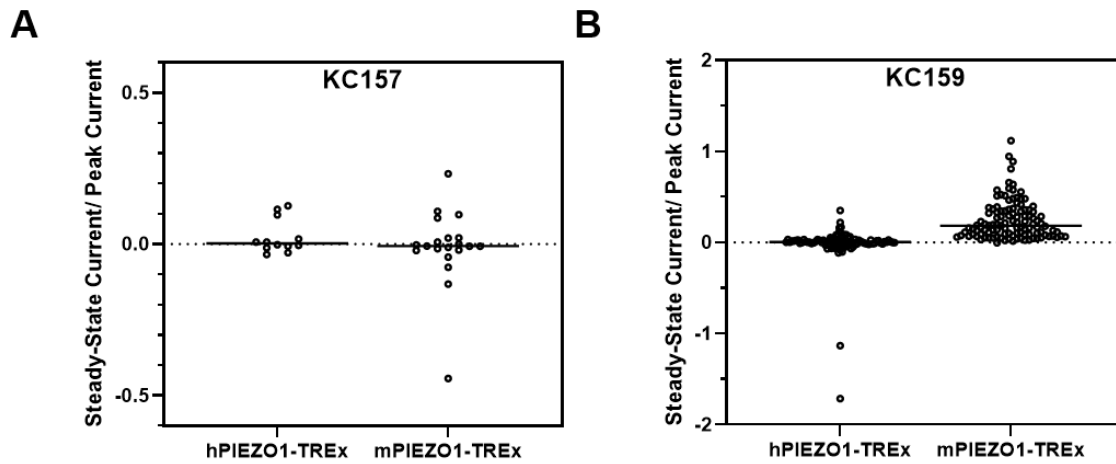
Figure 6 SI 1. Quantification of sustained current after application of KC157 and KC159.
Ratio of sustained current to peak current after application of (A) **KC157** and (B) **KC159** for
mouse PIEZO1 and human PIEZO1. (A) hPIEZO1-TREx M-Stim + KC157 (N=12), mPIEZO1-
TREx M-Stim + **KC157** (N=20). (B) hPIEZO1-TREx M-Stim + **KC159** (N=94), mPIEZO1-TREx
M-Stim + **KC159** (N=113). Bars indicate median values.

Figure 7
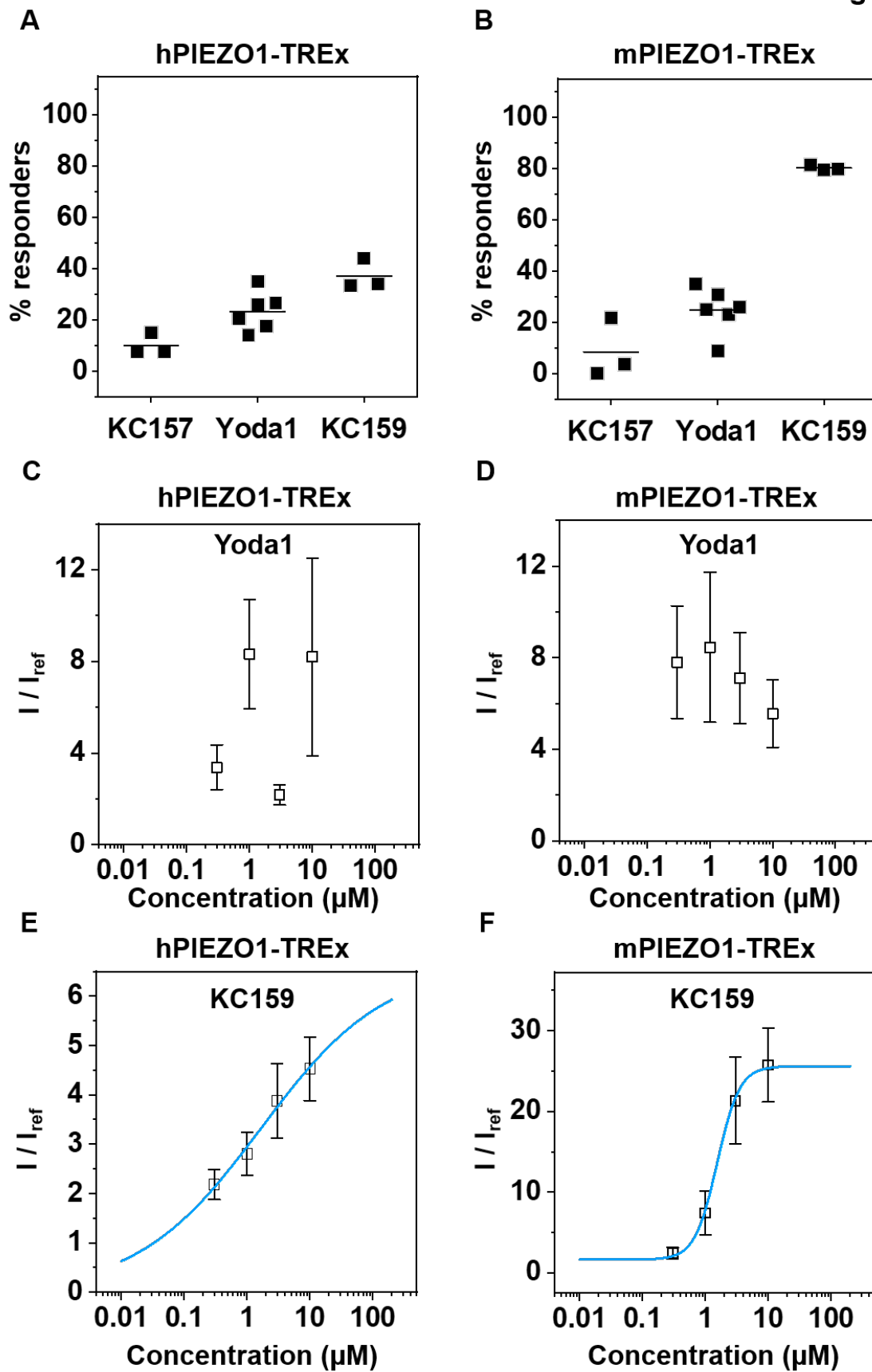
Figure 7. Automated patch-clamp comparison with Yoda1

1462   (A and B) Percentages of; (A) hPIEZO1-TREx and; (B) mPIEZO1-TREx cells responding to
1463   activation by 10 µM **KC157,** 10 µM Yoda1 and 5 µM **KC159**. Each square represents an
1464   independent experiment with mean values indicated by black bars. All groups contained 64
1465   cells per condition tested on the same chip, and the following numbers of valid cells were
1466   assessed for responsiveness in each repeat: (A) **KC157**, N=40, 40, 53; **Yoda1**, N=37, 50, 51,
1467   46, 39, 49; **KC159**, N=42, 50, 41. (B) **KC157**, N=48, 55, 46; **Yoda1**, N=42, 48, 56, 48, 43, 54;
1468   **KC159**, N=34, 25, 43. Because of the number of independent 384-well chips used was less
1469   than 5 in some cases (i.e., 3), we did not apply statistical testing to these data.
1470   (C and D) Dose-response data expressed as mean normalized activation ± SEM, obtained
1471   from; (C) hPIEZO1-TREx (N=108) and; (D) mPIEZO1-TREx (N=134) cells exposed to
1472   increasing concentrations (0.3, 1, 3 and 10 µM) of Yoda1. hPIEZO1 0.3 µM (N=27), 1 µM
1473   (N=25), 3 µM (N=28), 10 µM (N=28); mPIEZO1 0.3 µM (N=34), 1 µM (N=34), 3 µM (N=34),
1474   10 µM (N=32) The peak current in the presence of the agonist was normalized to the peak
1475   current in the presence of reference only.
1476   (E and F) Dose-response data expressed as mean normalized activation ± SEM, obtained
1477   from; (E) hPIEZO1-TREx (N=316) and; (F) mPIEZO1-TREx (N=250) cells exposed to
1478   increasing concentrations (0.3, 1, 3 and 10 µM) of **KC159**. hPIEZO1 0.3 µM (N=79), 1 µM
1479   (N=86), 3 µM (N=73), 10 µM (N=78); mPIEZO1 0.3 µM (N=65), 1 µM (N=58), 3 µM (N=63),
1480   10 µM (N=64). The peak current in the presence of the agonist was normalized to the peak
1481   current in the presence of reference only. Fitted curves (blue) were generated from the Hill
1482   equation.
1483

Figure 8
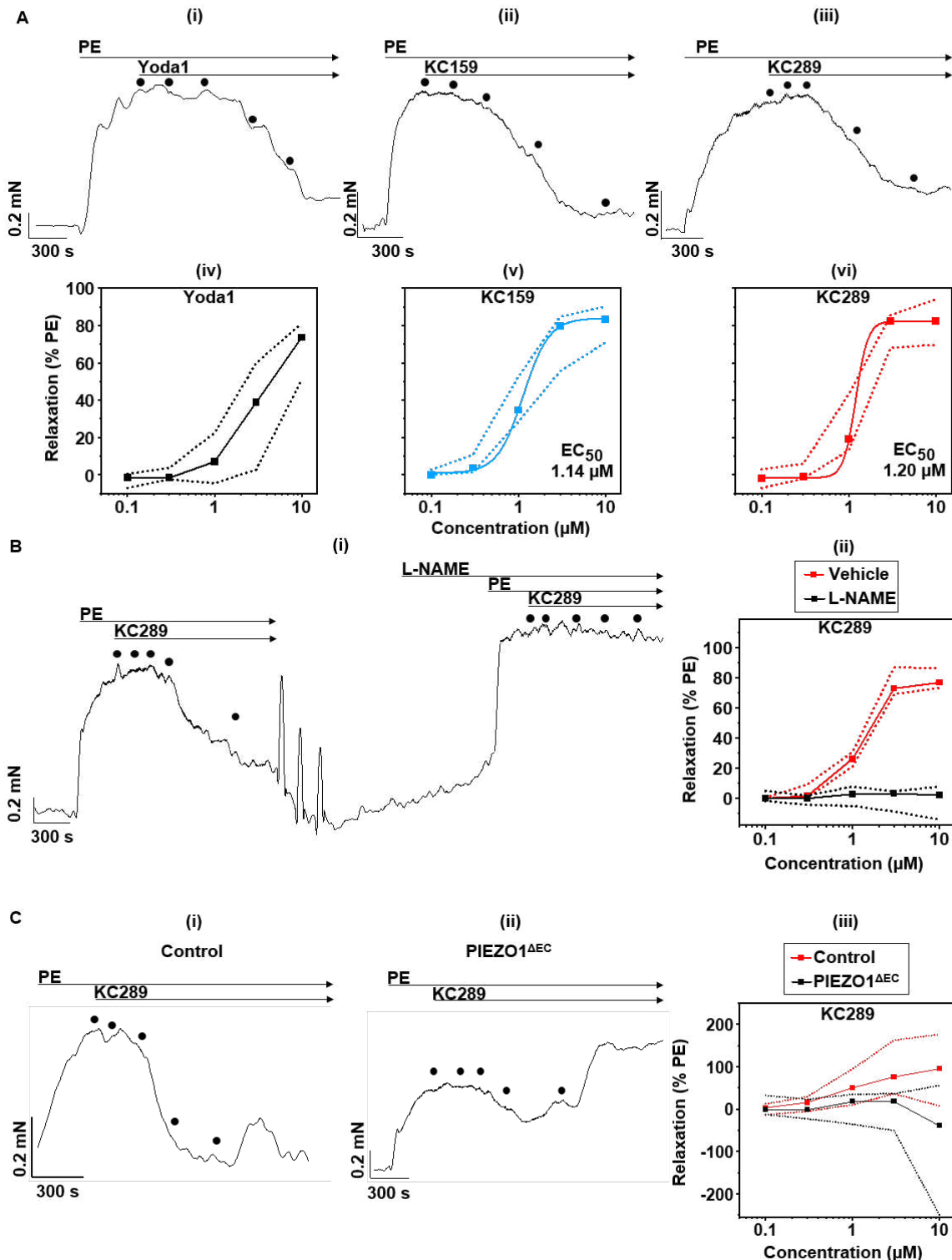
1484
1485 **Figure 8. NO- and endothelial PIEZO1- dependent vasorelaxation**
1486 Isometric tension of mouse portal vein possessing intact endothelium was measured following
1487 pre-constriction with 10 µM phenylephrine (PE) and exposure to increasing concentrations
1488 (0.1, 0.3, 1, 3 and 10 µM) of indicated compounds.
1489 (A) (upper panel) Isometric tension traces from single experiments (n=1) in which mouse
1490 portal vein segments were exposed to increasing concentrations of: (i) Yoda1; (ii) **KC159**; (iii)
1491 **KC289.** The dots indicate the sequential addition of rising concentrations of compounds.

1492 (lower panel) Corresponding dose-response data for: (iv) Yoda1 (n=8); (v) **KC159** (n=5); (vi)
1493 **KC289** (n=5) expressed as a % of the maximal PE-induced tension. Squares indicate median
1494 values and dotted lines indicate the data range from collated experiments. For Yoda1, curve
1495 fitting was not successful due to the lack of upper plateau. For KC159 and KC289, fitted curves
1496 generated from the Hill equation (Hill1 in OriginPro 2020 software) and their corresponding
1497 EC_{50} values are shown. (B) (i) Isometric tension response trace from a single experiment (n=1)
1498 in which increasing concentrations of **KC289** were added before and after a 30-minute pre-
1499 incubation of the vessel with 100 µM Nω-nitro-L-arginine methyl ester (L-NAME). (ii)
1500 Corresponding collated dose-response data expressed as a % of the maximal PE-induced
1501 tension (n=5). Median and range are shown.
1502 (C) (i-ii) Isometric tension response traces from a single experiment (n=1) in which increasing
1503 concentrations of **KC289** were added to portal veins from; (i) control and; (ii) PIEZO1$^{\Delta EC}$ mice.
1504 (iii) Corresponding dose-response data expressed as a % of the maximal PE-induced tension
1505 (control, n=9; PIEZO1$^{\Delta EC}$, n=9). Median and range from collated experiments are shown.
1506
1507

Figure 8 SI 1

(i)

Response to PE (mN)

1.5
1.0
0.5

Vehicle L-NAME

(ii)

Resting Basal Tension (mN)

2.0
1.5
1.0

Vehicle L-NAME
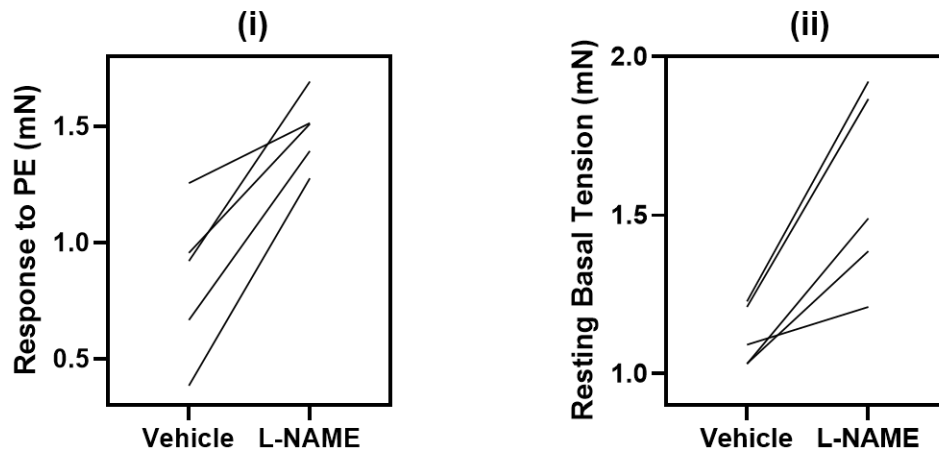
Figure 8 SI 1 Effects of L-NAME on vessel response to PE and resting basal tension
Paired comparisons of (i) tension responses to PE and; (ii) isometric basal tension measurements before and after a 30-minute pre-incubation of vessels with 100 µM Nω-nitro-L-arginine methyl ester (L-NAME). Each plot shows values from independent experiments (n=5).

1516

A　**Control**
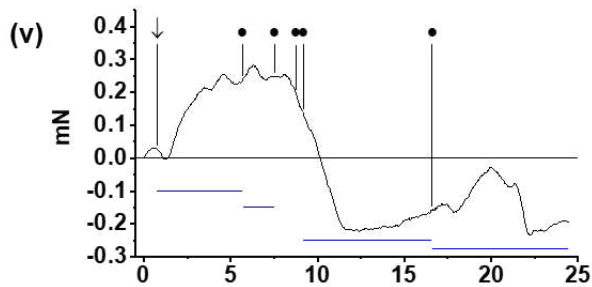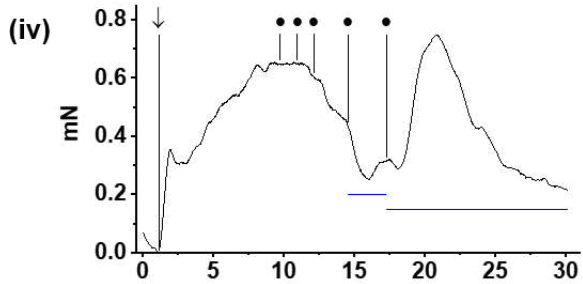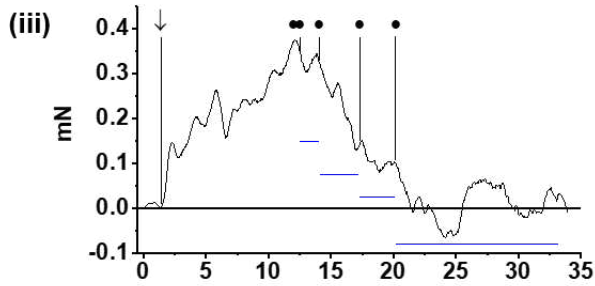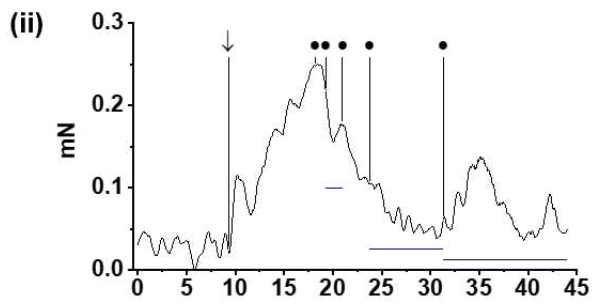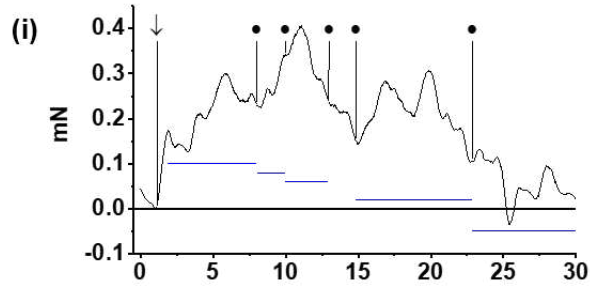
Figure 8 SI 2 (A)
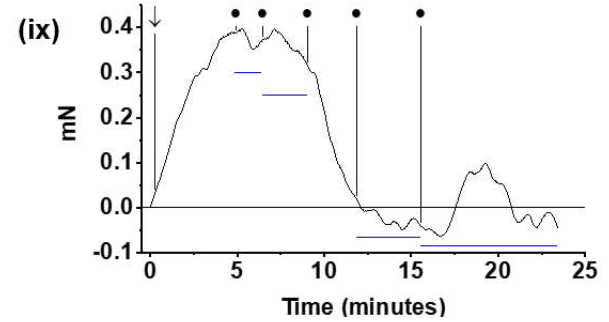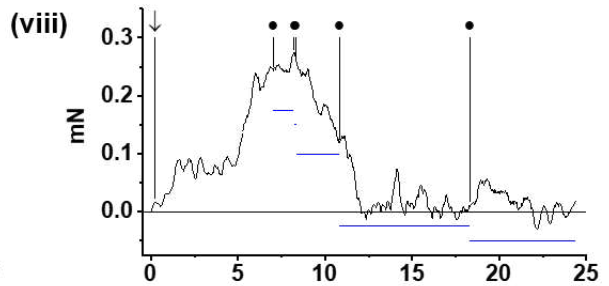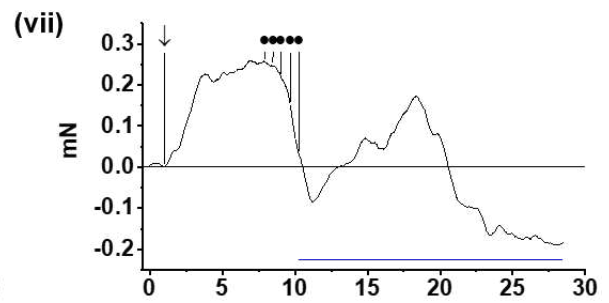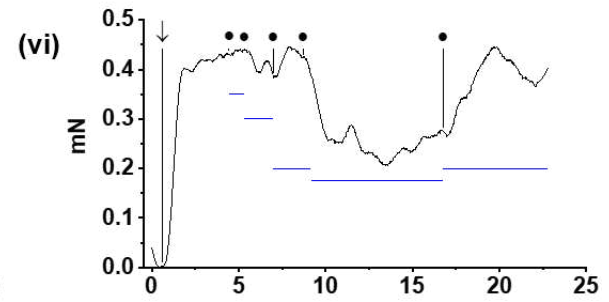
1517

B PIEZO1$^{\Delta EC}$
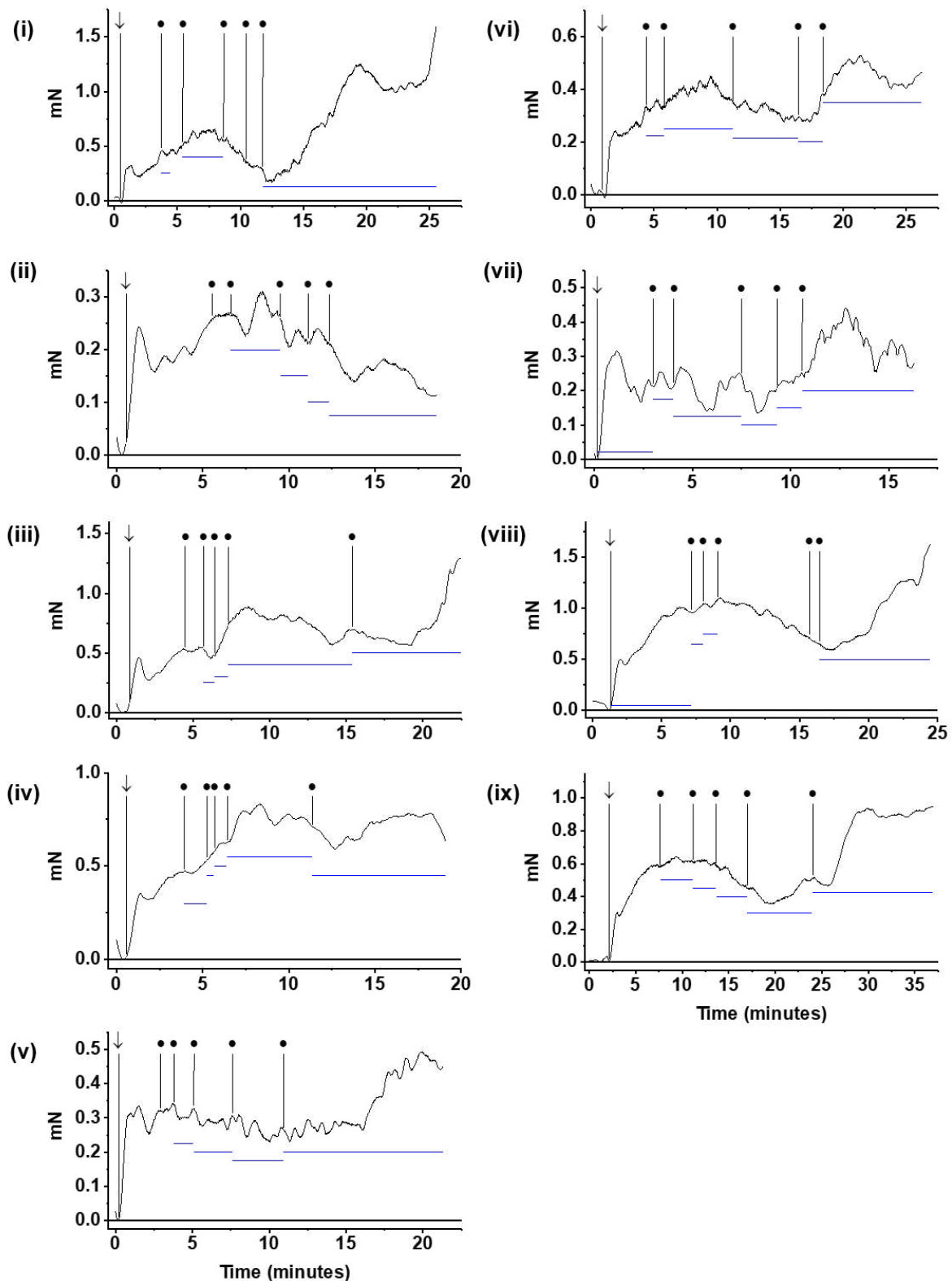
Figure 8 SI 2 (B)

1518
1519
1520 **Figure 8 SI 2 All original traces for the data of Figure 8C.**
1521 Isometric tension traces from single experiments in which (A) (i-ix) control mouse, or (B) (i -
1522 ix) portal vein segments possessing intact endothelium were exposed to increasing
1523 concentrations (0.1, 0.3, 1, 3 and 10 µM) of KC289 after pre-constriction with 10 µM

1524   phenylephrine (PE). The arrows indicate the addition of PE; dots indicate the sequential
1525   addition of rising concentrations of KC289. Blue lines annotate treatment periods in which
1526   spontaneous activity of the vessel made it difficult to determine if there were effects of the
1527   compound.
1528

Figure 8 SI 3
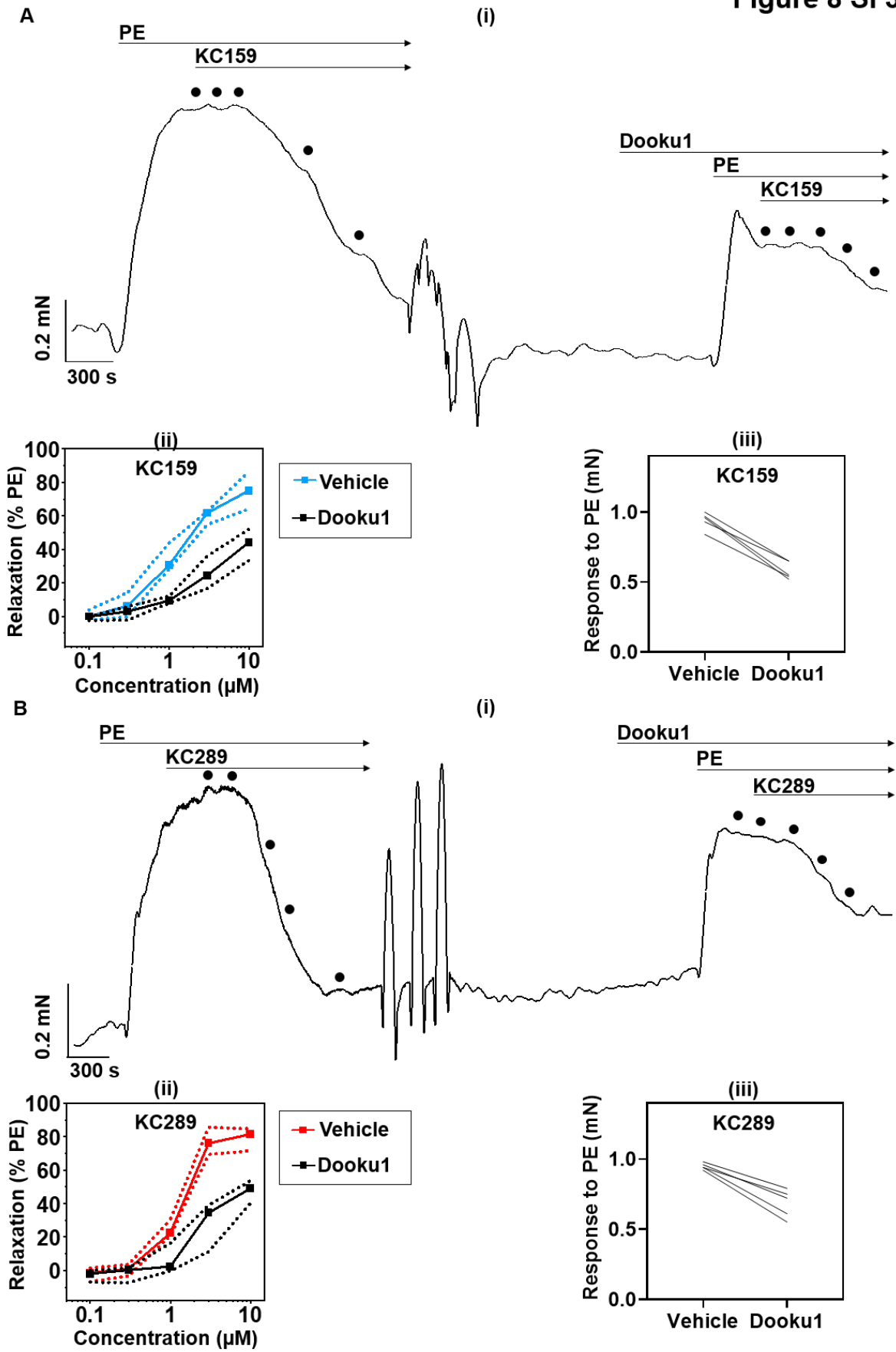
1529
1530 **Figure 8 SI 3 Dooku1 antagonises vasorelaxant effects of KC159 and KC289**

1531   Isometric tension responses observed on addition of increasing concentrations of: (A) **KC159**
1532   or; (B) **KC289** before and after a 30-minute pre-incubation of the vessel with 10 µM Dooku1
1533   or DMSO vehicle control. (A)(i) and (B)(i) show traces from individual experiments (n=1 each).
1534   The dots indicate the sequential addition of rising concentrations of compounds. (A)(ii) and
1535   (B)(ii) show corresponding dose-response data expressed as a % of the maximal PE-induced
1536   tension (n=5 for each compound). Median and range from collated experiments are shown.
1537   (A)(iii) and (B)(iii) show paired comparisons of vessel tension responses to PE. Each plot
1538   shows values from independent experiments (n=5).
1539
1540
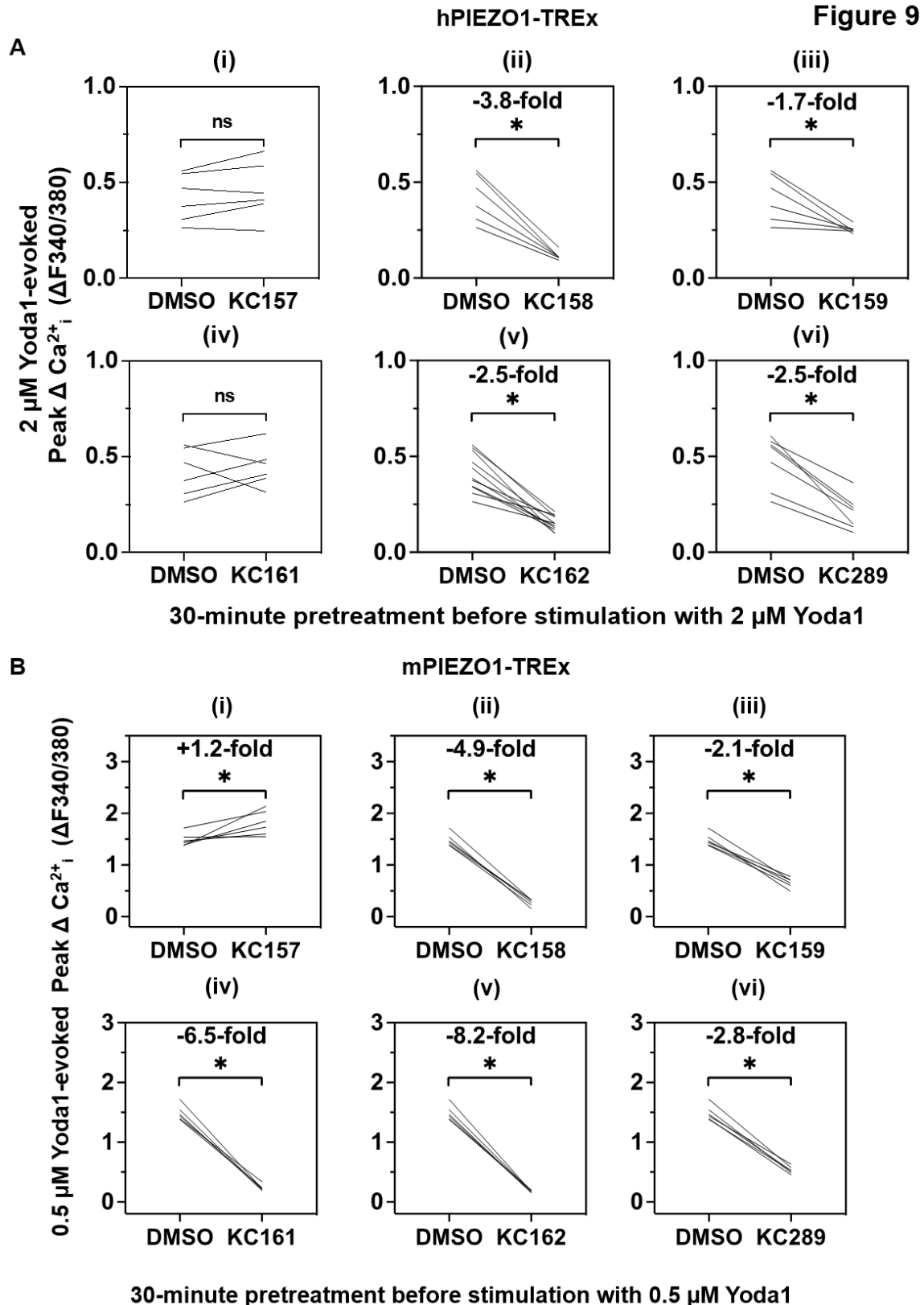
Figure 9. Effects of 3- and 4-benzamide and 3-benzoic acid analogues
(A and B) Paired, background-subtracted (Δ), peak intracellular Ca^{2+} measurement comparisons of: (A) hPIEZO1-TREx and (B) mPIEZO1-TREx pretreated with 10 μM indicated compound for 30 minutes prior to acute exposure to (ii – vi) the indicated Yoda1 stimulus. Each plot shows mean peak values from independent experiments. Independent experiment numbers for hPIEZO1-TREx experiments (A): **KC157**, n=6; **KC158**, n=6; **KC159**, n=6; **KC161**,

1548   n=6; **KC162**, n= 11, **KC289**, n=7). Independent experiment numbers for mPIEZO1-TREx
1549   experiments (B): (n=6 for all compounds). Paired sample Wilcoxon signed rank test results
1550   comparing the median values of the collated experiments are shown as: n.s (p > 0.05), * p <
1551   0.05. Median fold-differences compared to DMSO-pretreatment/ indicated Yoda1-stimulation
1552   are also shown.
1553
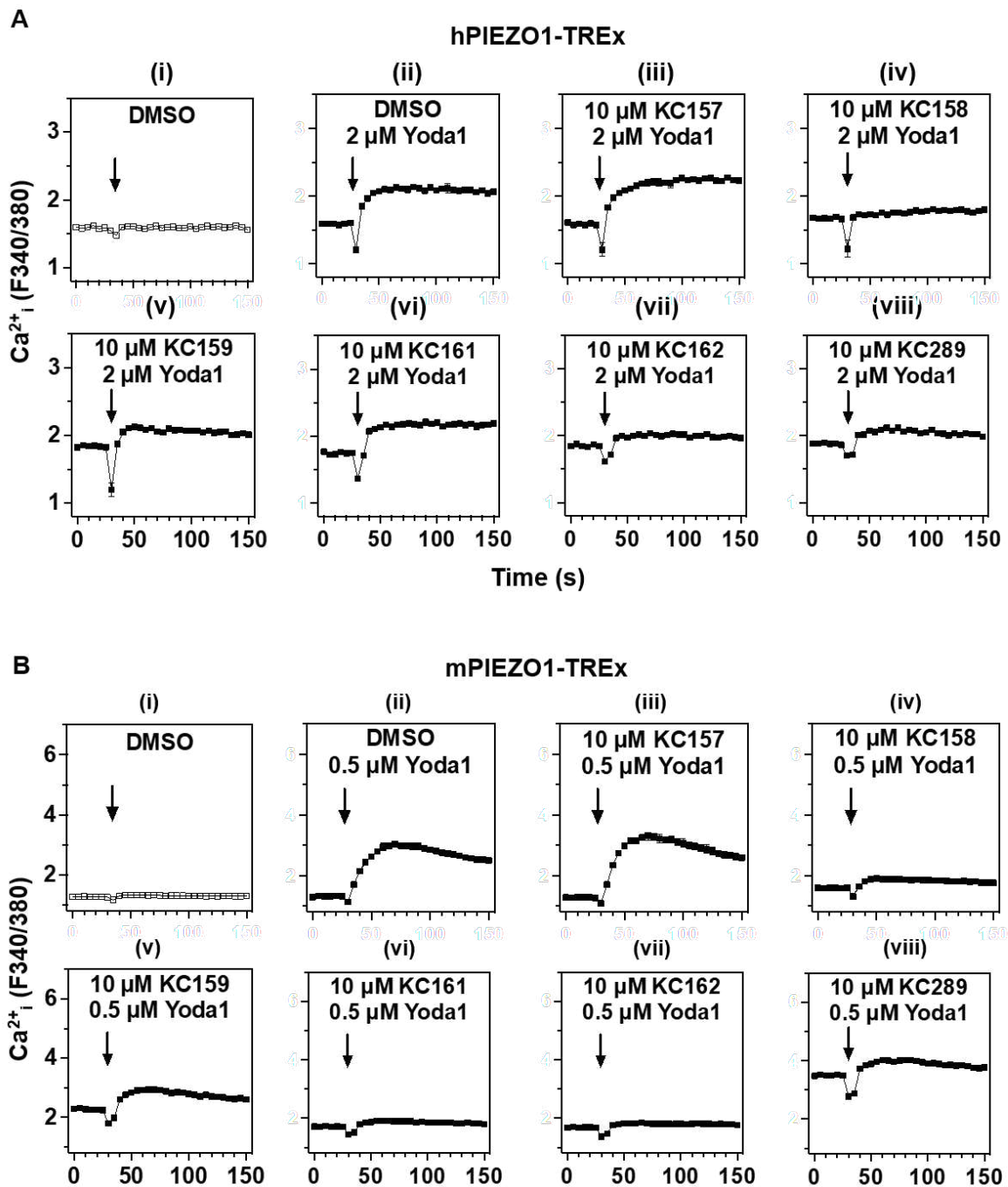
Figure 9 SI 1 Example single experiment data in support of Figure 9
Intracellular Ca^{2+} measurements from single experiments (n=1) in which; (A) hPIEZO1-TREx and; (B) mPIEZO1-TREx cells were pretreated with; (i - ii) DMSO vehicle, or 10 µM; (iii) **KC157**, (iv) **KC158**, (v) **KC159**, (vi) **KC161**, (vii) **KC162**, (viii) **KC289** for 30 minutes before stimulation with the indicated concentration of Yoda1. Arrows indicate the time at which Yoda1 was added to the cells, following a 30 s background read. Mean ± SEM values from between 3 and 5 technical replicates are shown.
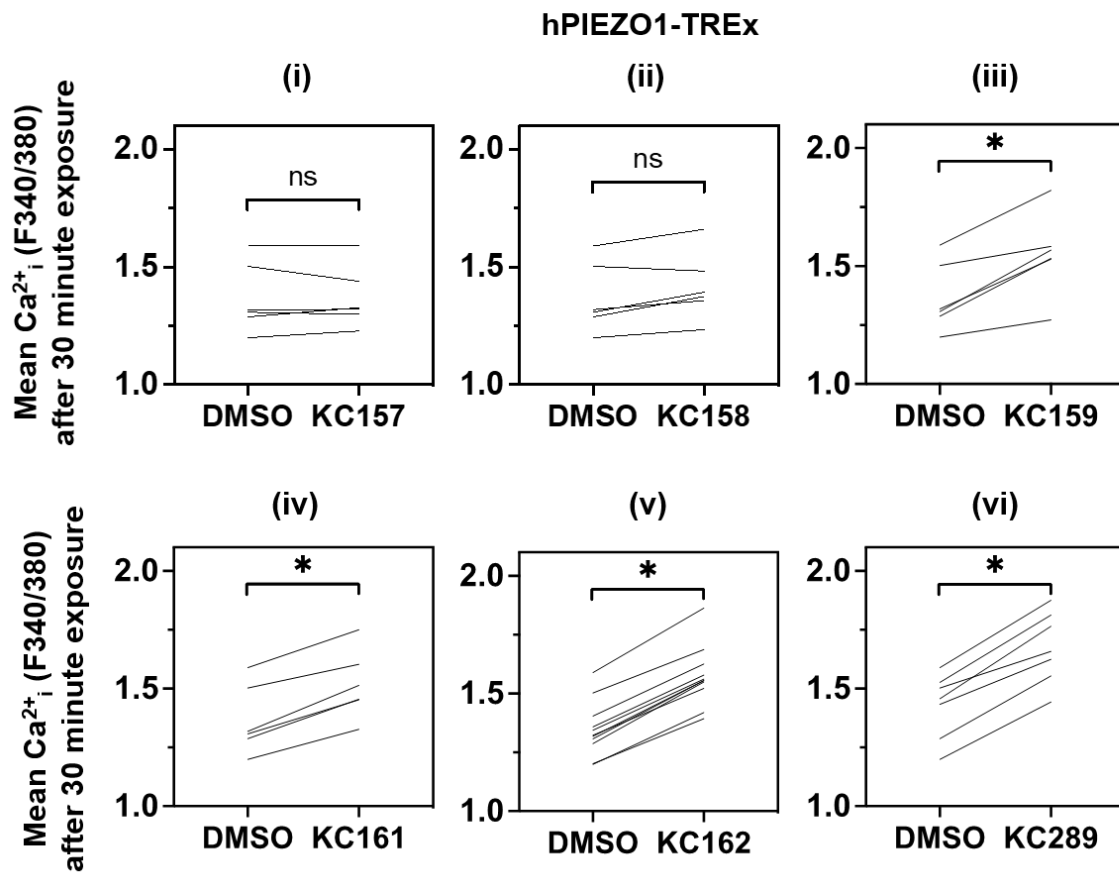
Figure 9 SI 2

Figure 9 SI 2 Further analysis of data in Figure 9 – effects of long exposure

Paired mean intracellular Ca^{2+} measurement comparisons of hPIEZO1-TREx treated with 10 µM indicated compound for 30 minutes. Each plot shows mean values from independent experiments. Independent experiment numbers: (i) **KC157**, n=6; (ii) **KC158**, n=6; (iii) **KC159**, n=6; (iv) **KC161**, n=6; (v) **KC162**, n= 11; (vi) **KC289**, n=7. Paired sample Wilcoxon signed rank test results comparing the median values of the collated experiments are shown as: n.s (p > 0.05), * p < 0.05.
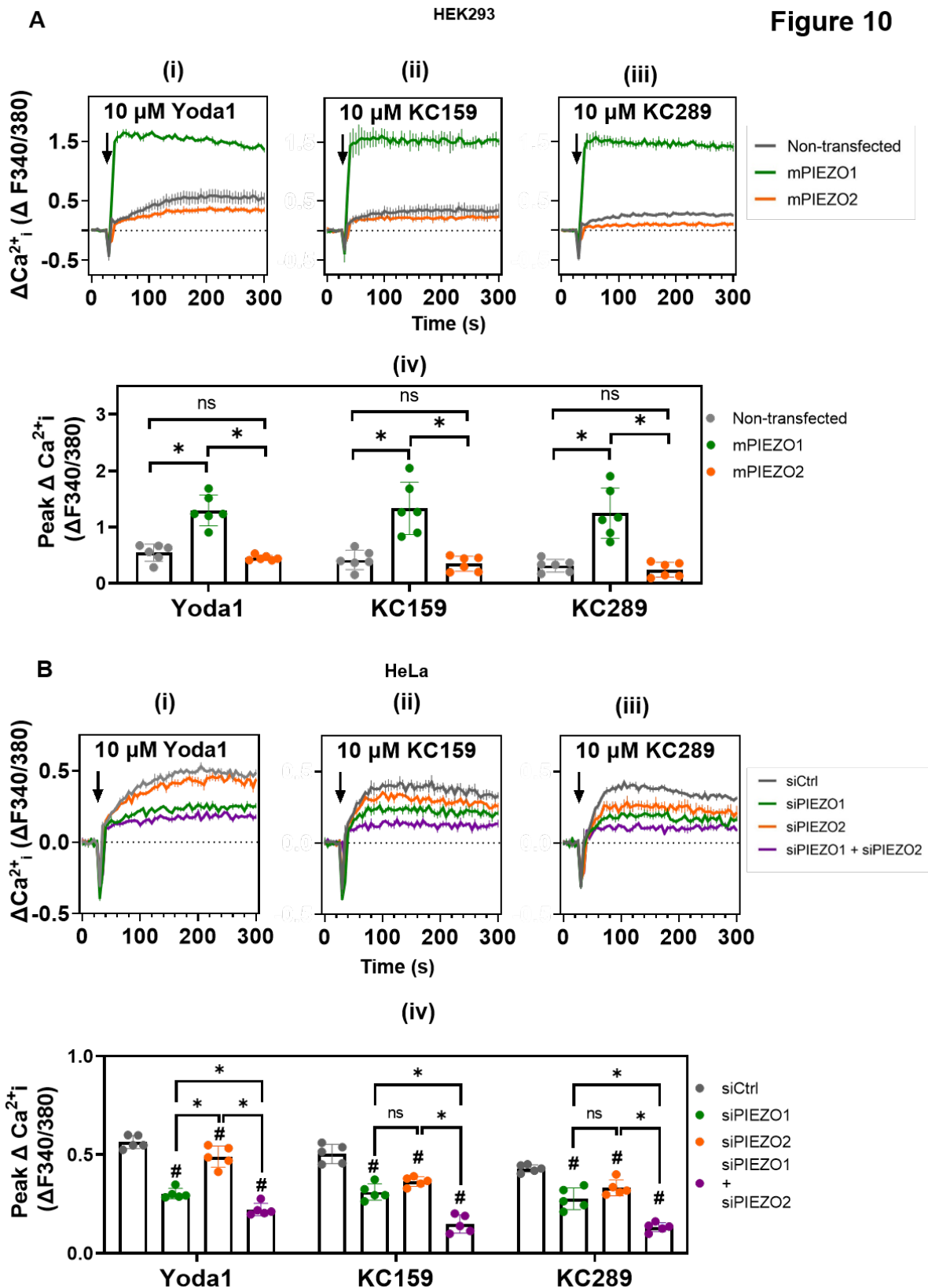
Figure 10 Relevance to PIEZO2

(A) Background-subtracted (Δ) peak intracellular Ca^{2+} measurements of HEK 293 cells overexpressing mPIEZO1, mPIEZO2 or non-transfected cells. Cells were exposed to 10 µM: (i) Yoda1; (ii) **KC159**; (iii) **KC289** . In each case, mean ± SEM values from 4 technical replicates are shown (n=1 each). (iv) Mean ± SD (n=6) for peak Ca^{2+} signals evoked by 10 µM

1579 Yoda1, **KC159** and **KC289**. (B) Background-subtracted (Δ) peak intracellular Ca^{2+}
1580 measurements of HeLa cells after siRNA mediated knockdown of hPIEZO1 (siPIEZO1),
1581 hPIEZO2 (siPIEZO2), both (siPIEZO1 + siPIEZO2) or transfected with a non-targeting
1582 (Control, Ctrl) siRNA (siCtrl). Cells were exposed to 10 µM: (i) Yoda1; (ii) **KC159**; (iii) **KC289**.
1583 Mean ± SEM values from 4 technical replicates are shown (n=1 each). (iv) Mean ± SD (n=5)
1584 for peak Ca^{2+} signals evoked by 10 µM Yoda1, **KC159** and **KC289**. RM-One way ANOVA
1585 followed by a Tukey's post-hoc test for multiple comparison performed on the mean values of
1586 the collated experiments are shown as: n.s (p > 0.05), # (p<0.05 vs siCtrl) * p < 0.05.
1587

A

HEK293

Figure 10 SI 1
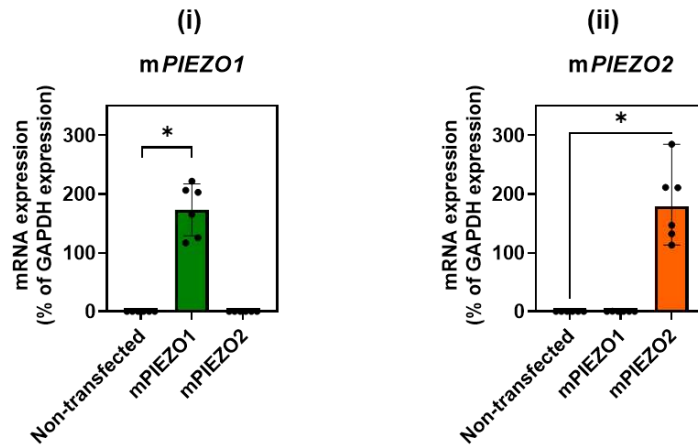
B

HeLa
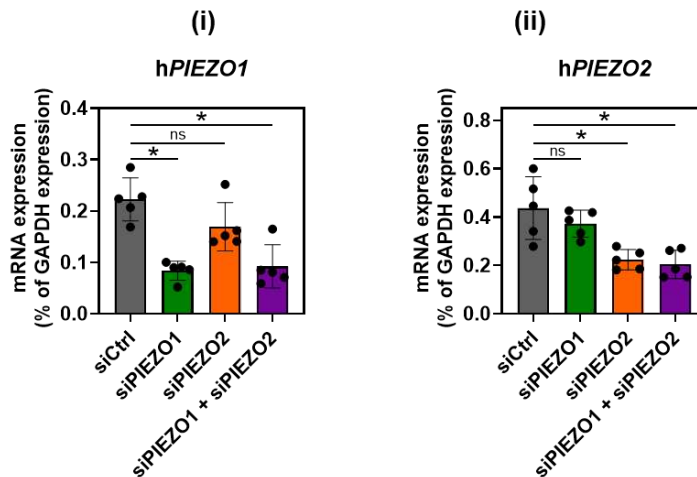
1588
1589 **Figure 10 SI 1 Validation of transfection efficiency in HEK 293 and HeLa cells**
1590 (A) mRNA abundance of (i) m*PIEZO1* and (ii) m*PIEZO2* (n=5) transcripts relative to h*GAPDH*
1591 mRNA in HEK 293 cells overexpressing mPIEZO1, mPIEZO2 or neither ("non-transfected
1592 cells"). (B) mRNA abundance of (i) h*PIEZO1* or (ii) h*PIEZO2* transcripts (n=5) relative to
1593 h*GAPDH* expression in HeLa cells after siRNA mediated knockdown of hPIEZO1 (siPIEZO1),
1594 hPIEZO2 (siPIEZO2), both (siPIEZO1 + siPIEZO2) or transfected with a non-targeting
1595 (Control, Ctrl) siRNA (siCtrl). Data expressed as Mean ± SD except in Aii, which is Median
1596 with Range because the data could not be confirmed as normally distributed. One way ANOVA
1597 followed by a Tukey's post-hoc test for multiple comparison was performed on the mean
1598 values of the collated experiments (Ai, Bi and Bii) and Friedmann test followed by a Dunn's
1599 post-hoc test for multiple comparison for (Aii): n.s ($p > 0.05$), * $p < 0.05$ for comparison against
1600 non-transfected and siCtrl only.
1601
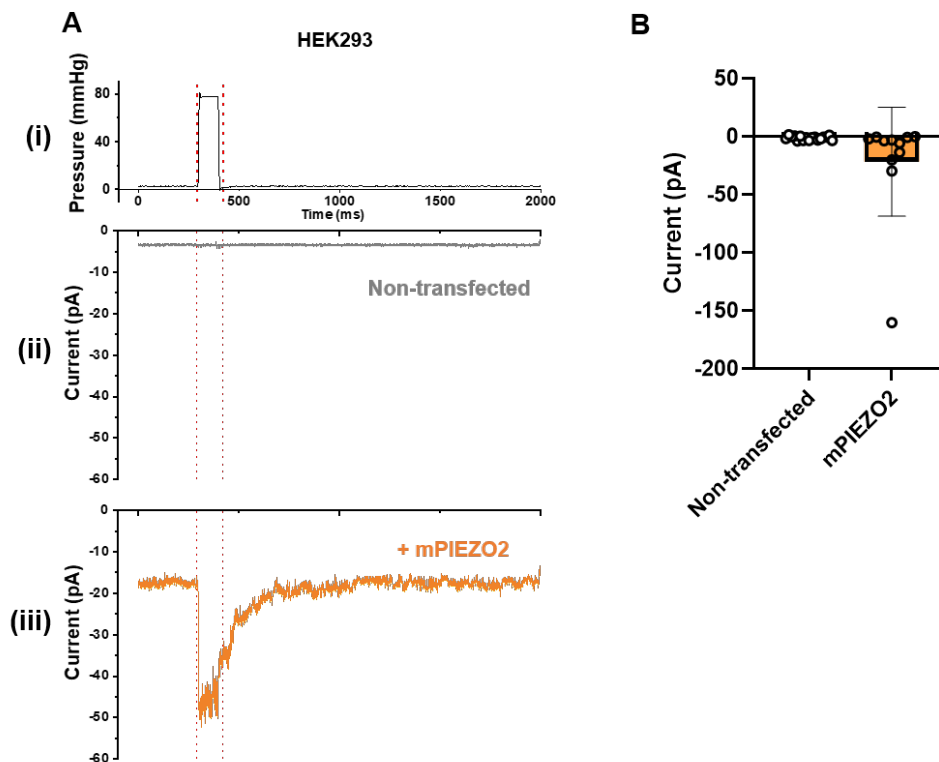
Figure 10 SI 2

Figure 10 SI 2 Detection of mechanically activated ionic current in HEK 293 cells overexpressing mouse PIEZO2

(A) Example (n=1) outside-out patch current recordings showing the response to (i) 100-ms 75 mmHg positive pressure pulse for (ii) non-transfected HEK 293 cells and (iii) HEK 293 cells overexpressing mPIEZO2. Traces in (ii) and (iii) are average currents from 3 consecutive pressure pulses. (B) Mean ± SD for peak inward currents activated by the pressure pulse as exemplified in (A): non-transfected cells (N=17 independent recordings) and HEK 293 cells overexpressing mPIEZO2 (N=11 independent recordings).

SUPPLEMENTARY INFORMATION (SI)

1612
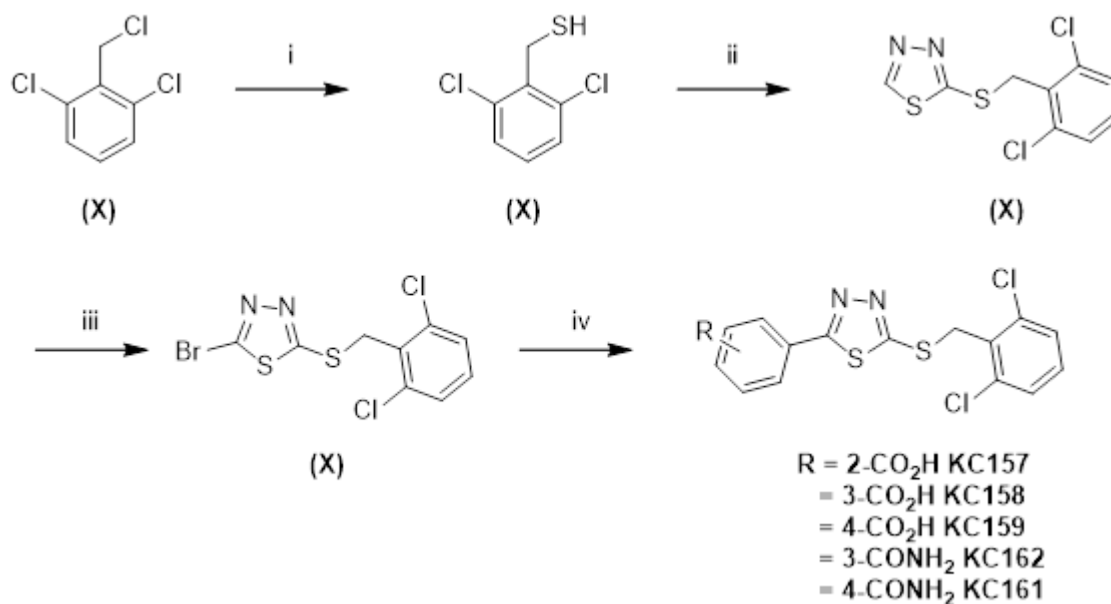
1613
1614

1615 **Scheme X**: i) a) thiourea (1.1 eq.), EtOH, reflux, 3h b) NaOH, EtOH, reflux, N_2, 3 h c) HCl
1616 (98%) ii) 2-bromo 1,3,4-thiadiazole (1.0 eq.), K_2CO_3 (1.2 eq.), DMF, 90 °C, 18 h (57%) iii) NBS
1617 (1.4 eq.), DCM, reflux, N_2, 48 h. (78%) iv) Appropriate boronic acid (1.0-3.5 eq.), K_2CO_3 (4.0
1618 eq.), Pd(PPh$_3$)$_4$ (0.1-2 eq.) dioxane, H_2O, 90 °C, N_2, 2-24 h (7-68%)

1619

1620 **Materials**

1621

1622 All purchased chemicals and solvents were used without further purification unless otherwise
1623 stated. All compounds were at least 95% pure by ^{1}H NMR.

1624

1625 **Physical Methods**

1626

1627 ^{1}H Nuclear Magnetic Resonance spectra were recorded at 500 MHz using a Bruker DRX 500
1628 instrument or at 400 MHz using a Bruker DPX 400. ^{1}H spectra are referenced based on the
1629 residual proton in the solvent (*e.g.* the CHCl$_3$, 0.01 % in 99.99 % CDCl$_3$). Coupling constants
1630 (*J*) are reported to the nearest 0.1 Hz. ^{13}C NMR spectra were recorded at 125 MHz on 500
1631 MHz spectrometers or at 100 MHz on 400 MHz spectrometers. HRMS was performed on a
1632 Burker Daltonics micrOTOF using positive electrospray ionisation (ES+). Automated column
1633 chromatography (ACC) was carried out using a Biotage Isolera Four EXP with Spektra.

1634

1635 **General Procedure A**

1636

1637 The desired aromatic halide (0.28 mmol, 1.0 eq. the desired boronic acid (0.28-0.98 mmol, 1-
1638 3.5 eq) and K_2CO_3 (1.12 mmol, 4.0 eq.) were dissolved in dioxane (2 mL) and H_2O (2 mL)
1639 then degassed with N_2 for 30 minutes. Pd(PPh$_3$)$_4$ (0.04 mmol, 0.15 eq.) was then added and
1640 the reaction was then heated to 90 °C for 2-24 h. Upon completion, the reaction was diluted
1641 with H_2O (20 mL), extracted with DCM (3 × 10 mL), dried over Na$_2$SO$_3$, filtered and reduced
1642 *in vacuo* to afford the crude or pure product.

1643

1644 **2,6-dichlorobenzyl thiol (X)**

1645

1646 2,6-dichlorobenzyl chloride (3.00 g 16.40 mmol) and thiourea (1.38 g, 18.40 mmol) were
1647 dissolved in EtOH (36 mL) and heated to reflux for 3 h. The solution was cooled to room
1648 temperature and dissolved in 2 M aq. NaOH (30 mL) and EtOH (10 mL) and the reaction was

refluxed for a further 3 hours. The solution was then cooled, quenched with 1 M HCl (60 mL), reduced *in vacuo*, and extracted with EtOAc (3 × 20 mL). The combined organic layers were then washed with sat. NaCl solution (2 × 20 mL), dried over Na_2SO_4 and evaporated to dryness to afford an off-white crystalline solid without further need for purification (2.90 g, 15.00 mmol, 98%). Rf 0.7 (9:1 Petroleum ether (40-60 °C):EtOAc (v/v)); δ_H (500 MHz, $CDCl_3$): 7.33 (2H, d, J = 8.0 Hz, benzyl 3-H), 7.15 (1H, t, J = 8.0 Hz, benzyl 4-H), 4.02 (2H, d, J = 8.5 Hz, benzyl CH_2), 2.12 (1H, t, J = 8.5 Hz, SH); δ_C (125 MHz, $CDCl_3$): 137.3 (benzyl 1-C), 134.6 (benzyl 2-C), 128.5 (benzyl 4-C), 128.5 (benzyl 3-C), 24.4 (benzyl CH_2).

2-((2,6-dichlorobenzyl)thio)-1,3,4-thiadiazole (X)

2,6-dichlorobenzyl thiol (2.85 g, 14.77 mmol), 2-bromo-1,3,4-thiadiazole (2.43 g, 14.77 mmol),& K_2CO_3 (2.38 g, 17.72 mmol) were dissolved in DMF (10 mL) and heated to 90 °C for 18 h. The reaction was diluted with H_2O (100 mL), extracted with EtOAc (3 × 40 mL) and the organic layers combined. These were washed with brine (3 × 40 mL), 10% LiCl (3 × 40 mL), dried over $MgSO_4$, filtered and reduced *in vacuo* to give brown residue (4.33 g). This was purified by ACC (0-30% EtOAc in petroleum ether (40-60 °C)) to afford white crystalline solid (2.33 g, 8.43 mmol, 57%) Rf 0.60 (7:3 Petroleum ether (40-60 °C):EtOAc (v/v)); δ_H (400 MHz, $CDCl_3$): 8.99 (1H, s, thiadiazole 5-H), 7.27 (2H, d, J = 8.5 Hz, benzyl 3-H), 7.13 (1H, t, J = 8.5 H, benzyl 4-H), 4.89 (2H, s, benzyl CH_2); δ_C (100 MHz, $CDCl_3$): 164.7 (thiadiazole 2-C), 152.1 (thiadiazole 5-C), 136.3 (benzyl 2-C), 131.7 (benzyl 1-C), 129.8 (benzyl 4-C), 128.5 (benzyl 3-C), 34.73 (benzyl CH_2); m/z ES+ Found MNa^+ 298.9235, $C_9H_6Cl_2N_2S_2$ requires MNa^+ 298.9242.

2-Bromo-5-((2,6-dichlorobenzyl)thio)-1,3,4-thiadiazole

2-((2,6-dichlorobenzyl)thio)-1,3,4-thiadiazole (2.33 g, 8.43 mmol), & N-bromosuccinimide (2.10 g, 11.80 mmol) were dissolved in DCM (10 mL) and refluxed for 48 h. The reaction was then cooled, quenched with sat. $Na_2S_2O_3$ (20 mL), partitioned and the aqueous extracted with DCM (2 × 15 mL). The organic layers were combined, dried over $MgSO_4$, filtered and reduced *in vacuo* to give an orange, oily crystals (3.15 g). This was purified by ACC (0-30% EtOAc in Petroleum ether (40-60 °C)) to afford a white crystalline solid (2.80 g, 7.87 mmol, 78 %) Rf 0.80 (7:3 Petroleum ether (40-60 °C):EtOAc (v/v)); δ_H (400 MHz, $CDCl_3$): 7.37 (2H, d, J = 8 Hz, benzyl 3-H), 7.24 (1H, dd, J = 8.5 & 7.5 Hz, benzyl 4-H), 4.92 (2H, s benzyl CH_2); δ_C (100 MHz, $CDCl_3$): 168.1 (thiadiazole 5-C), 138.1 (thiadiazole 2-C), 136.3 (benzyl 2-C), 131.5 (benzyl 1-C), 129.9 (benzyl 4-C), 128.6 (benzyl 3-C), 34.6 (benzyl CH_2); m/z ES+ Found MH^+ 356.8462, $C_9H_5BrCl_2N_4S_2$ requires MH^+ 356.8512.

2-(5-((2,6-Dichlorobenzyl)thio)-1,3,4-thiadiazol-2-yl)benzoic acid (KC157)

General procedure A was followed using 2-bromo-5-((2,6-dichlorobenzyl)thio)-1,3,4-thiadiazole (100 mg, 0.28 mmol), 2-(methoxycarbonyl)phenylboronic acid (43 mg, 0.28 mmol), K_2CO_3 (155 mg, 1.12 mmol), Pd(PPh$_3$)$_4$ (35 mg, 0.03 mmol), dioxane (2 mL) and water (2 mL) to afford a crude orange solid. This was triturated with DCM to afford a yellow powder (16 mg, 0.04 mmol, 14%). δ_H (400 MHz, D_6-DMSO): 7.91-7.88 (1H, m, benzoatyl 6-H), 7.73-7.67 (3H, m, benzoatyl 3, 4 & 5-H), 7.56 (2H, d, J = 8.0 Hz, benzyl 3-H), 7.42 (1H, t, J = 8.0 Hz, benzyl 4-H), 4.85 (2H, s, benzyl CH_2); δ_C (100 MHz, D_6-DMSO): 168.4 (carbonyl C), 167.9 (thiadiazolyl 2-C), 164.7 (thiadiazolyl 5-C), 135.7 (benzoatyl 6-C), 133.1 (benzoatyl 1 or 2-C or benzyl 1-C), 132.1 (benzoatyl 3, 4 or 5-C), 131.9 (benzoatyl 1 or 2-C or benzyl 1-C), 131.6 (benzoatyl 3, 4 or 5-C) 131.4 (benzyl 4-C), 131.3 (benzoatyl 3, 4 or 5-C), 130.3 (benzyl 2-C), 129.4 (benzyl 3-C), 128.9 (benzoatyl 3, 4 or 5-C), 34.9 (benzyl CH_2); m/z ES+ Found MH^+ 396.9635, $C_{16}H_{10}Cl_2N_2O_2S_s$ requires MH^+ 396.9639.

3-(5-((2,6-Dichlorobenzyl)thio)-1,3,4-thiadiazol-2-yl)benzoic acid (KC158)

1704 General procedure A was followed using 2-bromo-5-((2,6-dichlorobenzyl)thio)-1,3,4-
1705 thiadiazole (100 mg, 0.28 mmol), 3-(methoxycarbonyl)phenylboronic acid (43 mg, 0.28 mmol),
1706 K_2CO_3 (155 mg, 1.12 mmol), Pd(PPh$_3$)$_4$ (35 mg, 0.03 mmol), dioxane (2 mL) and water (2 mL)
1707 to afford a crude orange solid. This was triturated with DCM to afford a yellow powder (6 mg,
1708 0.02 mmol, 7%) δ_H (400 MHz, D$_6$-DMSO): 8.43 (1H, s. benzoatyl 2-H), 8.17 (1H, d, J = 8.0 Hz,
1709 benzoatyl 4 or 6-H), 8.13 (1H, d, J = 8.0 Hz, benzoatyl 4 or 6-H), 7.71 (1H, ap. t, J = 8.0 Hz,
1710 benzoatyl 5-H), 7.57 (2H, d, J = 8.0 Hz, benzyl 3-H), 743 (1H, t, 8.0 Hz, benzyl 4-H), 4.87 (2H,
1711 s, benzyl CH$_2$); δ_C (100 MHz, D$_6$-DMSO): 169.0 (carbonyl C), 166.9 (thiadiazolyl 2-C), 164.2
1712 (thiadiazolyl 5-C), 135.7 (benzyl 2-C), 132.4 (benzyl 1-C or benzoatyl 3-C), 132.2 (benzoatyl
1713 4 or 6-C), 132.0 (benzoatyl 4 or 6-C), 131.4 (benzyl 4-C), 130.5 (benzoatyl 5-C), 130.0 (benzyl
1714 1-C or benzoatyl 3-C), 129.4 (benzyl 3-C), 128.3 (benzoatyl 2-C), 35.1 (benzyl CH$_2$); m/z ES+
1715 Found MH$^+$ C$_{16}$H$_{10}$Cl$_2$N$_2$O$_2$S$_s$ requires MH$^+$ 396.9639.

1716

1717 **4-(5-(2,6-Dichlorobenzyl)thio)-1,3,4-thiadiazol-2-yl)benzoic acid (KC159)**

1718

1719 General procedure A was followed using 2-bromo-5-((2,6-dichlorobenzyl)thio)-1,3,4-
1720 thiadiazole (100 mg, 0.28 mmol), 4-(methoxycarbonyl)phenylboronic acid (43 mg, 0.28 mmol),
1721 K_2CO_3 (155 mg, 1.12 mmol), Pd(PPh$_3$)$_4$ (35 mg, 0.03 mmol), dioxane (2 mL) and water (2 mL)
1722 to afford a crude orange solid. This was triturated with DCM to afford an orange powder (77
1723 mg, 0.19 mmol, 68%) δ_H (400 MHz, D$_6$-DMSO): 8.09-8.04 (4H, m, benzoate 2 & 3-H), 7.56
1724 (2H, d J = 8.0 Hz, benzyl 3-H), 7.43 (1H, t, J = 8.0 Hz, benzyl 4-H), 4.88 (2H, s, benzyl CH$_2$);δ_C
1725 (100 MHz, D$_6$-DMSO): 168.8 (thiadiazolyl 2-C), 167.0 (thiadiazolyl 5-C), 164.8 (carbonyl C),
1726 135.7 (benzyl 2-C), 133.6 (benzoatyl 1 or 4-C), 133.3 (benzoatyl 1 or 4-C), 132.0 (benzyl 1-
1727 C), 131.4 (benzyl 4-C), 130.1 (benzoatyl 2 or 3-C), 129.4 (benzyl 3-C) 128.3 (benzoatyl 2 or
1728 3-C), 35.1 (benzyl CH$_2$); m/z ES+ Found MH$^+$ 396.9627, C$_{16}$H$_{10}$Cl$_2$N$_2$O$_2$S$_s$ requires MH$^+$
1729 396.9639.

1730

1731 **4-(5-((2,6-Dichlorobenzyl)thio)-1,3,4-thiadiazol-2-yl)benzamide (KC161)**

1732

1733 General procedure A was followed using 2-bromo-5-((2,6-dichlorobenzyl)thio)-1,3,4-
1734 thiadiazole (100 mg, 0.28 mmol), 4-(aminocarbonyl)-phenylboronic acid (46 mg, 0.28 mmol),
1735 K_2CO_3 (155 mg, 1.12 mmol), Pd(PPh$_3$)$_4$ (35 mg, 0.03 mmol), dioxane (2 mL) and water (2 mL)
1736 to afford a crude brown solid. This was purified by triturations with EtOAc and then DCM to
1737 afford a yellow solid (25 mg, 0.06 mmol, 21%). δ_H (400 MHz, D$_6$-DMSO): 8.03 (4H, bs,
1738 benzamidyl 2 & 3-H), 7.57 (2H, d, J = 8.0 Hz, benzyl 3-H), 7.43 (1H, t, J = 8.0 Hz, benzyl 4-
1739 H), 4.87 (2H, s, benzyl CH$_2$); δ_C (100 MHz, D$_6$-DMSO): 169.0 (carbonyl C), 167.4 (thiadiazolyl
1740 2-C), 164.3 (thiadiazolyl 5-C), 137.2 (benzamidyl 1 or 4-C), 135.7 (benzyl 2-C), 132.0 (benzyl
1741 1-C or benzamide 1 or 4-C), 131.9 (benzyl 1-C or benzamidyl 1 or 4-C), 131.4 (benzyl 4-C),
1742 129.4 (benzamidyl 2 or 3-C), 129.0 (benzyl 3-C), 128.0 (benzamidyl 2 or 3-C), 35.1 (benzyl
1743 CH$_2$; m/z ES+ Found MNa$^+$ 417.9608, C$_{16}$H$_{11}$Cl$_2$N$_3$OS$_2$ requires MNa$^+$ 417.9612.

1744

1745 **3-(5-((2,6-Dichlorobenzyl)thio)-1,3,4-thiadiazol-2-yl)benzamide (KC162)**

1746

1747 General procedure A was followed using 2-bromo-5-((2,6-dichlorobenzyl)thio)-1,3,4-
1748 thiadiazole (100 mg, 0.28 mmol), 3-(aminocarbonyl)-phenylboronic acid (46 mg, 0.28 mmol),
1749 K_2CO_3 (155 mg, 1.12 mmol), Pd(PPh$_3$)$_4$ (35 mg, 0.03 mmol), dioxane (2 mL) and water (2 mL)
1750 to afford a crude brown solid. This was purified by triturations with EtOAc and then DCM to
1751 afford a yellow solid (44 mg, 0.10 mmol, 36%). δ_H (400 MHz, D$_6$-DMSO): 8.39 (1H, s,
1752 benzamidyl 2-H), 8.10 (1H, d, J = 8.0 Hz, benzamidyl 4 or 6-H), 8.07 (1H, d, J = 8.0 Hz,
1753 benzamidyl 4 or 6-H), 7.99 (1H, ap. t, J = 7.5 Hz, benzamidyl 5-H), 7.56 (2H, d, J = 8.0 Hz,
1754 benzyl 3-H), 7.43 (1H, t, J = 8.0 Hz, benzyl 4-H), 4.86 (2H, s, benzyl CH$_2$); δ_C (100 MHz, D$_6$-
1755 DMSO):169.3 (carbonyl C), 167.3 (thiaidazolyl 2-C), 164.0 (thiadiazolyl 5-C), 136.9
1756 (benzamidyl 3-C), 135.6 (benzyl 2-C), 132.0 (benzamidyl 1-C), 131.3 (benzyl 4-C), 130.8
1757 (benzamidyl 4 or 6-C), 130.6 (benzamidyl 4 or 6-C), 130.1 (benzamidyl 5-C), 129.8 (benzyl 1-

1758   C), 129.4 (benzyl 3-C), 127.1 benzamidyl 2-C), 35.1 (benzyl CH$_2$); m/z ES+ Found MNa$^+$
1759   417.9609, C$_{16}$H$_{11}$Cl$_2$N$_3$OS$_2$ requires MNa$^+$ 417.9612.
1760
1761   **Potassium 4-(5-((2,6-dichlorobenzyl)thio)-1,3,4-thiadiazol-2-yl)benzoate (KC289)**
1762
1763   4-(5-((2,6-dichlorobenzyl)thio)-1,3,4-thiadiazol-2-yl)benzoic acid (20 mg, 0.05 mmol) and KOH
1764   (2.81 mg, 0.05 mmol) were dissolved in MeOH (3 mL) and heated to 60 °C for 18 h. The
1765   reaction was then reduced under pressure to give a white solid without further need for
1766   purification (20.92 mg, 0.05 mmol, 100%). δ$_H$ (500 MHz, D$_6$-DMSO): 7.97 (2H, d, J = 8.0 Hz,
1767   benzoatyl 2-H), 7.85 (2H, d, J = 8.0 Hz, benzoatyl 3-H), 7.56 (2H, d, J = 8.0 Hz, benzyl 3-H),
1768   7.43 (1H, dd, J = 8.5 & 7.5 Hz, benzyl 4-H), 4.85 (2H, s, benzyl CH$_2$); δ$_C$ (125 MHz, D$_6$-DMSO):
1769   170.0 (carbonyl-C), 167.5 (thiadiazolyl 2-C), 162.7 (thiadiazolyl 5-C), 135.6 (benzyl 2-C),
1770   132.1 (benzyl 1-C), 131.3 (benzyl 4-C), 130.4 (benzoatyl 1/2-C), 129.4 (benzyl 3-C), 127.2
1771   (benzoatyl 3/4-C), 35.1 (benzyl CH$_2$); m/z ES+ Found MH$^+$ 396.9628, C$_{16}$H$_{10}$Cl$_2$N$_2$O$_2$S$_s$
1772   requires MH$^+$ 396.9639.
1773
1774